4DCT as a tool to evaluate kinematic changes due to ACL injury

Determination of a workflow for the clinical setting

F.A.C. Oosterbaan

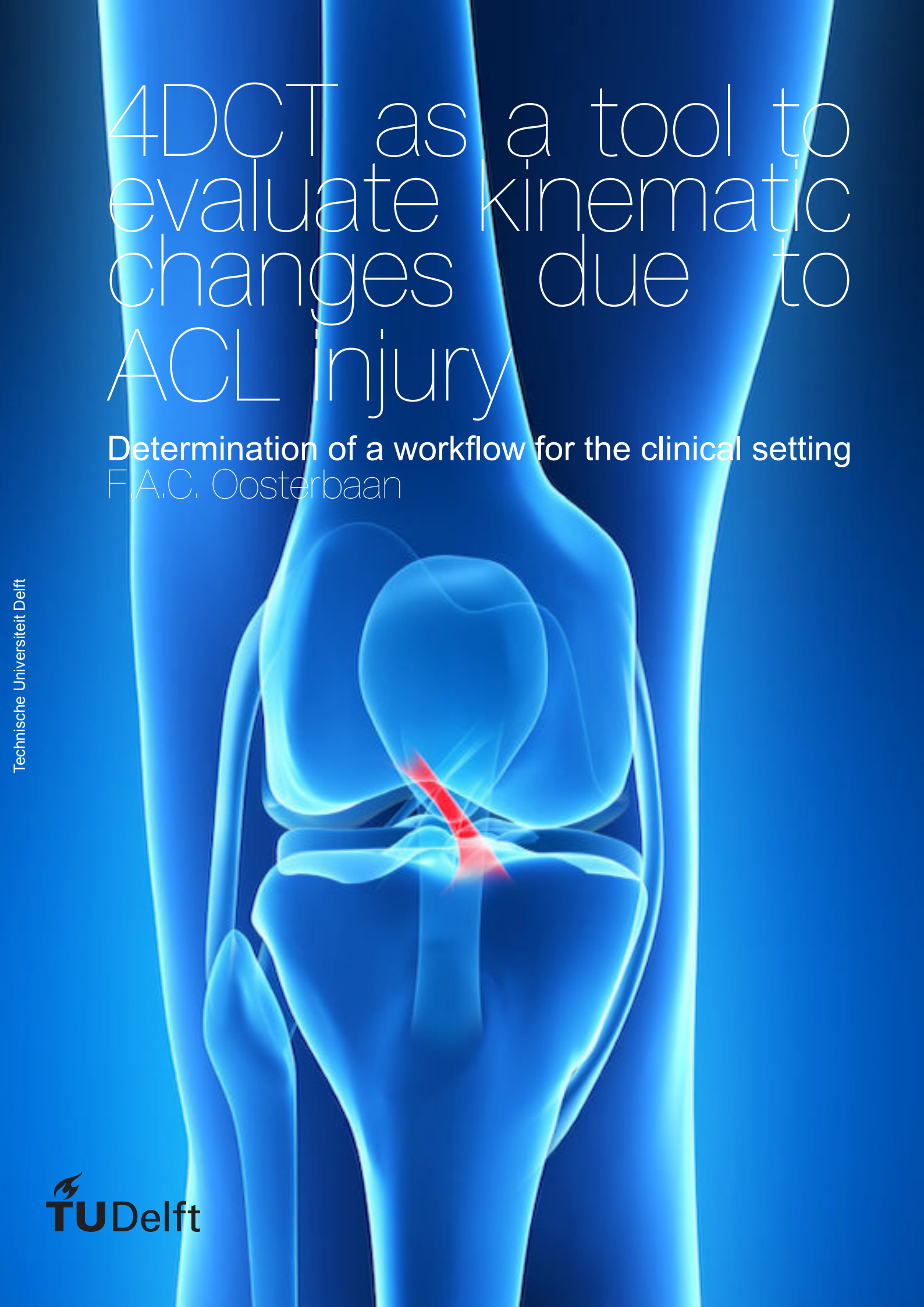

Technische Universiteit Delft

TU Delft

4DCT as a tool to evaluate kinematic changes due to ACL injury

Determination of a workflow for the clinical setting

by

F.A.C. Oosterbaan

to obtain the degree of Master of Science
at the Delft University of Technology,
to be defended publicly on Wednesday June 21, 2023 at 11:00 AM.

Student number:	4458613	
Course code:	BM51035	
Project duration:	June 2022 - June 2023	
Thesis committee:	Prof. dr. ir. J. Harlaar,	TU Delft, chair
	Dr. M.G.H. Wesseling,	TU Delft, supervisor
	Dr. T.M. Piscaer,	Erasmus MC, supervisor
	Prof. dr. H.E.J. Veeger	TU Delft

An electronic version of this thesis is available at http://repository.tudelft.nl/.
Cover figure adapted from http://physicalsolutionsli.com/acl-injuries/

TU Delft

Preface

When deciding on my education after high school, my interests were broad, and I went to various institutions to see what piqued my interest. I chose to come to Delft and decided on Mechanical Engineering. During my Bachelors, I joined one of the Dream Teams, the Human Power Team, which aimed to design the fastest human-powered vehicle on earth. Such a design requires a good interaction between the user and the vehicle. Even though this was not my responsibility within the team, I took an interest in the human aspect of technology this year and later chose to minor in health care. I found it very interesting, but also made me miss the engineering perspective. Altogether this is what led me to choose this Master's program.

For my thesis, I was looking for a challenge. That search resulted in this project which was something new for me. I did know the techniques required, as they were mentioned during the courses of my Master's program, but performing them myself was something I had never done. In addition, I found this project very interesting, and I still do, as it is a relatively new technique that I think has the potential to help the medical field in one way or another. During this project, I had to learn a series of new programs, which is very valuable and exciting, even though I may not always have been too excited about it. One example is Python, as I had only used Matlab before. Learning this program was a challenge at times, as it has a lot of similarities to Matlab, but they are just not quite the same, which led to quite some frustrations at times. However, now I know how to use this tool to automate the use of programs. Overall I can say I have learned a lot from this project, and I can undoubtedly say that I am happy that I never had to go through an ACL injury despite all my years of playing hockey, as it seems to be an injury that can affect you all your life.

I couldn't have written this thesis without the help of some people. Therefore, I want to thank my supervision team for all the help they have given me throughout the project. Mostly I want to thank Mariska and Tom for always being available to help me when facing an issue or to talk about the project so I could bounce some ideas off them. Moreover, I want to thank 'het meubulair' at Gezelschap Leeghwater. You know who you are. Even though I have seen a lot of you come and go, I was happy that there was always one of you on the couch during lunch with whom I could take a break from the study landscape. I want to thank Bas for helping me finalize this paper by proofreading it and helping me spot some silly mistakes I kept on overlooking. Lastly, I want to thank all my friends and family, especially Tom, Jessica and my parents. You were always there for me to vent when my scripts weren't working how I thought they should, which in most cases was due to a small error like missing a bracket that I would find two days later, which is part of the deal when programming, but still, it is very annoying.

With this thesis, my years as a student will come to an end. It has been years filled with some challenges, all of which I have managed to overcome. Now it is time for a new challenge, which I am very excited about, but first, some time off.

F.A.C. Oosterbaan
Delft, June 2023

Contents

List of Figures

List of Tables

List of abbreviations

Abbreviation	Definition
ACL:	Anterior cruciate ligament
MRI:	Magnetic resonance imaging
4DCT:	Four-dimensional computed tomography
CT:	Computed tomography
DoF:	Degrees of freedom
AP:	Anterior-posterior
ML:	Mediolateral
SI:	Superior-inferior
DICOM:	Digital imaging and communications in medicine
ICP:	Iterative closest point
LPS:	Left, posterior, superior
RAS:	Right, anterior, superior
ACS:	Anatomical coordinate system
SPM:	Statistical parametric mapping
JAM:	Joint and articular mechanics
SD:	Standard deviation
RMS:	Root mean square

Summary

Anterior cruciate ligament tears are a common injury, with over two million people affected annually. Typically, magnetic resonance imaging is used to diagnose the injury, but this technique is less sensitive in evaluating incomplete or concomitant injuries. Four-dimensional computed tomography is a relatively new technique that can become commonly available in the clinical setting. It allows for dynamic imaging, which may be suited for evaluating a change in knee kinematics after ACL in movements like flexion/extension. This may be used to gain insight into the function of the anterior cruciate ligament or surrounding ligaments which informs surgical decision-making and might prevent or alter intended surgeries.

This thesis aims to answer the following research question; How can four-dimensional computed tomography scans of the tibiofemoral joint made during unloaded flexion/extension movements be meaningfully visualized and can it be used to detect kinematic differences between a knee with a complete anterior cruciate ligament tear and an uninjured one? To do so, both knees of eight patients with a unilateral complete anterior cruciate ligament tear were scanned during a simultaneous flexion/extension movement in the four-dimensional computed tomography scanner. A workflow was created that consists of four steps; the segmentation, the registration, the definition of anatomical coordinate systems, and the visualization of the kinematic measures in three different ways. Almost all steps of this workflow were automated and open-source programs were used where possible throughout the workflow to facilitate easy usage. However, some manual steps are still required. The kinematic measures were expressed in three different ways. First, the rotations between the anatomical coordinate systems of the femur and tibia were calculated using Euler decomposition alongside the translations. In addition, a plot of the intercondylar axes was made, which shows the movement of the mediolateral axis of the femur relative to the tibia during flexion/extension. Finally, to obtain the kinematics at the articulation surface, an OpenSim Joint and Articular Mechanics simulation was set up to simulate the movement using the patient-specific information obtained from the four-dimensional computed tomography scans. Based on this simulation, the centres of proximity were plotted for both the tibia and the femur. The distances between the subsequent centres of proximity were then evaluated for a set of flexion angles to gain insight into the type of movement occurring (e.g., roll or slip).

Minor differences for the mean translations and rotations were seen between the anterior cruciate ligament deficient and the uninjured knees. Only in the anterior-posterior translation a statistically significant ($p=0.023$) increase could be seen at extension and the lower flexion angles ($\pm$-5° to $\pm$15°) for the anterior cruciate ligament deficient knees. No noteworthy differences were present for all other degrees of freedom. Differences were more apparent in the plots of the intercondylar axes. Here, the increased anterior-posterior translation was more prominent for anterior cruciate ligament deficient knees than for uninjured ones. Lastly, the centres of proximity showed substantial differences among patients, obscuring the determination of a pattern to distinguish between anterior cruciate ligament deficient and uninjured knees. However, these plots did show a substantial difference compared to the plots of the intercondylar axes. This may be due to slip occurring at the articulation surface and would mean that plotting the intercondylar axes does not adequately represent the kinematics of the articular surface throughout the whole range of motion of the knee.

Overall, some minor kinematic differences during flexion/extension can be seen in the graphs of the translations and rotations and the plots of the intercondylar axes. The plots of the intercondylar axes showed the most apparent differences, but they may not represent the situation at the articulation surface. Therefore the centres of proximity are better suited to gain information about the articulation surface. Still, due to the differences among patients, a pattern to distinguish between anterior cruciate ligament deficient and uninjured knees could not be determined. Altogether, this technique may not be suited as a tool to evaluate knee injuries in all patients, but only in patients that are expected to cope very well with the injury or where a concomitant injury is expected. However, future research should still evaluate the performance of the workflow for these situations.

1 Introduction

Over two million people worldwide tear their anterior cruciate ligament (ACL) annually, making this the most common knee ligament injury [28, 76]. About 70% of these injuries occur in non-contact situations such as during high pivoting movements or landing manoeuvres [14]. Because of this, these injuries are prevalent in sports like soccer and basketball. Recent studies have also shown that the incidence of these injuries in the pediatric and adolescent population has been rising despite prevention programs [29, 34, 32]. ACL injury, therefore, seems to be a growing problem, especially in a younger population.

Typically, patients with an ACL tear present with a malfunction of the knee expressed as altered knee kinematics during a specific task like flexion/extension [48]. Rehabilitation is of great importance and primarily aims to prevent recurrence and restore the original knee kinematics [16]. Two techniques form the basis of surgical decision-making; Magnetic resonance imaging (MRI) and manual tests. MRI is used to visualize the torn ACL, establish a surgical approach, and diagnose concomitant injuries [48]. However, this technique is less sensitive in visualizing partial tears of the ACL, and other ligaments are difficult to visualize using this technique [62, 77]. This may lead to incomplete diagnoses as partial tears concomitant injuries may have been missed. In addition, manual tests are used to assess the kinematic differences between the ACL deficient (ACLD) and uninjured knee for specific movements, but these tests are highly subjective [53]. Because of this, concomitant injuries or partial tears may be overlooked while requiring surgical repair, or surgeries may be performed when they are unnecessary, also because compensation strategies like muscle contractions are not accounted for in these two tests. Therefore, an alternative method that can adequately visualize all levels of ACL injury and concomitant injuries during daily movement would be preferred to properly assess the joint on which surgical decisions can be based.

Four-dimensional computed tomography (4DCT) is a relatively new technique that has previously helped to understand joint instabilities better [52]. It is a type of computed tomography (CT) that can visualize a moving structure over time. Currently, 4DCT is mainly used for planning radiotherapy or evaluating the heart and lungs, but recent studies also show an interest in the technique for skeletal applications, like the knee [52, 63]. As CT scanners are widely used, unlike tools such as motion capture labs, it has the potential to be an easily accessible technique to gain insight into the kinematic differences in ACLD and uninjured knees without the need for human interpretation of measurements like the manual tests. Using 4DCT, evaluating the changes in all six degrees of freedom (DoF) of the joint may be possible during continuous movement. Therefore, evaluating the kinematic differences between ACLD and uninjured knees may be possible during a functional task like a flexion/extension movement. As each ligament injury and its levels affect the knee kinematics differently, it should be possible to distinguish between them using this. Moreover, patients can perform the movement themselves which allows for insights into coping mechanisms like muscle contractions. Which, in turn, may reduce the kinematic changes due to injury and may even mean surgery is unnecessary. In addition, this technique allows for the evaluation of the movements of the bone directly without potential interference of soft tissue. Previous studies have evaluated the kinematics during flexion/extension movements but they required a series of separate static scans, which required patients to hold a specific position. This, in turn, could introduce relaxation and, thereby, differences from the actual movement in the joint [7].

This thesis aims to answer the following research question; How can four-dimensional computed tomography scans of the tibiofemoral joint made during unloaded flexion/extension movements be meaningfully visualized and can it be used to detect kinematic differences between a knee with a complete anterior cruciate ligament tear and an uninjured one? To answer this question, an automated workflow was developed to process the 4DCT scans of both knees of patients with a unilateral complete ACL injury. Subsequently, the kinematics were presented in three different ways to gain an understanding of the best way to interpret the data for this application and the differences between the calculated kinematic measures.

2

Terminology

Some of the terminology used throughout this thesis is common in the medical field but may be unfamiliar to some readers. Therefore, the following sections will explain the vital terminology used throughout.

2.1. Describing movements of the human body

The human body has three different planes, like the three that can be described in a three-dimensional coordinate system. These planes are named according to their orientation (see figure 2.1).

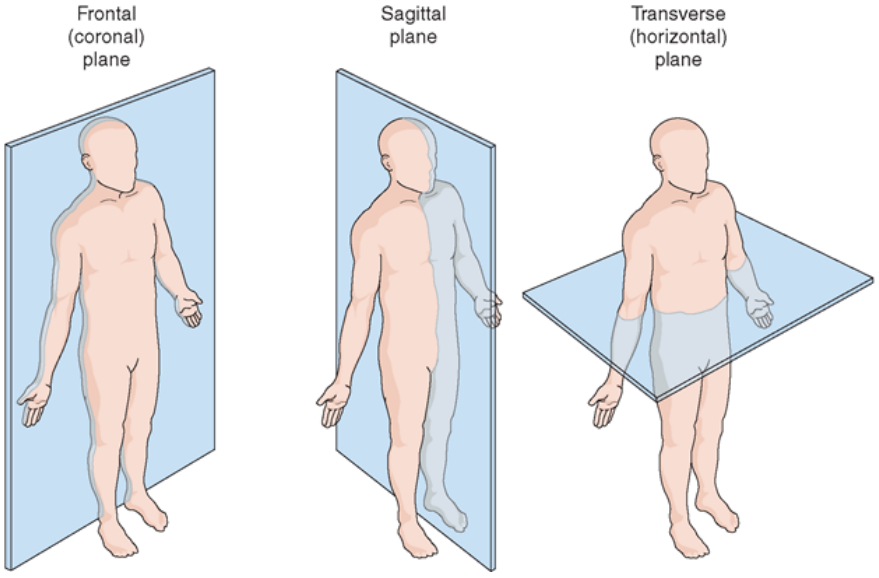

Figure 2.1: Anatomical planes [31].

Axes can be defined perpendicular to these planes. The anterior-posterior (AP) axis is perpendicular to the frontal or coronal plane. The axis perpendicular to the sagittal plane is the mediolateral (ML) axis, and the axis perpendicular to the transverse or horizontal plane is the superior-inferior (SI) axis.

These three axes can be used to describe the movement. Figure 2.2 shows the definitions of the positive translations and rotations used throughout this thesis. Here, extension is the positive rotation about the ML axis, while a movement in the opposite direction is flexion. A positive rotation about the AP axis can be called either varus or valgus, depending on the left or right knee. This difference is due to the definition of these rotations. Varus is when the tibia rotates inwards along the AP axis, which is in a different direction for both knees. Hence, a positive rotation for the right knee is varus, while that for the left knee is valgus, an outwards rotation of the tibia. The same holds for rotations about the SI axis, as internal rotation is defined as the inward rotation about the SI axis of the tibia compared to the

femur. Therefore a positive rotation about this axis is internal rotation for the right knee and external rotation for the left knee.

Lastly, locations can be described based on these axes and planes. A structure is superior when located higher along the SI axis. In contrast, when it is located lower, it is more inferior. Similarly, a position more forward along the AP axis is a more anterior position, and more backward is posterior. When comparing the position of a structure relative to the sagittal plane, it can be located more medial, which is closer to the plane or more towards the centre, or it can be situated lateral, which is further away from it. Lastly, a location in a limb can also be described in terms of its distance to the trunk. Here, a structure closer to the trunk is more proximal, and one further away is more distal.

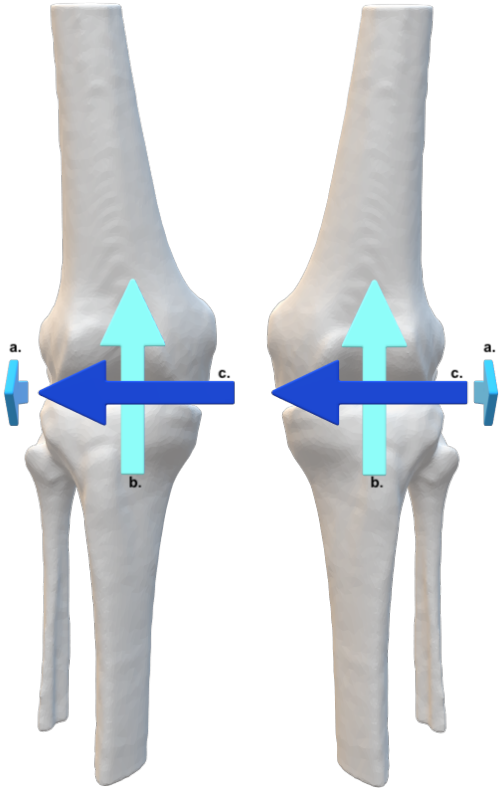

(a) Positive knee translations; a. (blue) Anterior translation. b. (light blue) Superior translation. c. (dark blue) To the right is positive, which is the medial translation for the left knee (right side of the figure) and lateral translation for the right knee (left side of the figure).

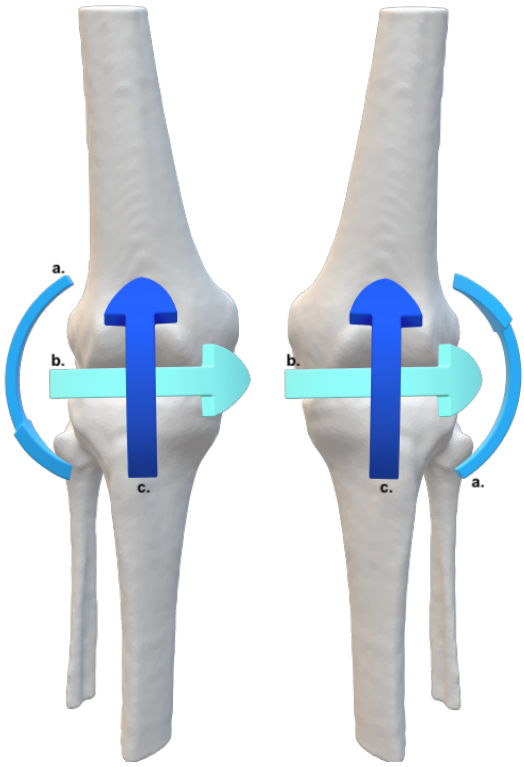

(b) Positive knee rotations; a. (blue) Extension. b. (light blue) External rotation for the left knee (right side of the figure) and internal rotation for the right (left side of the figure). c. (dark blue) Valgus for the left knee (right side of the figure) and varus for the right knee (left side of the figure).

Figure 2.2: Positive translations and rotations of the knee as seen from the anterior side.

2.2. Anatomy of the knee

The knee is a complex structure where four bones come together; the femur, patella, tibia, and fibula (see figure 2.3). As the condyles of the femur are convex and so is the lateral side of the tibial plateau, the joint is unstable based on the bony morphology only. Several ligaments and the meniscus between them help increase joint stability by restricting movement in undesired directions while muscles attach to the bones to facilitate movement [30]. In this thesis, the ACL is of particular interest as participants with this injury were evaluated. It is approximately 38 mm in length and has a width of about 10 mm, and connects the anteromedial area of the intercondylar area on the tibia to the posterolateral side of the lateral condyle of the femur as shown in figure 2.3 [59, 60]. Together these ligaments enable the knee to function as a complex hinge joint where the rotation axis changes over time [43]. Two ligaments provide the main restrictions for this hinging movement; the ACL and the posterior cruciate ligament. These two ligaments restrict movement at different points, and the ACL will restrict movement in a more anterior position while the posterior cruciate ligament is more relaxed. In a more flexed position, this is the other way around. The two ligaments also allow for some rotational movement, in which the

medial- and lateral collateral ligaments aid in stabilizing. Altogether this results in the complex hinge movement that is known for the knee joint.

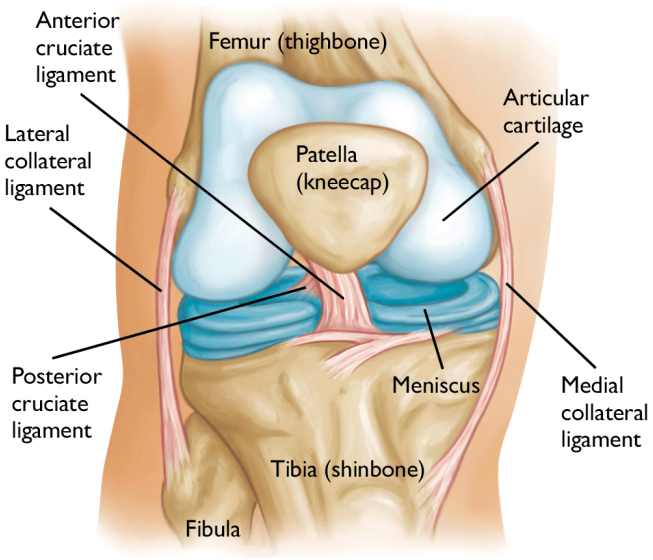

Figure 2.3: Anatomy of a healthy knee [65].

3

ACL injury

Damage to a ligament will result in a knee malfunction and therefore altered knee kinematics. To better understand ACL tears and the consequences thereof, the following sections will elaborate on the different aspects of this injury.

3.1. Kinematic consequences of an ACL tear

Commonly, the ACL can injure when a valgus or anterior stress is put on the knee when extended [66]. Still, it can also result from other loading mechanisms, such as an extreme internal rotation. This makes it a widespread injury in sports such as soccer and basketball due to the frequent pivoting movements, which put a rotational loading on the ACL. Patients suffering from ACL tears have reported hearing a popping sound at the time of injury in addition to pain, instability, and swelling [16, 60].

The ACL primarily restricts anterior tibial translation relative to the femur [30, 60, 70]. In addition, it also restricts internal and external rotation when the knee is in extension. Therefore, injury to this ligament is expected to increase the range of AP translation and internal-external rotation.

3.2. Risk factors

Multiple risk factors exist, which can be categorized into four categories; environmental, anatomic, hormonal, and biomechanical [16, 38]. The first category, environmental, includes factors such as the gear used during sports, like the shoes worn, as higher friction between the shoes and the playing ground increases the risk of injury [79]. Anatomic factors include the geometry of the bones, their alignment, and the length of the ACL, which, in contrast to the environmental factors, are non-modifiable [60]. Studies have also shown that hormones affect the incidence of this injury, like the study by Slauterbeck et al. [82], who have shown an increase in ACL tears in the first days of the menstrual cycle. These two factors explain the higher incidence of ACL injury in women than men, which can be related to the different anatomical structures and the hormone balances [16]. Lastly, biomechanical factors that influence the risk of ACL tears are neuromuscular control strategies of a person and, with that, their movement patterns.

3.3. Diagnosis of an ACL tear

Physical examination is commonly the first evaluation technique used to diagnose ACL injury. Well-known manual tests are the anterior drawer, Lachman, and Pivot-shift test [67]. These three tests evaluate the kinematics of the knee joint for different types of movements, which are affected by an ACL tear mentioned in section 3.1. Even though these manual tests can give insight into the movement of the knee, a more objective test is preferred for a more precise evaluation of the ACL and surrounding structures [53]. Therefore MRI and radiography are commonly added to the diagnostic evaluation [49, 67]. MRI is used to detect the ligament injury due to its increased soft tissue contrast, while radiography is primarily used to determine if a patient also suffers from a fracture or dislocation [11, 86]. In addition to identifying ACL injuries, MRI can diagnose additional soft tissue injuries such as concomitant ligament injuries, but it is less sensitive for these types of injuries than it is for complete ACL tear [62, 77].

3.4. Treatment

The primary goal of rehabilitation after ACL injury is to restore the original knee kinematics and to prevent recurrent injuries [16]. The treatment of an ACL tear relies on a patient's lifestyle and can be conservative or surgical. Commonly, surgery is recommended for patients who want to return to sport, are very young, have an additional injury, or are substantially hindered in daily life [57, 68]. During surgery, the damaged ACL is replaced with either an auto or allograft. In the case of an autograft, the tissue will be harvested from the hamstring or patellar tendon as this tissue is similar to that of the ACL [58]. Independent of surgical or conservative treatment, the process can be divided into three phases; the acute, recovery, and functional phase [60]. In the acute phase, goals include reducing pain and swelling, preventing scarring, regaining some movements, and starting with some weight bearing. The recovery phase focuses on regaining the full range of motion or at least a sufficient range of motion for the patient's lifestyle. The final phase is focused on regaining strength and returning to sport. Physical therapy is essential to the whole rehabilitation process and crutches and bracing could also help stabilize the joint or lower the weight put onto it [16].

Rehabilitation of an ACL tear can take three to nine months [28]. However, one-third of the patients sustain another tear in the same or contralateral knee within two years after injury, especially during sport [69]. The incidence is highest in the first year and decreases with time. Therefore, a prolonged period of rehabilitation before returning to sport is preferred.

4

Methods

A workflow was developed to process the digital imaging and communication in medicine (DICOM) files obtained from the CT. Subsequently, the obtained kinematic measures were presented in three different ways to gain an understanding of the best way to interpret the data for this application and the differences between the calculated kinematic measures. An overview can be found in figure 4.1. An elaboration on each step can be found in different sections of this chapter.

To facilitate easy usage in a clinical setting, almost all workflow steps were automatized using Python [72]. In addition to the automation, all programs used were open source and freely available for download online. The primary reason for this was the accessibility, as program licenses can be expensive, especially if this would be the only application within an institution. These licenses are no longer required when using open-source programs . Use is also very transparent, as the source code is available online. However, maintenance and development are not guaranteed for these programs, and they are generally not approved for clinical use. Figure 4.2 shows an overview of the workflow on script level. The scripts themselves can be found at `https://gitlab.tudelft.nl/clinical-biomechanical-lab/4d-ct-knee-kinematics`.

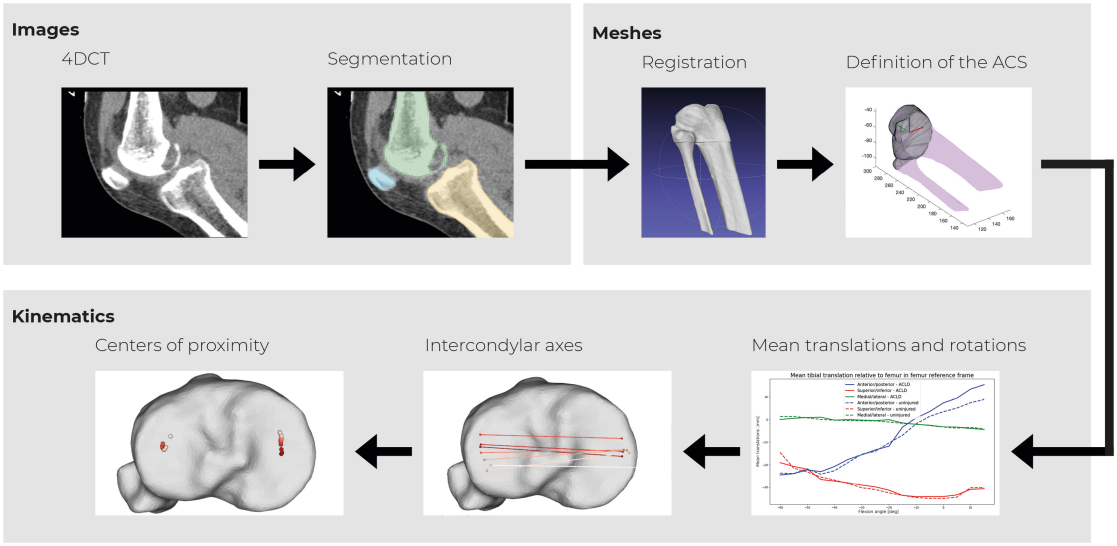

Figure 4.1: Workflow of the project.
The workflow starts with the obtained 4DCT images at the top right, to the segmentation and registration followed by the definition of the ACSs at the top left. Finally, the three ways the kinematic measures were presented can be seen in the bottom row. **Abbreviations:** four-dimensional computed tomography (4DCT), anatomical coordinate system (ACS).

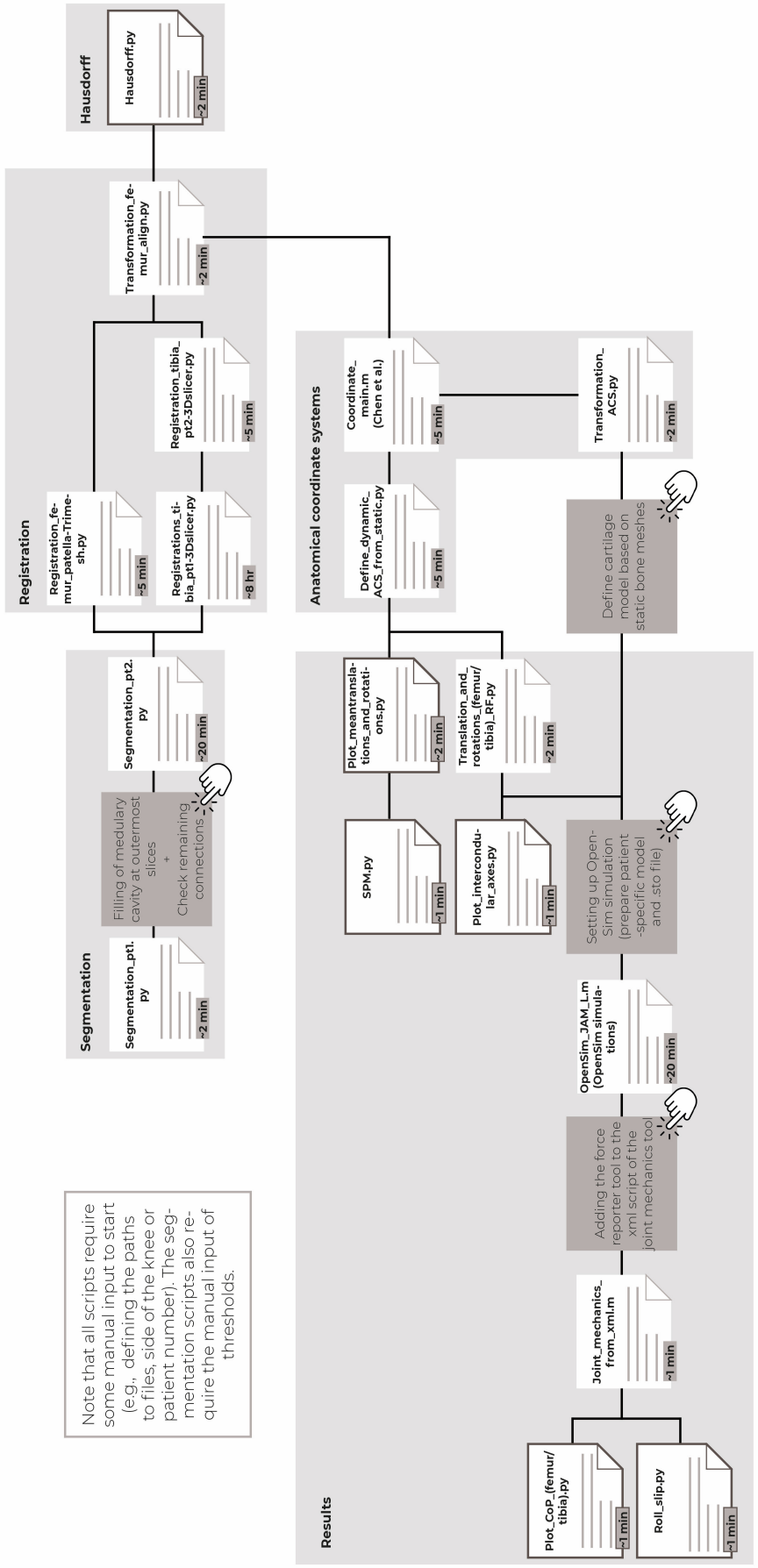

Figure 4.2: Workflow through the scripts developed for this application, the approximated run times and required manual steps.
Here, the white blocks represent the scripts, and the darker blocks with the hand represent the manual steps. The white blocks with dark outlines represent the scripts generating the final figures and tables. **Abbreviations:** Four dimensional computed tomography (4DCT), anatomical coordinate system (ACS).

4.1. Patients

All scanning was performed before this thesis by Dr. T. Piscaer and T. Hoedemakers at the Erasmus MC. A total of eight patients with a unilateral complete ACL tear that were scheduled for reconstruction at the Erasmus MC gave informed consent and were included in this thesis. The numbers of the scans were used to refer to the patients throughout the thesis. The seventh scan was made with a different orientation for another project and was therefore excluded prior to this thesis. Hence the included patients will be referred to as patients 001-006, 008, and 009. Two of the included patients were male, and six were female. The mean age of the patient group was 25.1 (range: 18-29). Among patients 001 to 004, three suffered from concomitant meniscal injuries, of whom two had an added anterolateral tenodesis. Another patient suffered from an additional partial tear to the medial collateral ligament. No data was available on the eventual concomitant injuries of patients 005, 006, 008 and 009.

4.2. Data acquisition

A TSX-301A-Aquilion ONE scanner from Canon Medical Systems [17] at the IJsselland Hospital was used for scanning. Both a static and a dynamic scan were made for each patient. The field of view for the static scan was more extensive than that of the dynamic scan to facilitate a more accurate definition of the anatomical coordinate system (ACS) at a later stage of the project. The settings differed between the two scans, but the matrix size was set to 512x512 voxels for both. The other settings can be found in table 4.1.

Table 4.1: Settings of the CT scanner for the static and dynamic scans.

Parameter	Static scan	Dynamic scan
Field of view mm)	320	160
Slice thickness (mm)	1.0	0.5
Increment (mm)	0.8	0.5
Pitch	0.813	
Peak potential (kV)	120	100
Radiation time (s)	0.50	0.35
Duration (s)	-	10
Radiation dose (mAs)	100	35
Effective dose (mSv)	0.0888	0.3944

Patients were asked to lie in the scanner pronely with their lower leg and knee hanging over the scanning bed. This prone position was chosen to aid patients in reaching full extension, which is known to be difficult for patients suffering from ACL injury [26]. First, a static scan of the ACLD and contralateral knee was made in full (hyper)extension, directly followed by a series of dynamic scans. For this, the patient was asked to flex both knees simultaneously to 70° within eight seconds. They were told that the focus was on the first part of the movement and that it was preferred they moved too slow than too fast. Before scanning, the movement was practised at least three times with an instructional video with a timer. The dynamic scans were made over 10 seconds while the patients performed the movement with the aid of the same instructional video. The CT data were then assembled in DICOM files for further use.

4.3. Segmentations

The soft tissue scans in the set of DICOM files acquired from static and dynamic CT scans were segmented to obtain a three-dimensional surface model. The soft tissue scans were used here instead of the bone scans, which were also available. This was because the contrast between the soft tissue and bones in these scans is higher than in the bone scans. The images had to be divided into multiple regions; the left and right femur, patella, and tibia and fibula. The tibia and fibula were kept together as the joint space between them was too small to split into two separate segments accurately with an automated program. Moreover, it was not expected to influence the workflow substantially as registration was performed between two meshes that both contained the fibula, and the ACS of the tibia is defined based on the tibial plateau only. 3D Slicer [1, 2] was used for the segmentations, as it allows

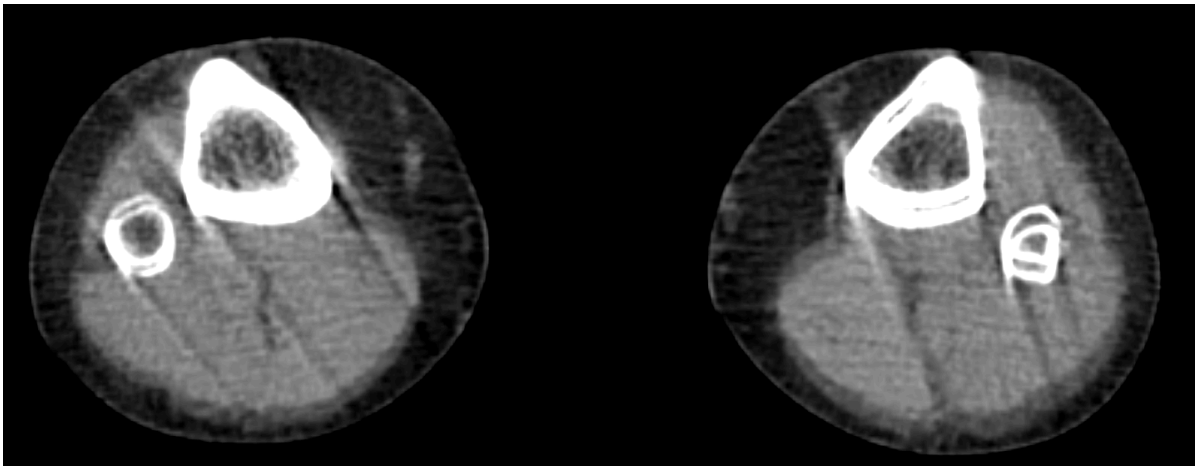

Figure 4.3: Example of movement artefacts in one of the 4DCT images

the user to work directly with the DICOM data. During the segmentation process, one step could not be performed automatically (discussed in the next paragraph). Therefore, the segmentation consists of two separate Python scripts with a manual step. Before segmenting the images, the distal part of the tibial shaft that contained the most movement artefacts was cut off. This was done because the images contained too many artefacts due to the movement, which would complicate the registration later. An example of the movement artefacts can be seen in figure 4.3. To exclude part of the shaft, a markup volume was defined around the area that should be included in the segmentation for each patient specifically. This volume included the full portion of the femur that was scanned, the patella and the tibial head.

The segmentation process consisted of multiple steps, which are briefly listed in table 4.2. The thresholds in this table may vary slightly depending on the patient. During the manual step, the medullary cavity had to be filled in the outermost slices of the scans to close the outer surface of the segments completely. This was required to enclose the bone cavities, which could then be deleted by inverting the segment. Excluding these bone cavities was required for the registration because they would have complicated the registration. This is due to the cancellous bone which is a complex structure that is inconsistently segmented from the scans, while it could now be performed based on the outer surfaces only which can be segmented more consistently. As seen in table 4.2, a closing tool is available. However, to close the medullary cavity, the kernel size had to be set to a very high value that would have also closed the gap between the femoral condyles.

As a manual step was already required, it could also be used to check the initial segmentation as, in some cases, minor connections remained between the femur and patella or femur and tibia, which would lead to improper splitting of the segments. During the splitting islands step, a minimum size was set for the segments, and all segments smaller than that were excluded. In all dynamic scans, this resulted in a list of six different segments representing each bone separately ordered according to their size. In the static scans, the field of view was more extensive, resulting in a larger portion of the scanning bed being included in the scans, which would not be excluded based on size. However, the size of this scanning bed was always larger than that of the patellae and smaller than the femur and tibia, which meant it could be appropriately named. This way, all six (or seven in the case of the static scans) segments could be individually saved to mesh (.stl) files for further processing.

4.4. Registration

The registration consisted of two steps. First, the longer static mesh was transformed onto the short, dynamic mesh to obtain more information at each point of the movement. This was followed by an additional registration step to compensate for the movement of the femur, as all patients moved slightly during scanning.

Table 4.2: Steps and parameters of the segmentation process.

Step	Parameter	Effect
Markup volume	Size: [200, 200, 60] Origin: [0, 0, 335]	Select the portion of the image to segment
Threshold	∼177-max	Separate the bone geometry from surrounding soft tissue structures.
Smoothing	3 mm, median	Smoothen surface and reducing some artefacts.
Save	-	Save files to .mrb files for manual step.
Manual step	-	Fill the medullary cavity at the outermost slices and check for potential remaining connections between the bones.
Islands	Split islands to segments, min segment size: 20.000 voxels	Split the overall segmentation into separate segments for each bone. A threshold was added to exclude small segments like artefacts and the fragments of the scanning bed. Segments were ordered according to size, where the first segment was the largest.
Smoothing	8 mm, closing	Close remaining gaps on the bone surface.
Invert	-	Invert each segment separately.
Islands	Keep largest island	Keep the largest segment, thereby deleting the bone cavities for each bone
Invert	-	Invert each segment again to obtain solid bone segments.
Naming segments	LR threshold: 0 SI threshold: ∼320	Label segments with the correct names based on the center of mass and order given during split islands.
Save	-	Save files to .mrb and .stl files for further use.

Abbreviations: Left-right (LR), superior-inferior (SI).

4.4.1. Static-dynamic registration

A registration step was performed to determine the transformation matrix defining the position of the dynamic scan relative to the static scan. As the static and dynamic positions of the femur and patella are relatively close together, they could be registered with an iterative closest point (ICP) algorithm directly. This algorithm requires a good initial estimate to prevent it from finding a local minimum [12]. It searches for the smallest distance between the vertex of a moving mesh to a target mesh and minimizes the mean square error between the two and keeps iterating until it converges [12]. The resulting transformation matrix then describes the position of the target mesh relative to the moving mesh. Applying the transformation will then transform the moving mesh to the position of the target mesh. This algorithm could be applied in Python directly through the Trimesh package. For this thesis, the dynamic mesh was registered onto the static one as that scan had a larger surface, making the registration easier to perform. This resulted in the transformation matrix describing the position of the static scan relative to the position of the dynamic one, which is the opposite of what was of interest here. Therefore the inverse of this matrix was applied to the static meshes as this gives the correct transformation.

The movement of the tibia was substantially more extensive than that of the femur and patella, which led to an increased amount of movement artefacts on this mesh and an increased distance between the meshes. The ICP algorithm could, therefore, not be applied directly to the tibia. Therefore, multiple options for this pre-registration step were evaluated (see appendix A), but finally, the Surface Fragments Registration available through the Surface Fragments Registration toolbox in 3D Slicer was used [4]. The registration tool consists of two steps. First, it performs a pre-registration based on a method by Horn [44]. Here, a least-squares problem is solved using quaternions. After the pre-registration, an ICP algorithm is applied to obtain the final registration. However, the ICP algorithm used in this tool allows for deformations over the surface of the mesh which is unwanted because of the use of patient-specific geometries. Therefore, we performed an additional rigid registration, registering the static mesh onto the already registered but slightly deformed static mesh. In this registration step, it

was possible to directly use the ICP algorithm through the Model Registration tool from the IGT package in 3DSlicer, as the meshes were almost identical, simplifying the registration. To check the accuracy of the registrations, the Hausdorff distances between all dynamic and static meshes were calculated using Mesh Lab 2022.02 [20] (see appendix B).

As mentioned, some registrations were performed using 3D Slicer, while others used the Trimesh package in Python. Because of this, the resulting transformation matrices are based on two different coordinate systems as, Python (and Matlab) [46], uses the LPS (left, posterior, superior as positive directions) convention and 3D Slicer uses RAS (right, anterior, superior as positive directions). This means the transformation matrices had to be mirrored along the frontal and coronal planes when using one from 3D Slicer in Python and vice versa. In addition, 3D Slicer exports transformation matrices as two vectors that must be rewritten into matrices before use (see explanation on `https://discourse.slicer.org/t/saving-linear-transformation-matrix/1192`).

4.4.2. Eliminating femoral movement

During the flexion-extension movement, the upper legs of the patients moved by a few centimetres (maximum Hausdorff distance between two meshes: 29.15mm). For further analysis, we wanted to compensate this movement to only describe the movement of the tibia with respect to the femur. The transformation matrices resulting from the registration between the dynamic and static meshes of the femur defined the movement. Therefore, the inverse of this transformation matrix could be applied to all bone meshes in 3D Slicer to compensate for the movement.

4.5. Definition of the anatomical coordinate systems

For analysis, the ACSs of the bones were required. For these ACSs, the x-axis is in the AP direction, the y-axis is in the SI direction, and the z-axis is pointed to the right along the ML axis. To obtain the

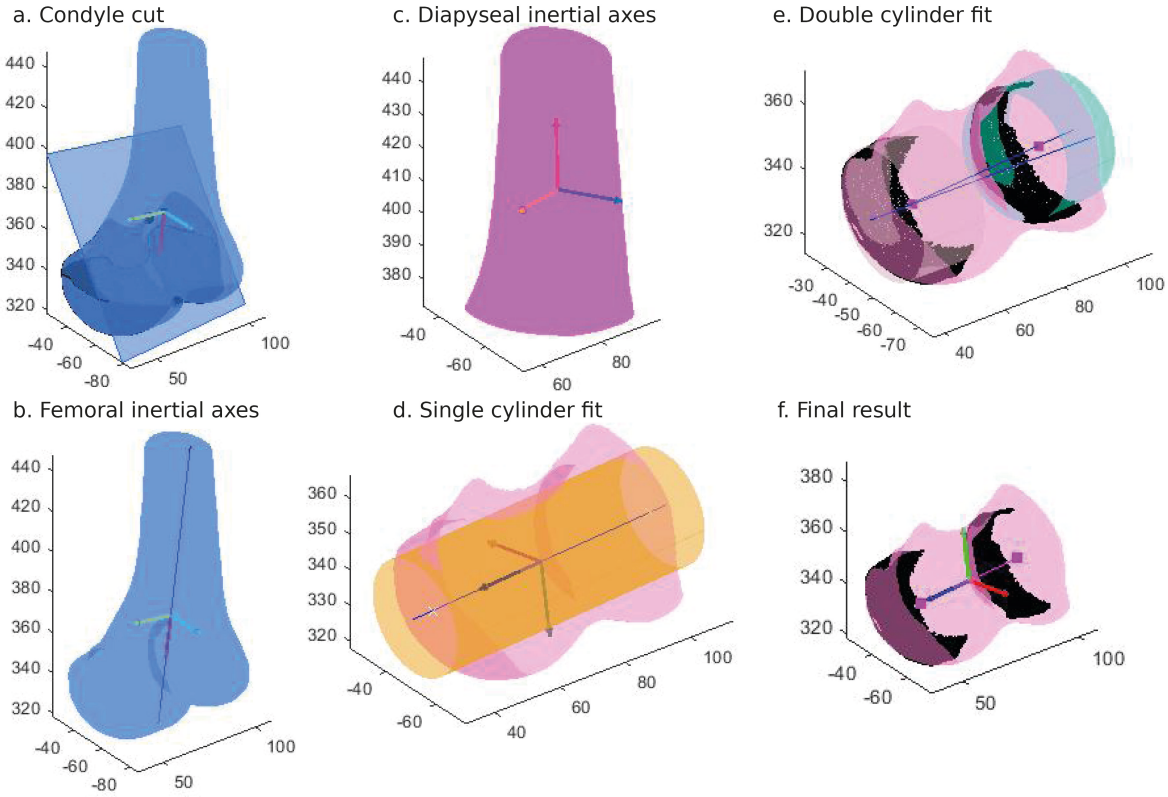

Figure 4.4: Workflow to determine the femoral ACS as defined by Chen et al. [19].
a. Definition of the plane to cut off the condyles. b. Definition of the femoral inertial axes. c. Definition of the diaphyseal inertial axes. d. Fitting of the cylinder onto the condyles. e. Fitting of the two cylinders on the separate condyles. f. The final definition of the femur ACS.

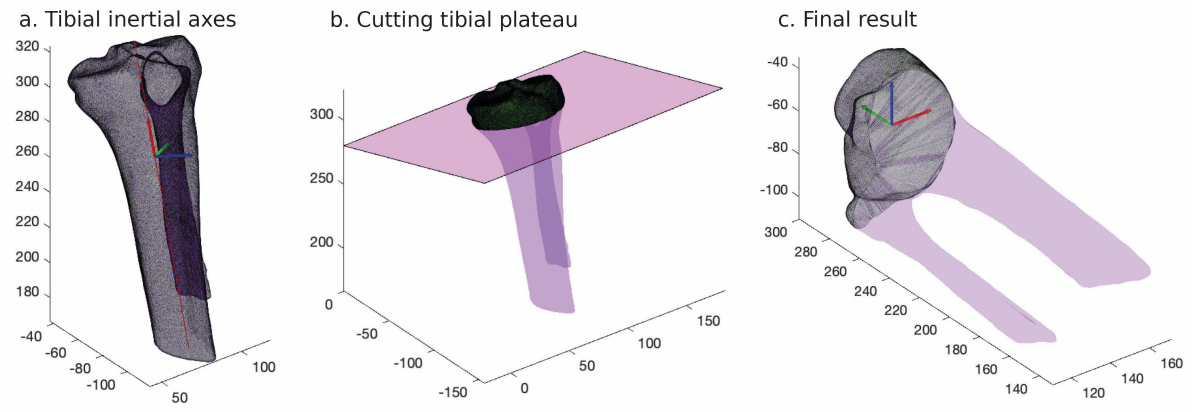

Figure 4.5: Workflow to determine the tibial ACS as defined by Chen et al. [19].
a. Definition of the tibial inertial axes. b. The plane used to separate the tibial plateau. c. The final definition of the tibial ACS.

ACSs of the static meshes, we used an algorithm by Chen et al. [19], which aims to approximate the ML axis as the flexion-extension axis and is available as a Matlab file online [41][1]. This algorithm uses a similar technique to that of Miranda et al. [61], where the femur condyles are first separated using a plane with a normal defined by the cross product of the line between two points and the femoral inertial axis pointing in the ML direction (see fig 4.4.a). The two points were defined using the diaphyseal and femur inertial axes (see figure 4.4.b and 4.4.c). The first point is the distal intersection of the 3rd inertial axis of the diaphysis. The second point is defined at the height of a plane at half the maximum cross-sectional area of the femur along the 3rd diaphyseal inertial axis. The location is then defined as the posterior intersection point of the femoral inertial axis approximating the AP direction. Subsequently, a cylinder is fitted through the condyles (see figure 4.4.d). The direction of this cylinder crossed with the vector through the two points is then used for a second iteration of the plane to cut off the condyles onto which a cylinder is fitted again. In contrast to Miranda et al. [61], this algorithm uses two cylinders fitted to each condyle instead of one, to allow for asymmetry. The two condyles were therefore separated by rotating the previously defined plane perpendicular to the defined cylinder. The separate cylinders were then fitted through the articulating surfaces of the two condyles (see figure 4.4.e). The articulating surfaces of the condyles were defined based on a set of geometrical criteria, and the cylinders fitted through both condyles. The ML axis is defined by projecting the surface centres of the articular surfaces onto the cylinder axis and connecting the two points (see figure 4.4.f). The origin was then defined as the middle point on this line. The AP axis was defined to be perpendicular to the ML axis and the 3rd inertial axis of the femur. Finally, the SI axis was defined by the cross-product of the ML and AP axis.

For the tibia, the techniques of Chen et al. [19] and Miranda et al. [19] are identical (see figure 4.5). The axes of inertia are defined first (see figure 4.5.a). The cross-sectional area is then calculated along the 3rd inertial axis. Subsequently, the tibial plateau is cut off at the largest cross-sectional area calculated (see figure 4.5.b). The inertial axes are then defined for the plateau only to obtain the three axes of the ACS. The origin was then determined as the centre of mass of the plateau (see figure 4.5.c). As the fibula was still attached to the tibia, it may be possible that part of the fibula head was included in the cut off of the tibial plateau and therefore also in the definition of the inertial axes thereof. However, as it is substantially smaller than the tibial plateau, the effect was assumed to be small.

For the patella, the inertial axes were defined first (see figure 4.6.a), based on which the anterior surface of the patella was determined [41, 42]. The AP axis was then defined as the axis perpendicular to this plane (see figure 4.6.b). The SI axis was defined as the axis connecting the centroid to the most inferior point for which the closest vertex perpendicular to AP is used (see figure 4.6.c). Lastly, the axis perpendicular to these two is the ML axis.

The ACSs of the dynamic meshes of a patient were then determined based on the ACS of the static scan of the same patient and the rotation matrices obtained during the two registration steps (static-dynamic and elimination of the femoral movement). As the movement of the femur was eliminated, the ACSs of the dynamic meshes were identical to that of the static mesh. Therefore, the two rotation

[1]A second algorithm to define the ACS by Renault et al. [75] was found online [74]. However, this algorithm used one single cylinder like Miranda et al. [61], which led to the choice for the algorithm from Chen et al. [19]

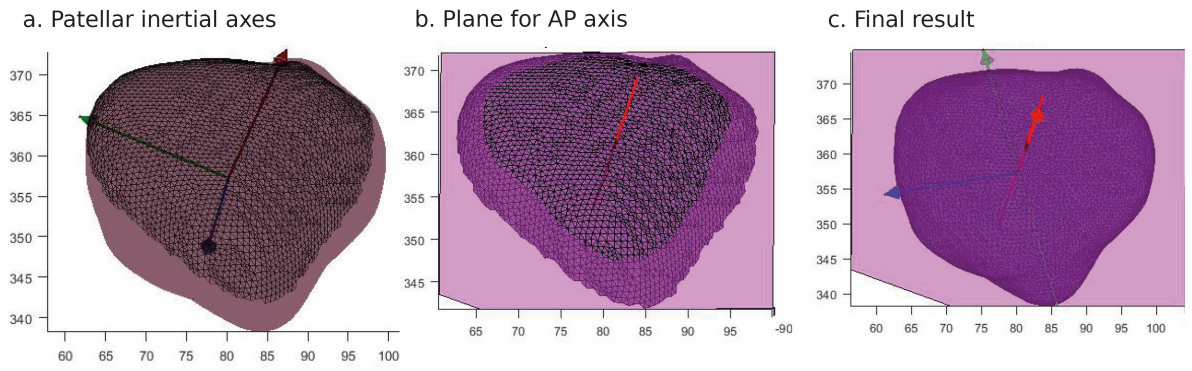

Figure 4.6: Workflow to determine the patellar ACS as defined by Chen et al. [19].
a. Definition of the patellar inertial axes. b. The plane used to define the AP axis. c. The final definition of the patellar ACS.

matrices were only applied to the static ACSs of the patella and tibia to obtain the locations of the dynamic ACSs of these.

4.6. Mean translations and rotations

Based on the ACSs, the translations and rotations of the tibia and patella relative to the femur were calculated. The same approach was used for both, but only the tibia will be mentioned in the descriptions below for clarity.

First, the transformation matrix between the ACS of the femur and that of the tibia (R_{tf}) had to be defined, which was done using equation 4.1 [3]. Using the resulting transformation matrix, the translations and rotations could be calculated between the femur and tibia, expressed in the femur ACS. The Rotation module from Scipy in Python was used to obtain the Euler angles based on the rotation order defined by Grood et al. [39] and the calculated rotation matrix. The transformations were already given by the fourth column of the transformation matrix defined with equation 4.1.

$$T_{tf} = (ACS_{femur})^{-1} * ACS_{tibia} \tag{4.1}$$

The translations and rotations of the ACSs were plotted separately against each patient's flexion angles and the image number. Outliers were defined based on the calculated translations and rotations and were mainly visible for the rotations (see appendix C.4). Data points were excluded when a peak of >5° was visible for at least one rotational direction, and a sudden peak was also visible for the other two rotations in the same image. Subsequently, a plot of the mean values against the flexion angle was plotted between -60° and 15°. These mean values were evaluated using a non-parametric, paired t-test and a two-tailed statistical parametric map (SPM) using the SPM1d tool available for Python [71]. Here, α was set to 0.05.

4.7. Intercondylar axes

The graphs of the translations and rotations give insight into each DoF separately. However, all occur simultaneously. To gain insight into the overall movement of the femur compared to the tibia, we plotted the intercondylar axis of the femur (ML axis) in the transverse plane of the tibia for different flexion angles. Based on the angles found previously, a range of 10° to -50° with 10° increments was chosen. To plot the intercondylar axes, an arbitrary point on the ML axis of the femur was chosen and mirrored along the sagittal plane to obtain a second point. These two points were then transformed to the tibia ACS to plot them with a line fitted through both. An interpolation step was required to obtain the values for each specific flexion angle. To do so, a cubic spline interpolation technique was used as it allows for a smooth curve fitted through the given dataset which is also expected during the flexion/extension movement [47, 88, 10, 91].

4.8. Centers of proximity

The plots of the intercondylar axes provide insight into the simultaneously occurring translations and rotations of the joint. However, these kinematics are only visualized at the femur level, not at the articulation surface. Therefore, we also plotted the centres of proximity on the tibia and femur using a musculoskeletal simulation in OpenSim. This way, a visualization of the kinematics at the articulation surface could also be provided.

4.8.1. Model

OpenSim was used to make a patient-specific knee model [80, 23]. This open-source program allows users to develop musculoskeletal models and evaluate that for different situations. More specifically, the program's Joint and Articular Mechanics (JAM) plugin was used. This plugin allows for more detailed joint mechanics, extending the OpenSim capabilities to represent joints with 6DoF. The model by Lenhart et al. [54] was used as a base for our model. This is a full-body model where the bone, ligaments, and cartilage of the knee are obtained from the MRI scan of a healthy adult female. In this model, the ligaments are modelled as a bundle of non-linear springs, which are sometimes wrapped around a structure to obtain the appropriate positions around the bone structures. The 12DoF knee model is incorporated into a model by Arnold et al. [6] with a 6DoF pelvis, 3DoF hip, and 1DoF ankle. The Lenhart2015 model was initially made for the evaluation of the right knee. Therefore, Dr. M. Wesseling had previously mirrored the model for the left knee, so both were used as a base for their respective sides.

4.8.2. Preparation for the simulation

Patient-specific meshes of the bones (distal femur, proximal tibia, and patella) and cartilage were required to accustom the Lenhart2015 model to our patients. These bone geometries were already obtained from the 4DCT scans (see section 4.3). However, two adaptations had to be made before they could be included in the Lenhart2015 model. First, the coordinate system of the mesh files had to be transformed as that was still that of the CT scanner. To do so, the matrices of the ACSs could be used as these are essentially the transformation matrices from the coordinate system of the CT scanner to the anatomical one. Moreover, the meshes were still very fine, resulting in long computational times and errors as the maximum number of nodes the model can handle was reached. Therefore, the meshes had to be simplified, which was done in Mesh Lab 2022.02 [20]. In this program, the Quadric edge collapse decimation tool was used to simplify the mesh. The targets for the number of faces were set to 15.000 for both the femur and tibia and 3.000 for the patella, as these reduced the size of the meshes significantly without sacrificing the geometry (mean edge length: about 1.5 mm).

Unfortunately, the geometry of the cartilage could not be extracted from the 4DCT scans. Therefore, the cartilage models had to be made based on the bone geometry of the patients. The cartilage was modelled with a constant thickness of 3mm. This thickness was chosen based on the thicker portions of the cartilage found in literature [9, 21, 55], and the existing Lenhart2015 model, which also used 3mm. To define the shape of the cartilage, the bone meshes were opened in 3D Slicer. Subsequently, a selection was made manually to define the cartilage shape based on the curvatures of the bone. The mesh was then enlarged by 3mm using the dynamic modeler module of 3D Slicer, and the contour of the cartilage was projected onto this mesh. To obtain the cartilage's surface model, the contour's outside was erased using the same module, and the inside was saved to a .stl file for further use in the OpenSim model. The cartilage of the tibia consists of a medial and a lateral part which were modelled separately to be able to calculate the centres of proximity for each side separately.

Lastly, the translations and rotations of the joint had to be provided in the femur coordinate system to define the movement for the model. These were already defined earlier (see section 4.6) and could be applied directly as the model contained the patient-specific geometries and coordinate systems. Still, some minor adaptations had to be made, as OpenSim defines translations in meters instead of millimetres, and flexion is defined as positive rotation instead of extension. In addition, a pelvis angle of -90° was given as input to simulate the prone position the patients were in during scanning. All values were stored in a .sto file coupled to the time intervals of the scans (0.5 sec) and an additional 1.5 seconds for the initialization.

4.8.3. Simulation

Both base models for the left and right knee were adapted to include the patient-specific information by importing the meshes based on their 4DCT scans and scaling them to fit the definitions of OpenSim (e.g., millimetres to meters). No changes were made to the positions and properties of the ligaments, muscles, or wrapping surfaces. This was done because it would not affect the simulation as translations and rotations in all directions were imposed onto the model, making the tibiofemoral movement fully constrained based on the scans. Moreover, there was no patient-specific information on these.

For the JAM simulation, the Passive Flexion example was used as a base and adapted for our application, as the simulated movement was the same only not passive. The example was provided as a Matlab script. Therefore, this step was performed in Matlab, but the program also has a Python interaction, so it would be possible to use Python instead if necessary. The example used two tools from the JAM plugin. First, the Forsim tool, which performs a forward simulation using an implicit integrator, was used to define all states of the whole model. A forward simulation tool is also standardly available in Opensim. However, that tool uses an explicit integrator [83]. The implicit integrator is preferred because it performs better for simulations involving contact, like our simulation. Hence this tool was chosen [83]. It allows for three types of inputs; the effects of muscles and actuators, the external loads, and the prescribed coordinates. Of these three, only the latter was used as no external loads were applied, and no data was available on the muscle activations. In addition, all DoFs were defined based on the 4DCT, and the effects of muscles, like the ligaments, would not affect our simulation. The results from the Forsim tool were then used as input for the Joint Mechanics tool. This tool performs a simulation, which can, among other data, calculate the centres of proximity and locations of the articular surface and bone meshes [84]. Results are written to .vtp files, allowing the visualization of this data for each timestep.

Most settings used here were kept as they were initially set in the example. Only the reported time steps were reduced as the simulation was substantially longer than the example's, which would have resulted in unnecessarily large files and long computational times. The 6DoF of the patella were left undefined in most simulations as the tibiofemoral contact was the one of interest to us. However, in some instances, this resulted in long computational times or errors, which could be resolved by defining the patellar translations and rotations. A force reporter tool [40] was manually added to the Joint Mechanics tool setup file, as the direct implementation did not work correctly in the Matlab script. This tool was added as it writes a file containing the locations of the centres of proximity that were calculated during the simulation. As this tool had to be manually added, and the Matlab script would overwrite the setup file, another script was written to run this tool separately after the initial simulation.

To visualize the results, a similar type of plot to that of the intercondylar axes was chosen. Only here the locations of the centres of proximity on the tibia and femur were plotted instead of the axes. The same range was used in both plots (e.g., 10° to -50°). However, in these plots, the increments were changed to 5° to better show the movement's flow. Again, a cubic spline interpolation was used to obtain the same flexion angles for all patients. Subsequently, the distances between two consecutive centres of proximity were calculated for those of the tibia and the femur (see equation 4.2). These two distances were then compared by dividing the distance on the femur by that on the tibia to evaluate if either slip or roll occurred between the two (see equation 4.3).

$$\Delta d_{femur/tibia} = \sqrt{(CoP_{x2} - CoP_{x1})^2 + (CoP_{y2} - CoP_{y1})^2 + (CoP_{z2} - CoP_{z1})^2} \tag{4.2}$$

$$d_{inter\ articular} = \frac{\Delta d_{femur}}{\Delta d_{tibia}} \tag{4.3}$$

The primary occurrence was said to be roll when the interarticular motion was between 0.5 and 1.5 (see equation 4.4), as the movement on both surfaces is equal in this situation (see figure 4.7). However, pure roll or slip will never occur, hence the more extensive range. All values between 1.5 and 5 were considered a combination of roll and slip, and any value above 5 was considered to be pure slip.

$$d_{inter\ articular} = \begin{cases} \text{roll} & \text{if } 0.5 < d_{inter\ articular} < 1.5 \\ \text{roll \& slip} & \text{if } 1.5 < d_{inter\ articular} < 5 \\ \text{slip} & \text{if } 5 < d_{inter\ articular} \end{cases} \tag{4.4}$$

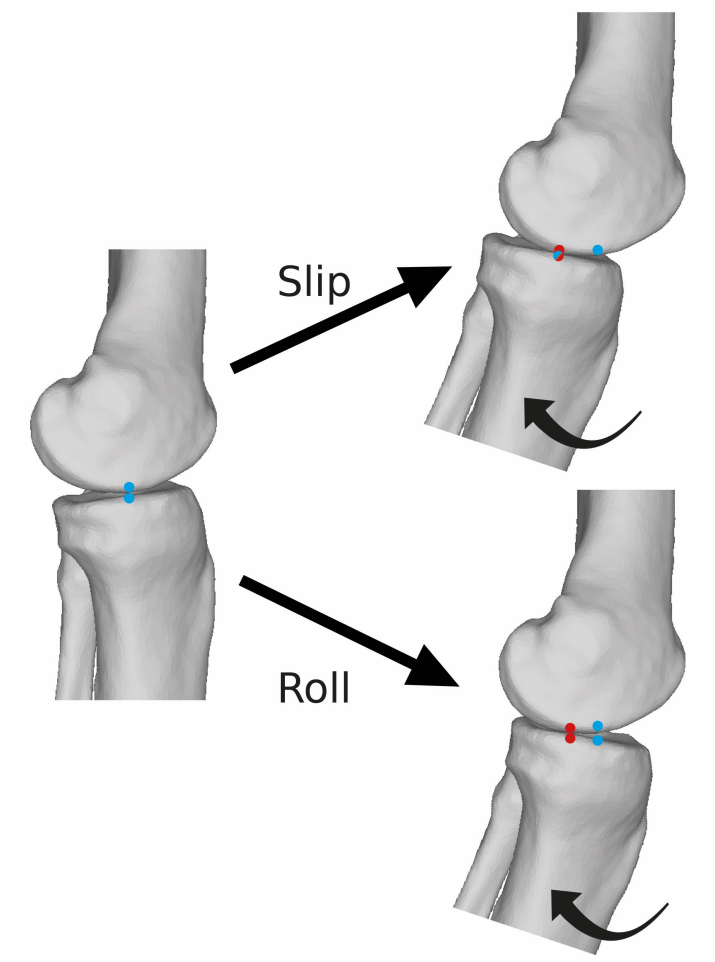

Figure 4.7: Difference between slip and roll.
The blue points represent the initial position, and red is the rotated position. Note that in slip, the contact point on the tibia remains the same, while in roll, the contact point changes.

5 Results

Different techniques were used to visualize the kinematic measures. First, a series of graphs were plotted to visualize all translations and rotations against the flexion angles (see Appendix C). In these graphs, one patient presented with a substantial amount of outliers due to fast movement during scanning (see figures C.3a and C.3b in Appendix C). Because of this, the outliers could not be separated from the actual movement, and this patient (002) was excluded from subsequent analysis.

Based on the translations and rotations calculated for the remaining patients, plots of the mean values over the patient group were made, which are presented in section 5.1. These graphs do give insight into the separate translations and rotations. However, in the actual movement, all occur simultaneously, which is represented in the plots of the intercondylar axes in section 5.2. Finally, the centres of proximity between the femur and the tibia were plotted onto the bone surfaces which can be found in section 5.3.

5.1. Mean translations and rotations

Figures 5.1a to 5.1f show the mean translations of the origin of the tibial ACS compared to that of the femur for the included patients. Note that not all patients reached the same angles (see secondary x-axes in the figures) and that these graphs are flipped compared to the actual movement. This is due to the definitions of the rotations where extension is positive and, therefore, on the right end of the x-axis in the plots. The SPMs were also plotted, but only for the angles that all patients reached (e.g., -35° to 0°). A statistical difference (p=0.023) can be seen in the AP direction from extension towards the lower flexion angles ($\pm$ 15° to $\pm$ -2.5°). Here, the ACLD knees present with an increased anterior tibial translation compared to the uninjured knees. At the higher flexion angles (-2.5° and below), there is no longer a difference between the ACLD and uninjured knees as is the case for the SI and ML directions.

Figures 5.1g to 5.1j show the mean rotations. But no statistical difference between the ACLD and uninjured knees is visible for either of the rotations.

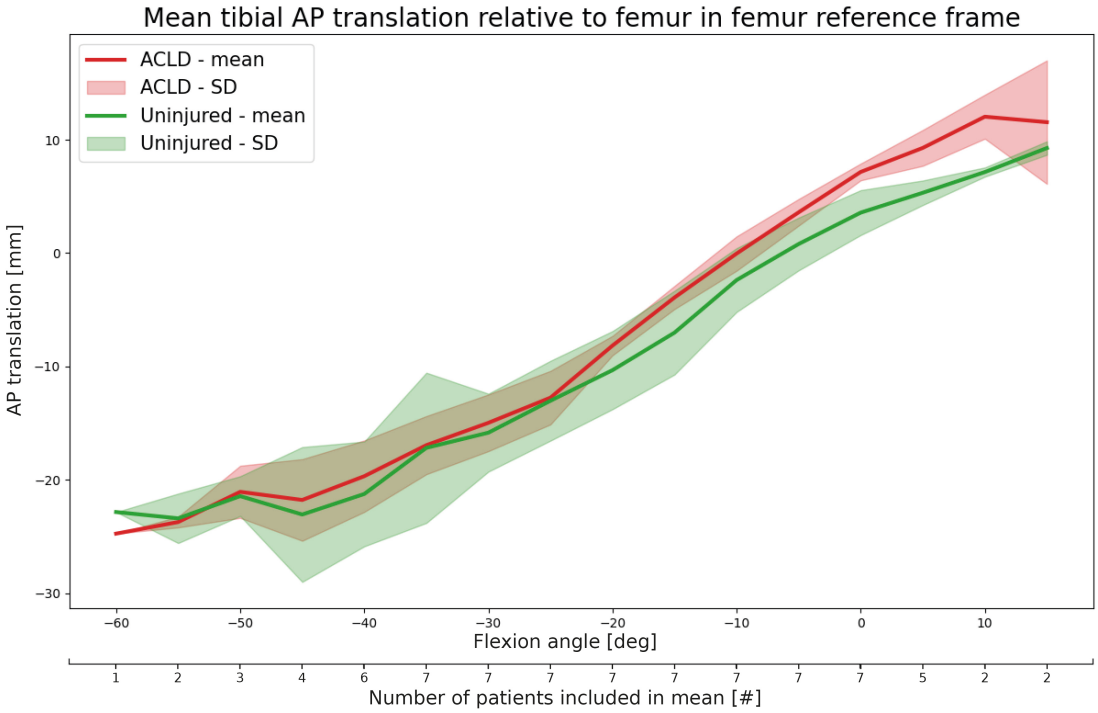

(a) Mean AP translation, anterior positive.

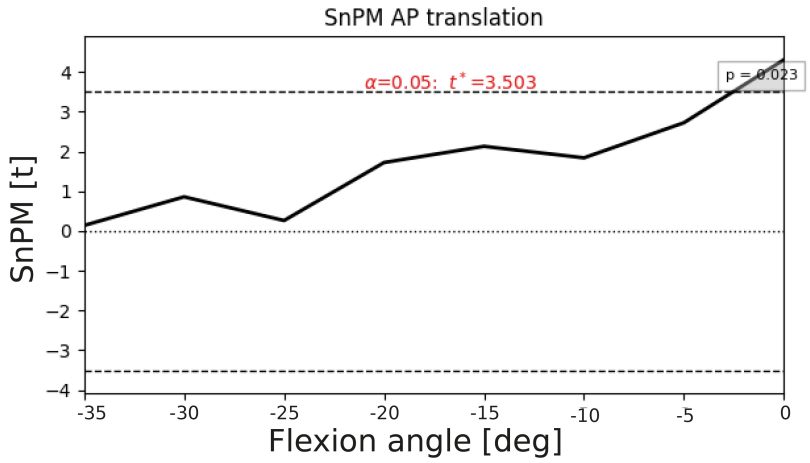

(b) SPM AP translation.

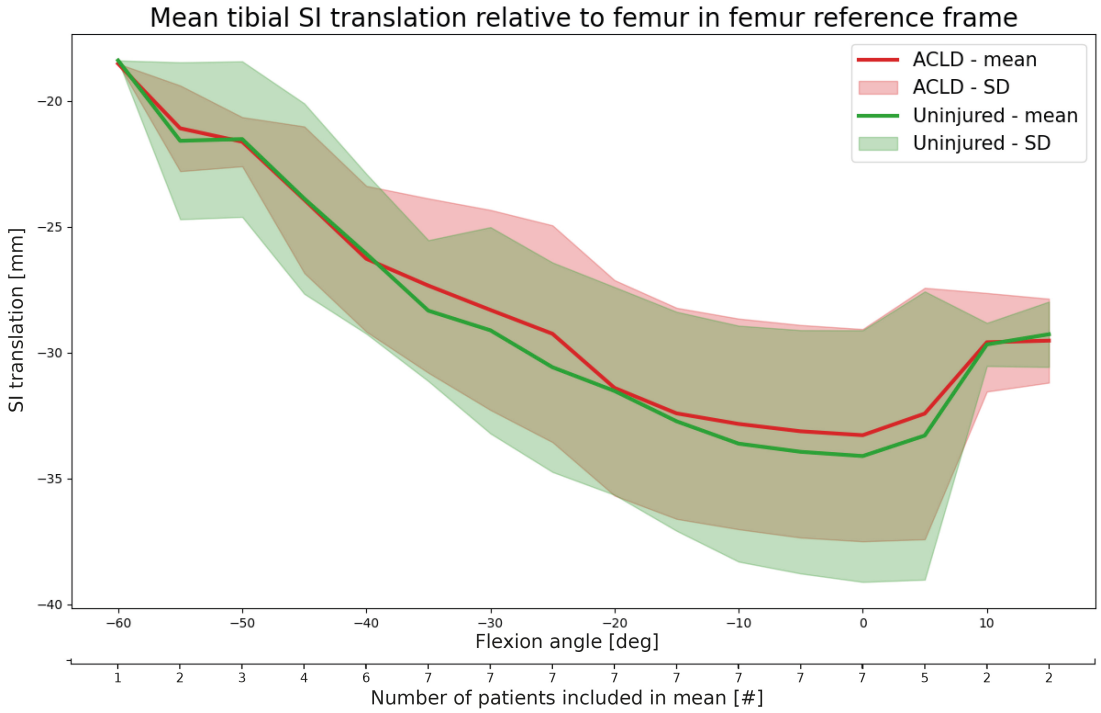

(c) Mean SI translation, superior positive.

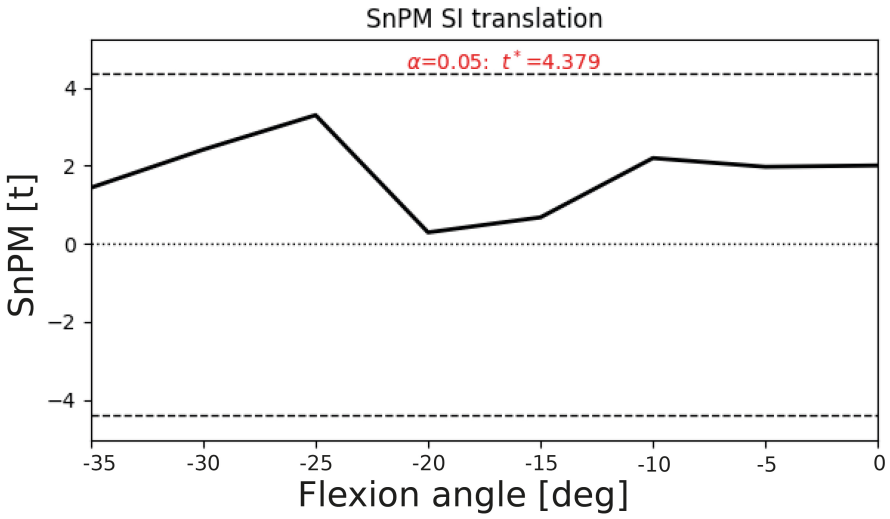

(d) SPM SI translation.

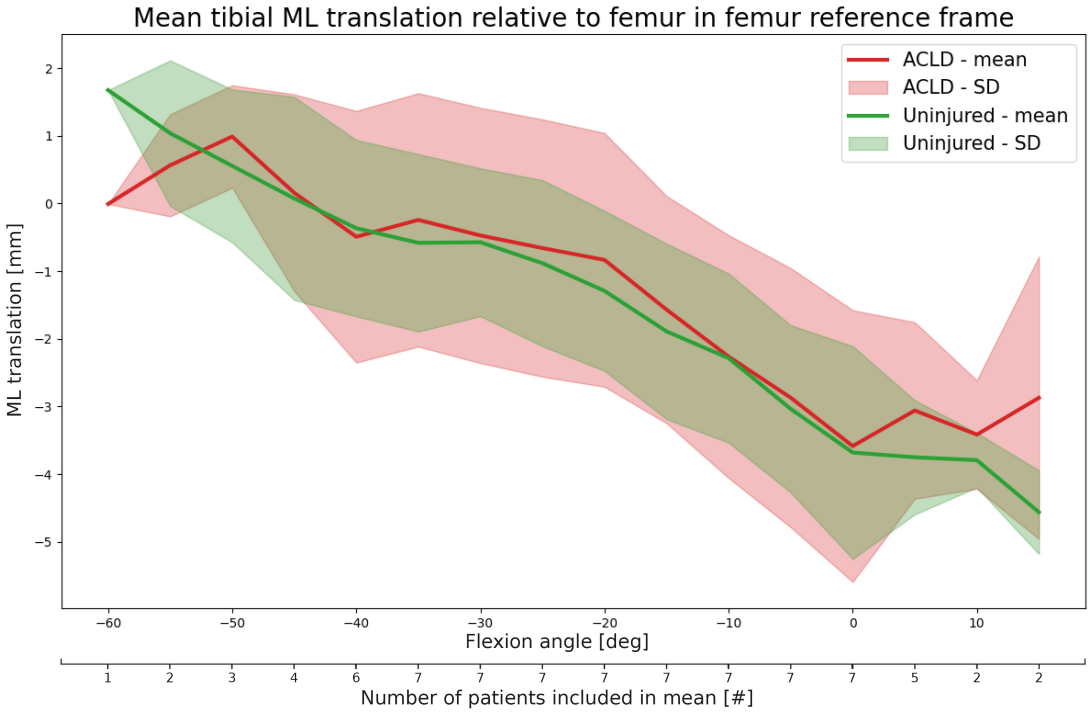

(e) Mean ML translation, medial positive.

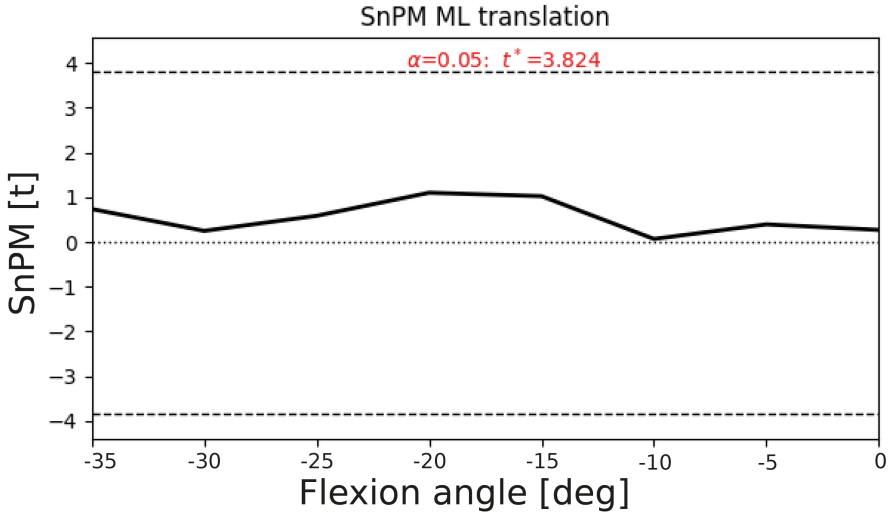

(f) SPM ML translation.

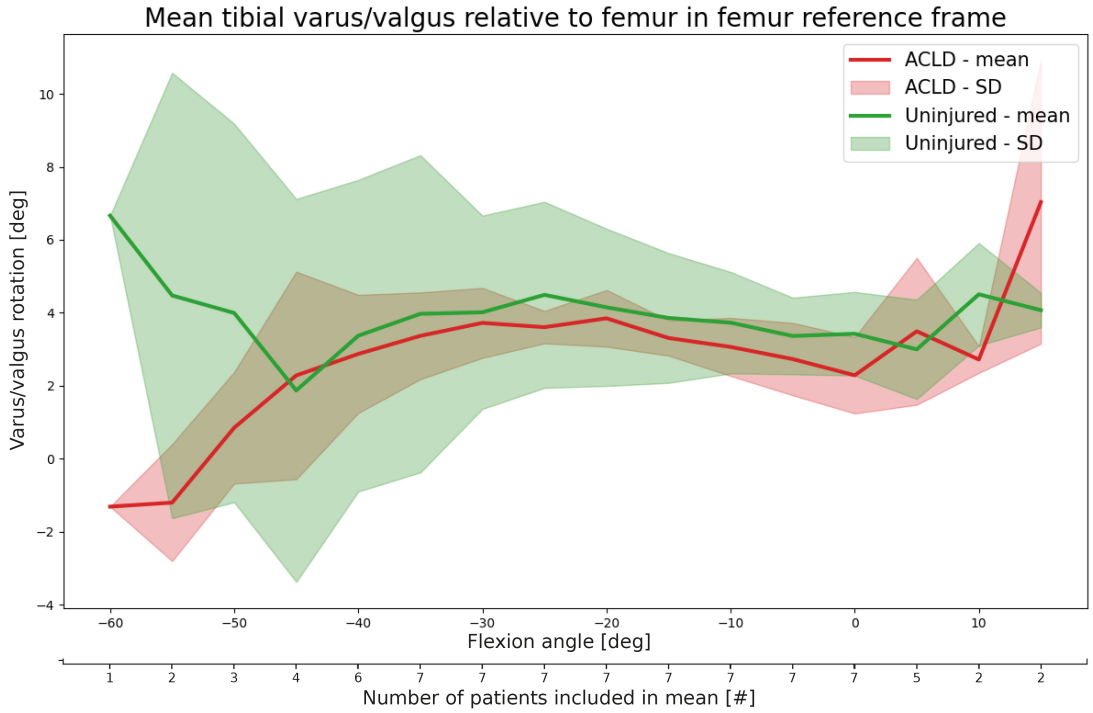

(g) Mean varus/valgus rotation, varus positive.

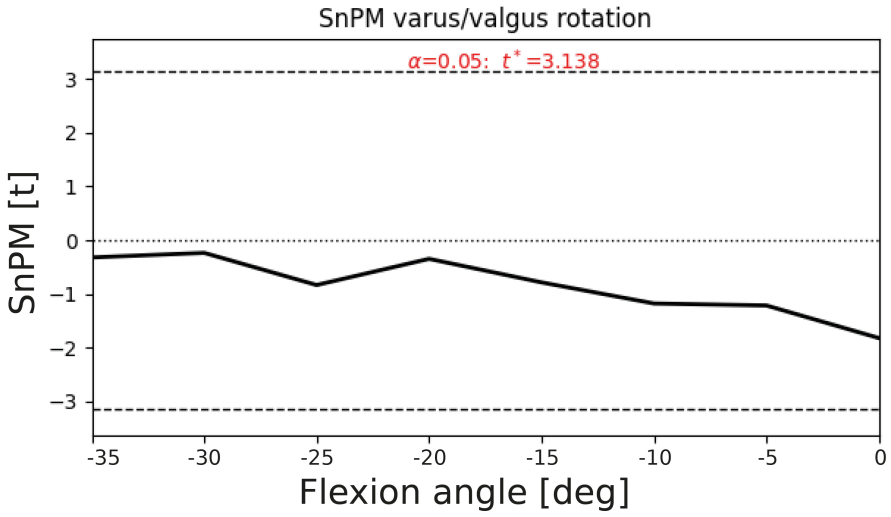

(h) SPM varus/valgus rotation.

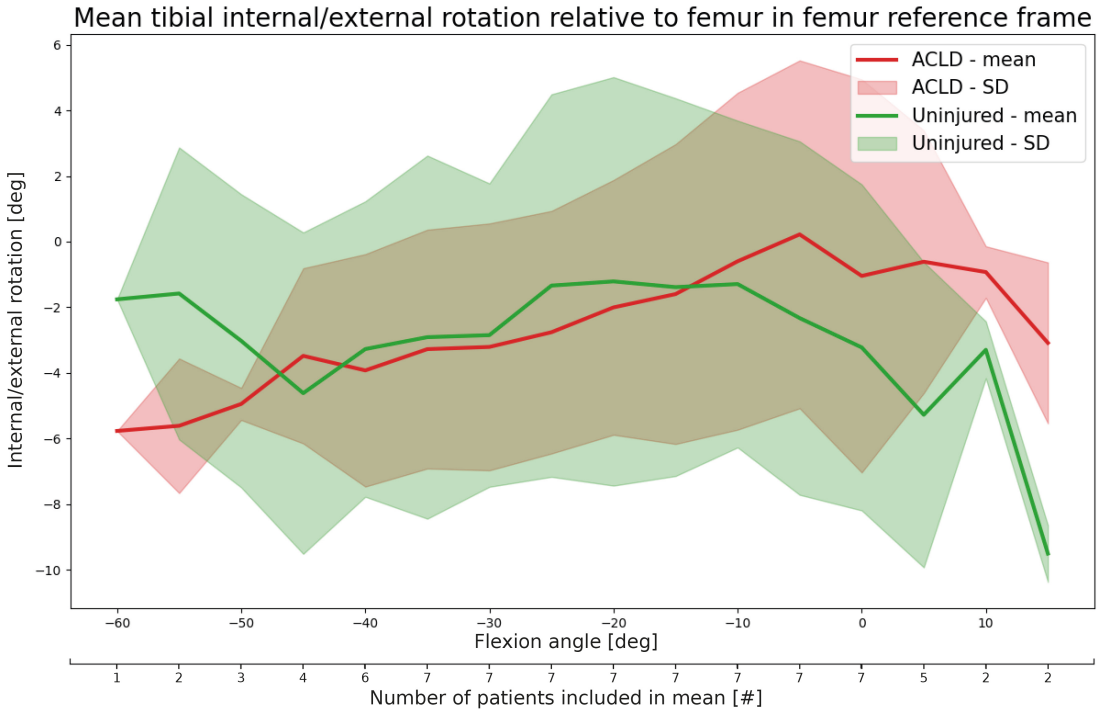

(i) Mean internal/external rotation, internal positive.

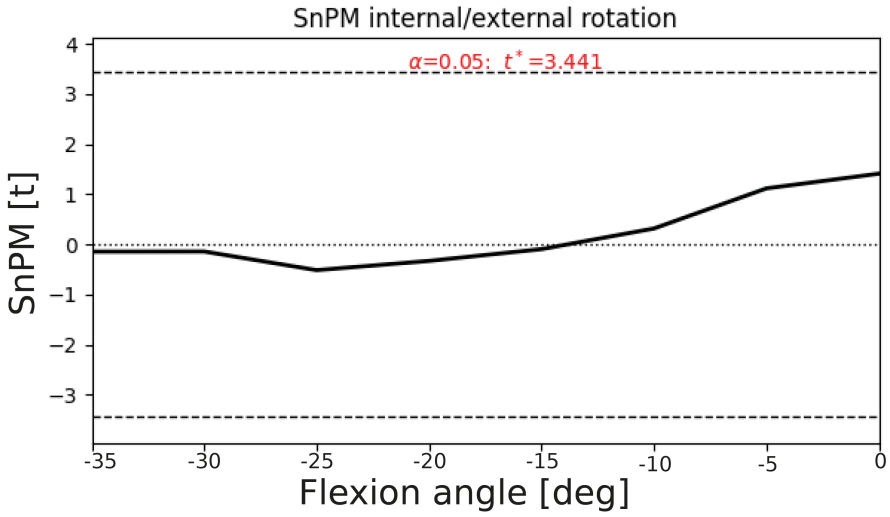

(j) SPM internal/external rotation.

Figure 5.1: Mean translations and rotations and the respective SPMs.
Note that the outermost portions of the mean and standard deviations (SD) are based on fewer data, the graphs of the SPMs, therefore, only contain the flexion angles that all patients reached (e.g., -35° to 0°. The number of patients included in the mean and SD can be found on the second x-axis of the figure. Moreover, these graphs are flipped compared to the actual movement due to the definitions used (e.g., extension is positive and flexion negative), causing the flexion angles to be plotted at the left. **Abbreviations:** Anterior-posterior (AP), anterior cruciate ligament deficient (ACLD), standard deviation (SD), degrees (deg), number (#), statistical non-parametric map (SnPM), level of significance (α), critical t-value (t^*), superior-inferior (SI), mediolateral (ML).

5.2. Intercondylar axes

The plots of the intercondylar axes for each patient can be seen in figures 5.2a to 5.2g. The left and right knees were plotted in the same figure to ease comparison. Angles between 10° and -50° with increments of 10° where plotted when possible. However, not all patients reached the same range. Therefore, some lack data for these angles in the figures.

Apparent differences can be seen between the ACLD and uninjured knees. Overall, the increased AP translation is most clearly visible as the intercondylar axes of the ACLD knees move over a larger range than in the uninjured knees on both the medial and lateral sides, which is especially visible in patients 001 and 003 (figures 5.2a and 5.2b). The intercondylar axis is first located at the posterior surface of the tibia in both the ACLD and uninjured knees. From there, it moves anteriorly in the ACLD knees to its most anterior location at about 30° flexion, from here it starts moving posteriorly again, as can be seen by the darkest lines, which are situated around the centre in the ACLD knees. However, a similar movement can also be seen in the uninjured knees but with a smaller range.

The effect on the internal/external rotation is also visible but may be less apparent and varies more among the patients. Rotations are most prominent in the first parts of the movement (e.g., moving from extension to the first degrees of flexion) in the ACLD knees. In these knees, some rotation can be seen at the beginning of the movement, after which the rotation reduces, and the intercondylar axes can be seen to be oriented more parallel to each other. More prominent rotations can be seen in the uninjured knees. Here, the rotation seems to continue throughout the flexion/extension movement, as seen in patient 003, where the intercondylar axis still rotated considerably between 30° and 50° flexion. Moreover, the phenomenon of the medial pivot is visible in the uninjured knees. In this phenomenon, the lateral femoral condyle presents with more of a sliding movement toward the anterior side of the tibia plateau. In contrast, the medial condyle presents with more of a pivoting movement [78]. This medial pivot is less visible on the ACLD side where the movement seems more consistent between the two sides.

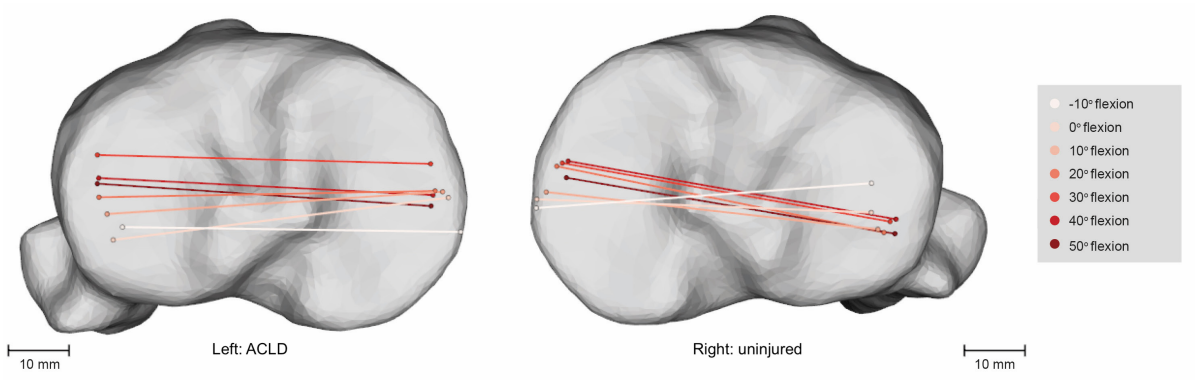

(a) Patient001.

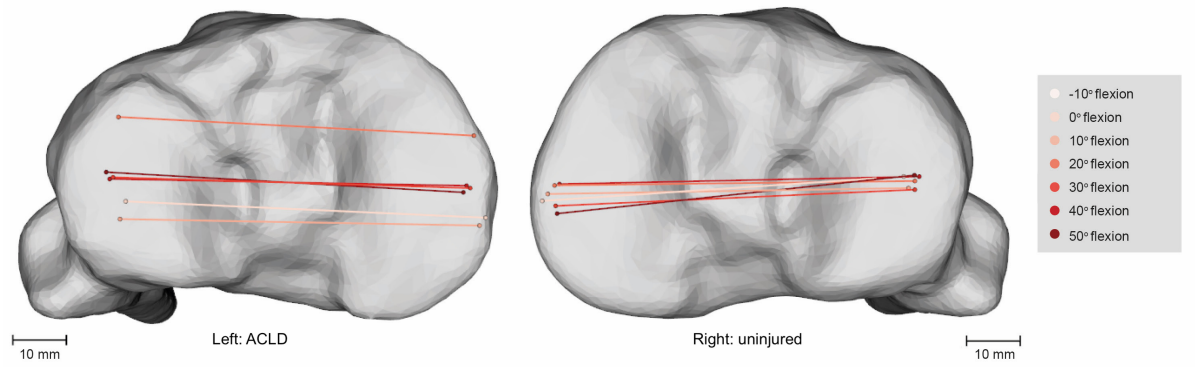

(b) Patient003.

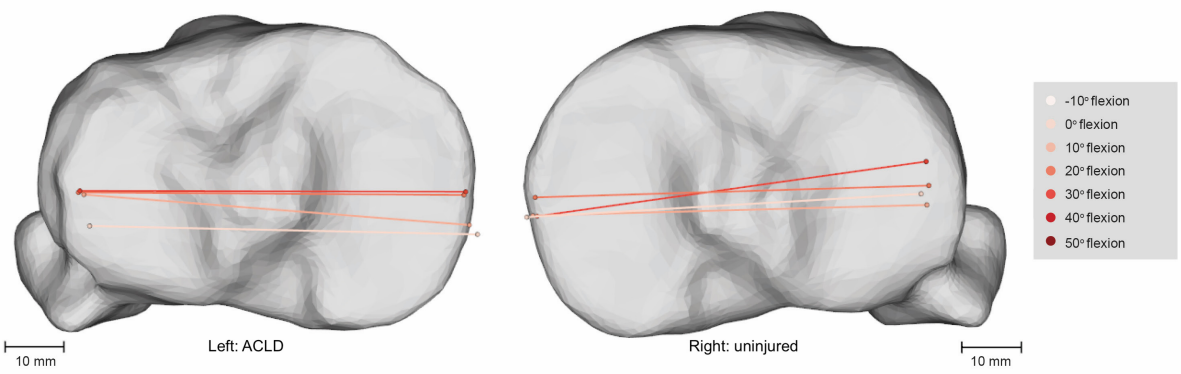

(c) Patient004.

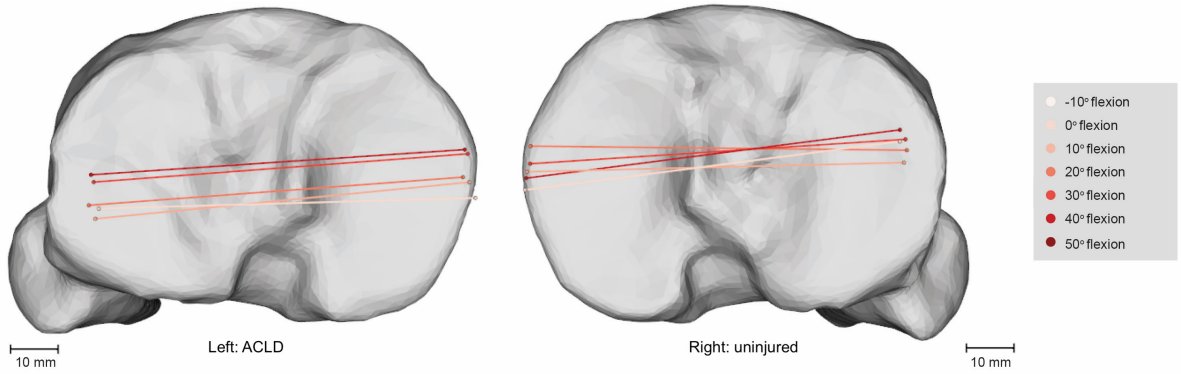

(d) Patient005.

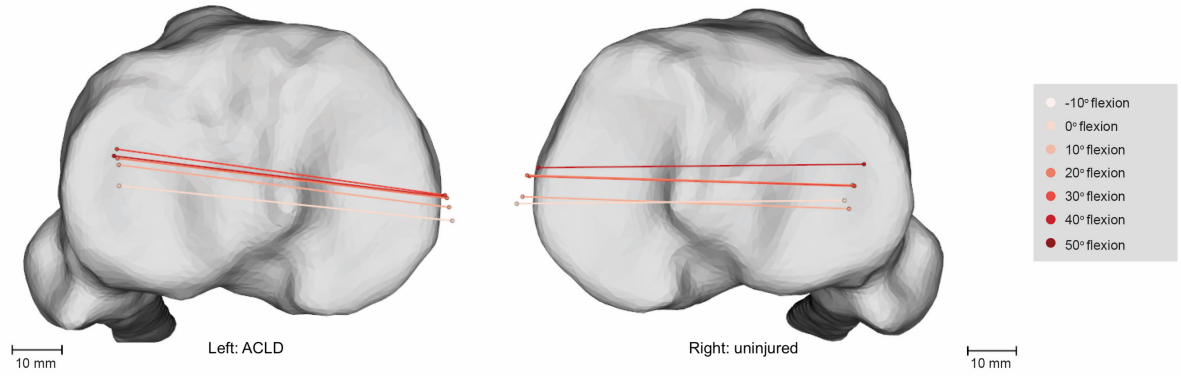

(e) Patient006.

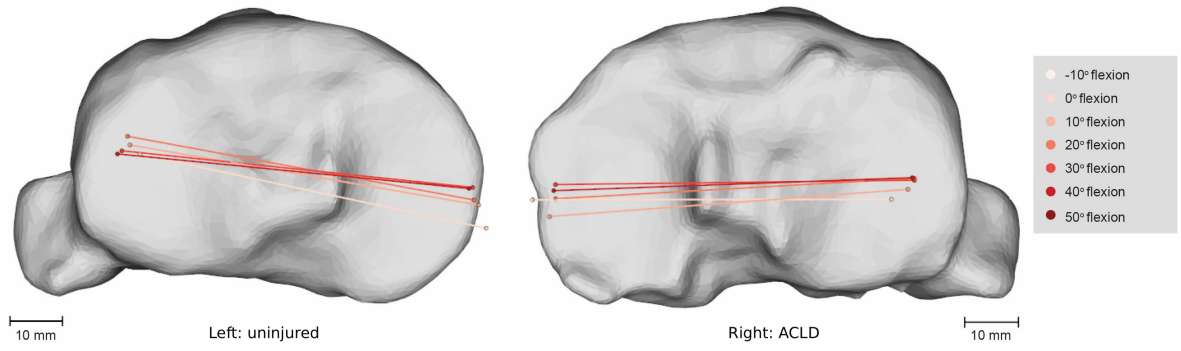

(f) Patient008.

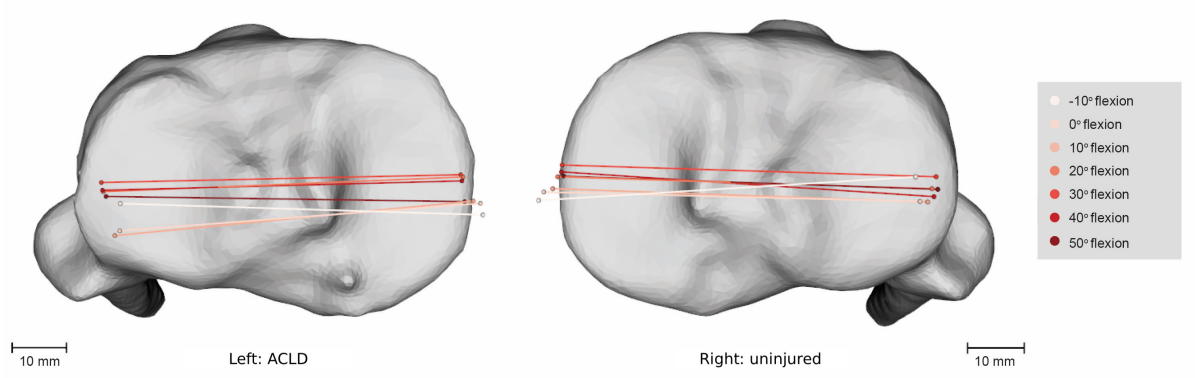

(g) Patient009.

Figure 5.2: Intercondylar axes of the femur for different flexion angles plotted onto the transverse plane of the tibia. Note that not all patients reached the same flexion angles, hence the missing data at certain angles. Movement ranges from the lighter reds at extension towards the darker reds in flexion. **Abbreviations:** Anterior cruciate ligament deficient (ACLD).

5.3. Centers of proximity

Figures 5.3a to 5.3g show the plots of the centres of proximity for different flexion angles on the tibia. Those for the femur are shown in figures 5.4a to 5.4g. The same range of flexion angles as that in the plots of the intercondylar axes was reported in these plots, only now with 5° increments to better visualize the path along which the centres of proximity moved. Again, not all patients reached the same range, so for some participants, data is missing on the outer regions of the flexion range.

These plots show apparent differences in the movement patterns of different patients as movements between left and right knees are similar, but patterns across patients vary substantially. A phenomenon seen in almost all tibial plots is that the medial movement is larger than the lateral movement. In addition, movement in the uninjured knee is always from the anterior surface toward the posterior surface. Interestingly, in the ACLD knees, this movement seems to be in the opposite direction at the lateral side as the centres of proximity move from the posterior towards the anterior side or from anterior to posterior and then anterior again.

When looking at the relative movements between the femur and tibia at the level of articulation in tables 5.1 and 5.2, it can be seen that slip is the phenomenon occurring most throughout flexion/extension (an overview of the distances for the femur and tibia specifically can be found in Appendix D). A slight increase of this slip movement can be seen in the ACLD knees for most patients, which mainly occurs at the lateral side.

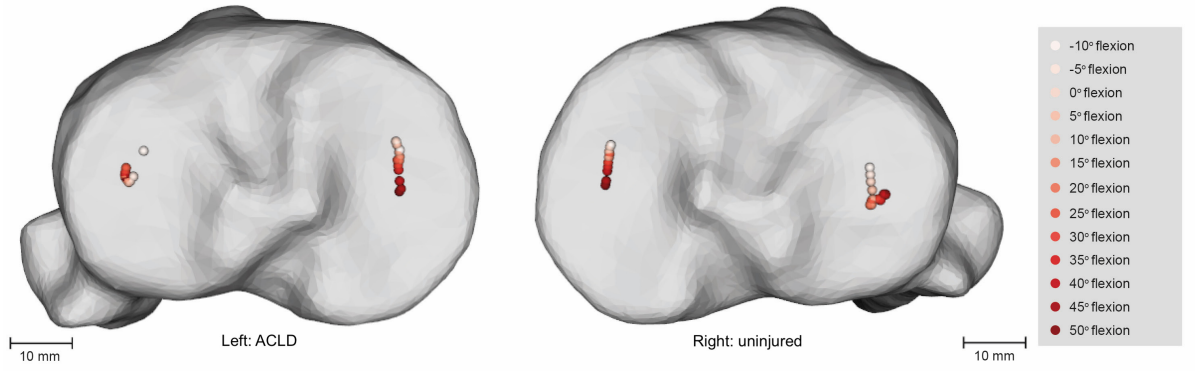

(a) Patient001.

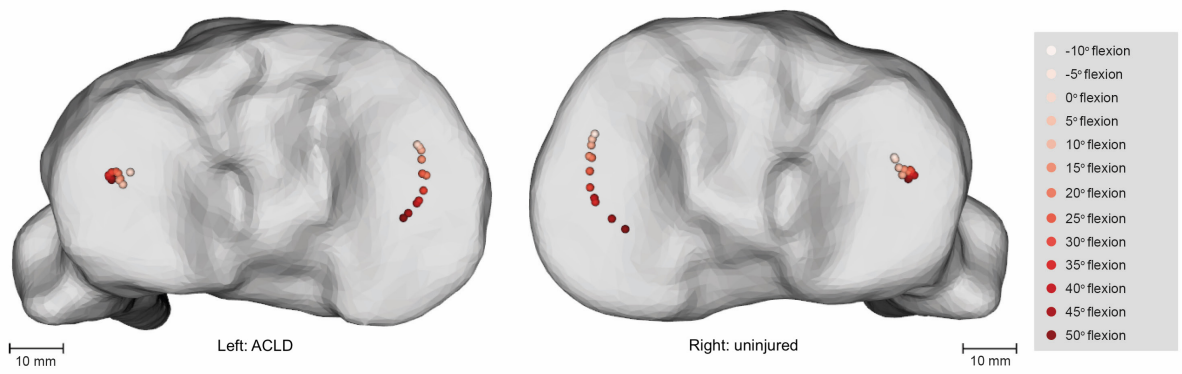

(b) Patient003.

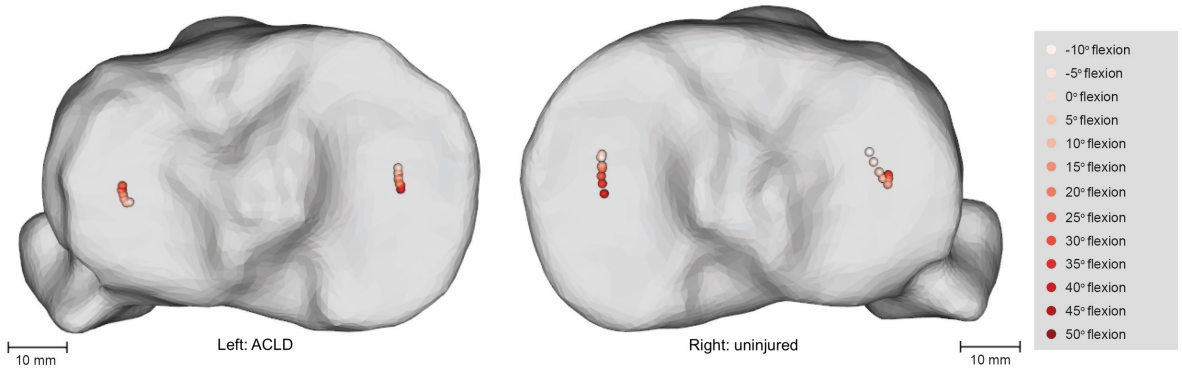

(c) Patient004.

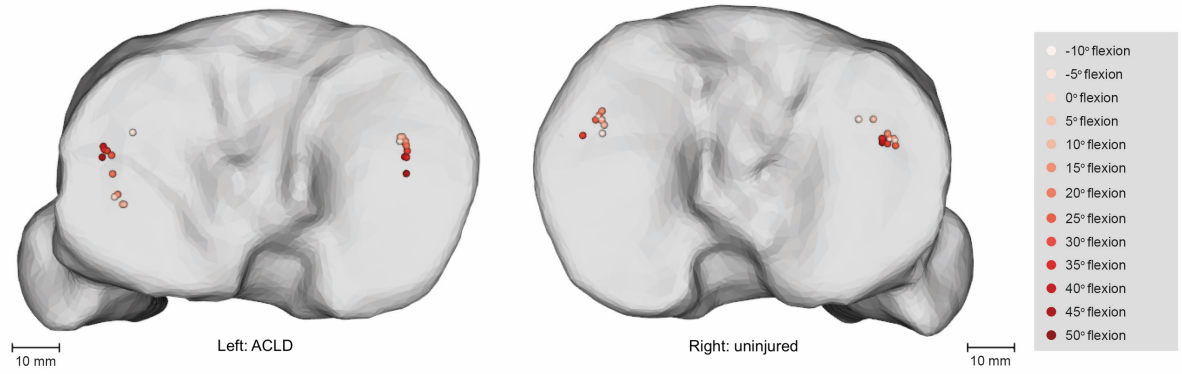

(d) Patient005.

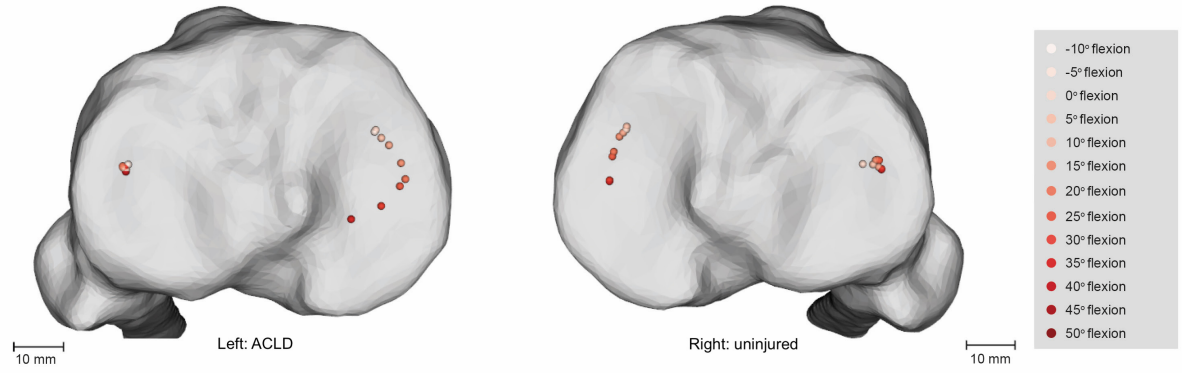

(e) Patient006.

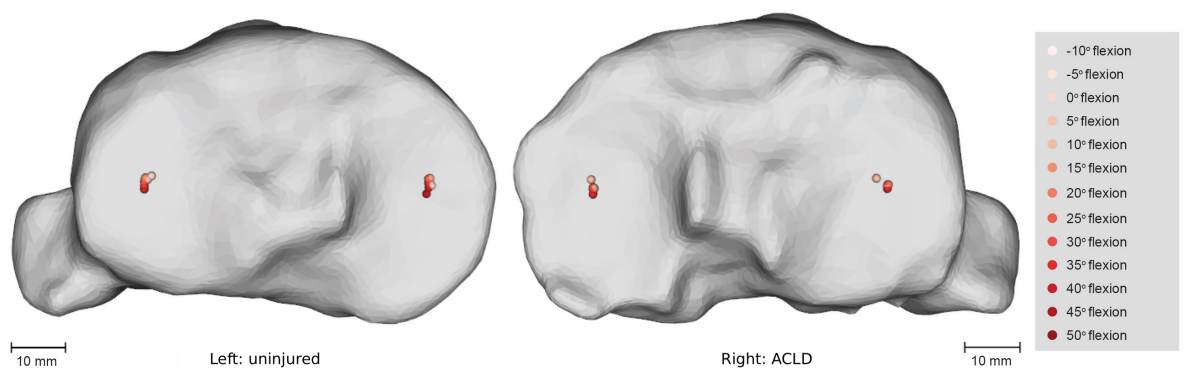

(f) Patient008.

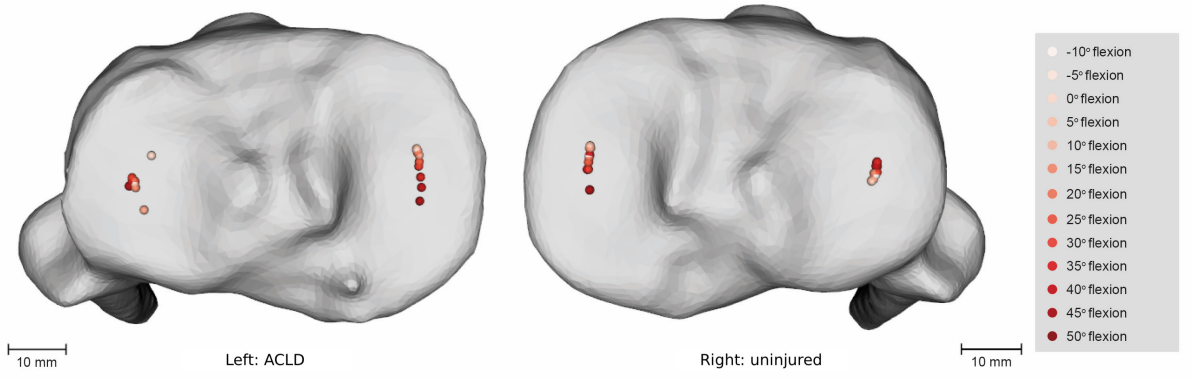

(g) Patient009.

Figure 5.3: Plots of the centres of proximity on the tibia for different flexion angles.
Note that not all patients reached the same flexion angles, hence the missing data at certain angles. Movement ranges from the lighter reds at extension towards the darker reds in flexion. **Abbreviations:** Anterior cruciate ligament deficient (ACLD).

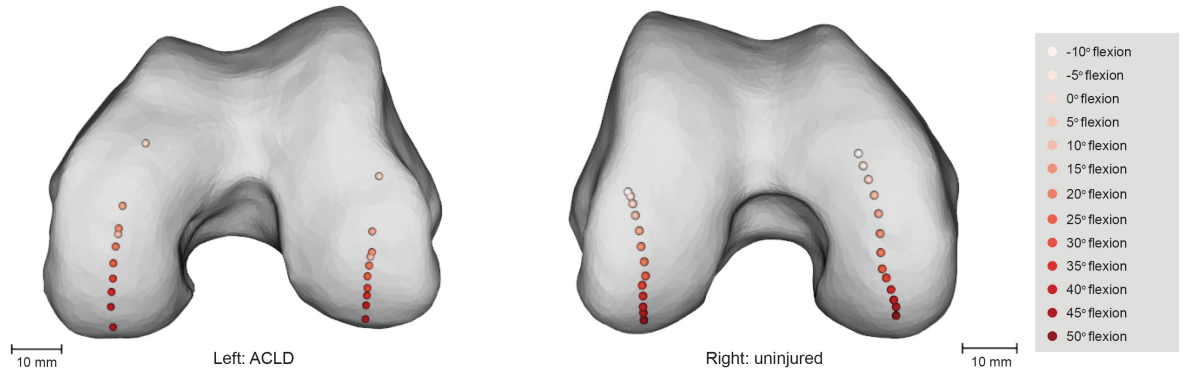

(a) Patient001.

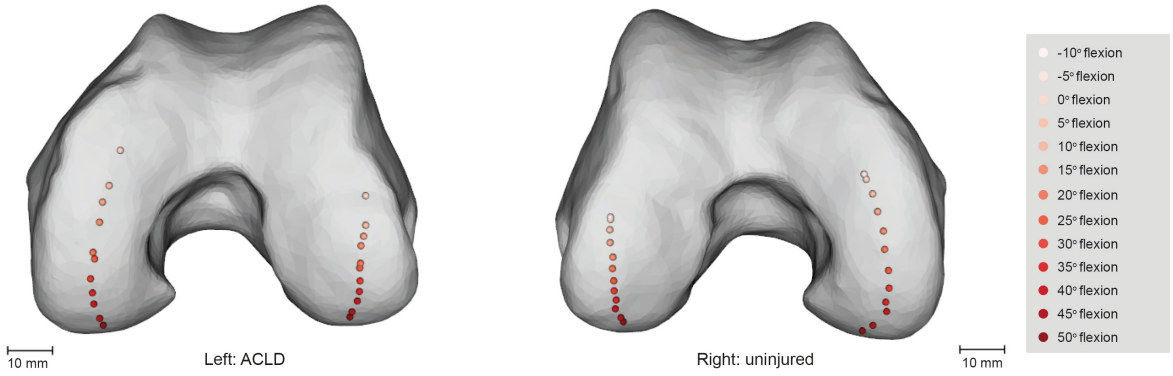

(b) Patient003.

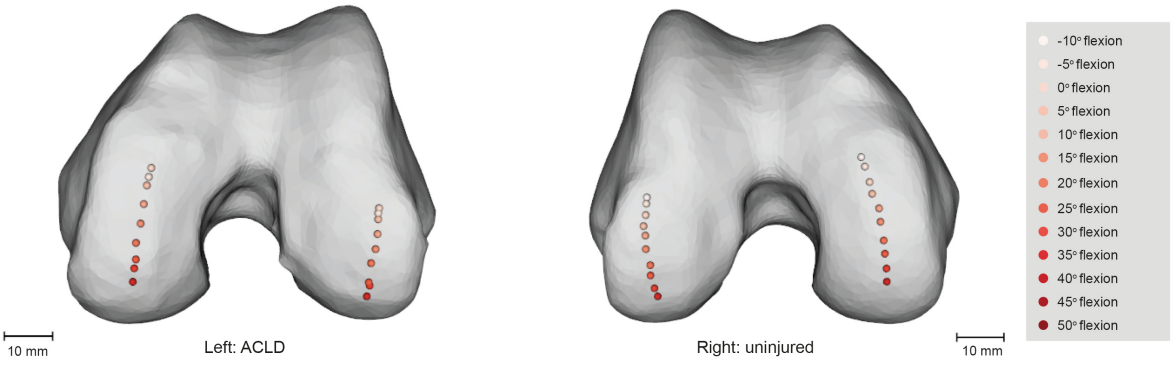

(c) Patient004.

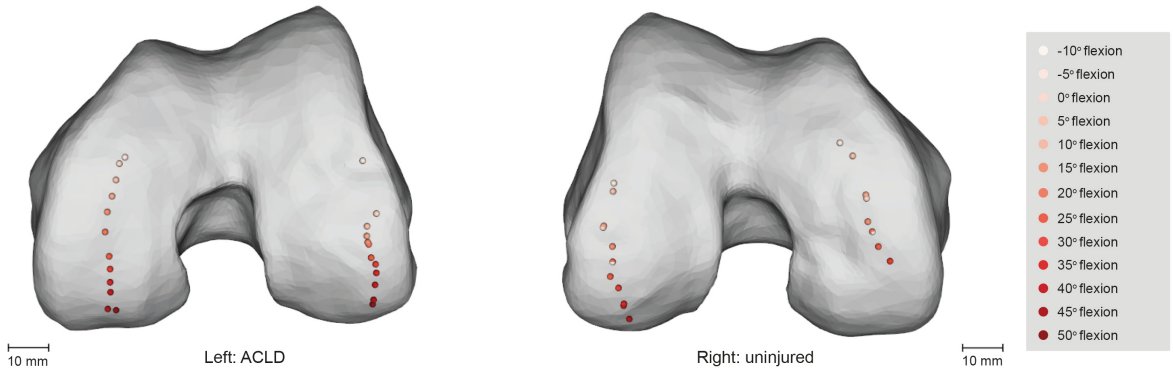

(d) Patient005.

(e) Patient006.

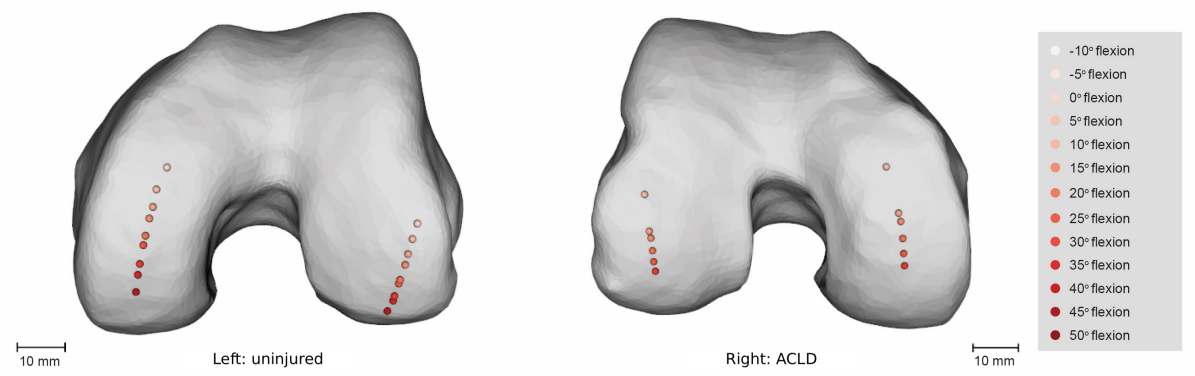

(f) Patient008.

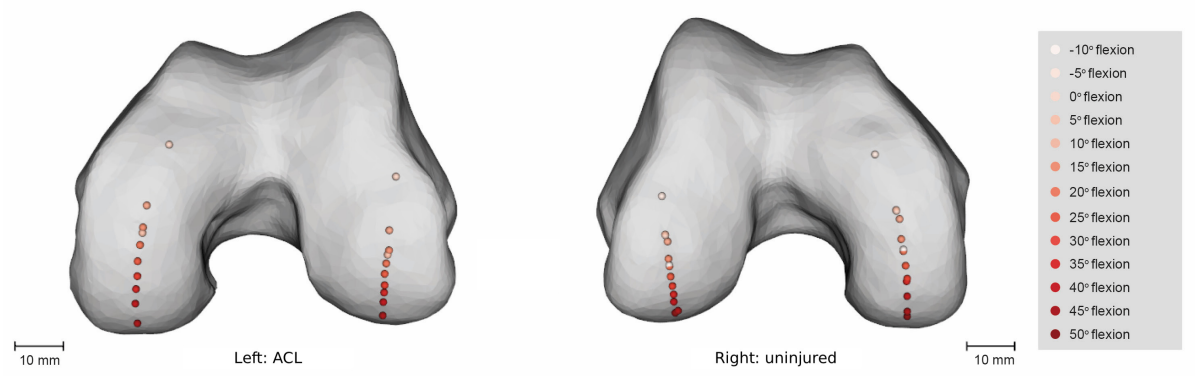

(g) Patient009.

Figure 5.4: Plots of the centres of proximity on the femur for different flexion angles.
Note that not all patients reached the same flexion angles, hence the missing data at certain angles. Movement ranges from the lighter reds at extension towards the darker reds in flexion. **Abbreviations:** Anterior cruciate ligament deficient (ACLD).

Table 5.1: Movement of the centres of proximity on the tibia compared to those on the femur for the ACLD knee.

ACLD KNEE	Patient001		Patient003		Patient004		Patient005		Patient006		Patient008		Patient009	
Flexion angle	L	M	L	M	L	M	L	M	L	M	L	M	L	M
-10	0.82	4.08												
-5	3.69	26.92			3.37	8.96	0.91	2.30						
0	10.14	5.82	2.36	13.61	3.99	3.87	1.45	46.45	5.48	2.31			2.76	128.87
5	12.37	2.40	2.34	5.12	4.15	4.57	8.11	8.23	17.22	2.35	3.32	6.45	1.04	4.52
10	11.88	2.46	7.05	2.57	3.91	3.96	0.66	3.48	21.73	1.59	6.94	12.14	0.99	5.60
15	6.40	5.82	3.61	2.17	3.76	5.67	0.12	5.00	15.02	1.98	28.48	33.50	2.29	11.61
20	5.08	19.52	2.33	1.94	5.89	3.65	0.85	21.06	4.72	2.25	18.37	19.24	17.00	2.12
25	0.49	1.65	3.75	1.50	1.06	1.02	1.45	2.37	6.28	1.36	6.57	10.64	3.24	4.27
30	0.71	1.32	3.59	1.79	19.61	4.44	3.55	2.65	13.66	1.22	7.11	3.00	2.55	1.52
35	63.07	1.41	7.74	5.15			5.09	7.73			12.11	3.25	24.77	1.98
40	5.48	1.87	6.83	1.83			2.06	1.52					4.83	2.35
45	9.50	3.47	10.36	1.95										

Values below 1.5 (blue) are considered roll, those between 1.5 and 5 (purple), a combination of roll and slip, and over 5 (red) slip. **Abbreviations:** Anterior cruciate ligament deficient (ACLD), lateral side (L), medial side (M).

Table 5.2: Movement of the centres of proximity on the tibia compared to those on the femur for the uninjured knee.

UNINJURED KNEE	Patient001		Patient003		Patient004		Patient005		Patient006		Patient008		Patient009	
Flexion angle	L	M	L	M	L	M	L	M	L	M	L	M	L	M
-10	0.81	68.99												
-5	1.23	7.70			1.21	9.15	1.22	4.96						
0	1.52	3.66	1.29	3.10	1.88	4.39	1.39	8.47	0.76	4.99			5.27	2.98
5	1.89	3.80	1.90	3.57	1.56	2.30	1.41	8.77	2.21	2.34	9.09	3.48	3.88	5.27
10	3.26	117.37	3.05	2.09	3.42	13.93	3.14	3.16	2.80	5.07	12.67	134.28	3.53	26.67
15	11.02	6.19	2.64	7.40	9.80	12.17	3.70	2.35	12.77	2.07	13.32	11.25	5.97	1.67
20	4.07	32.82	6.38	1.93	10.60	2.17	1.90	3.20	2.16	1.42	1.76	9.32	7.49	4.00
25	1.77	1.46	8.02	1.41	5.66	2.49	2.13	1.03	3.27	1.64	4.60	6.72	17.32	2.50
30	5.21	3.69	5.71	1.29	6.10	1.79	3.13	0.98	1.97	1.10	2.25	3.09	1.24	0.24
35	2.26	3.62	3.95	3.50			1.38	0.98			37.82	3.37	3.08	1.54
40	4.57	1.05	3.67	1.03			13.77	0.98					15.91	1.14
45	21.38	3.25	4.18	1.00										

Values below 1.5 (blue) are considered roll, those between 1.5 and 5 (purple) a combination of roll and slip, and over 5 (red) slip. **Abbreviations:** lateral side (L), medial side (M).

6

Discussion

The translation and rotation graphs showed little difference between the ACLD and uninjured knees. Only the AP translations showed an increase in extension and the lower flexion angles for the ACLD knees. The intercondylar axes showed more evident differences between the two knees. Here, it could be seen that the ACLD knees translated more anteriorly than the uninjured knees. The centres of proximity showed apparent kinematic differences among the individual patients included but showed a less conclusive pattern to distinguish between the ACLD and uninjured knees. Moreover, differences between the centres of proximity on the tibia and the femur showed that slip is a frequent occurrence in the joint that increases with ACL deficiency. In addition, these plots showed interesting differences from the plots of the intercondylar axes, showing that these intercondylar axes do not accurately represent the interarticular kinematics throughout the whole range of motion of the knee. Overall, the findings in this thesis support that kinematic differences during a flexion/extension movement can to some extend be visualized between ACLD and uninjured knees using this workflow. However, differences are only small.

6.1. Mean translations and rotations

The graphs containing the translations and rotations show a statistical increase in AP translation between the ACS from the femur and tibia for the ACLD group at extension and the lower flexion angles. The no statistical difference were visible between -35° and 0° for the other translations or either of the rotations.

This was an expected finding as the ACL restricts movement in the AP direction, especially in extension and the lower flexion angles [24, 70]. However, the differences were smaller than expected based on previous literature. An explanation for this difference may be that previous literature mainly evaluates the joint in weight-bearing conditions such as during lunging [22] or with weights [13], which may increase the kinematic differences during movement. Another explanation could be the definitions of the translations, as these are calculated for specific points and may be different when calculating them for a different set of points.

For the rotations, no noteworthy differences could be seen, which is in contrast with our expectations as an increase in the internal rotation was expected for the ACLD knee based on literature [70, 87, 35, 63]. However, not all studies reported significant differences for internal/external rotation, such as Yim et al. [93], who evaluated the differences during gait. An explanation may be that the unloaded conditions caused the differences to become too small to distinguish. As mentioned, other studies frequently apply a loading like body weight [15] or external forces [27] when evaluating differences between ACLD and uninjured knees that may enlarge the changes. Another option may be that this patient group compensated well for the injury through muscle contractions. These compensation strategies would not be visible in studies that used tests where the examiner or an instrument applies a movement or force like the in pivot shift test [53] or a passive flexion [27], as these tests are passive and patients are discouraged from tensing their muscles. Therefore muscular compensation strategies are not taken into account in these measurements.

Overall the SDs were large, and the sample size was small, which may give an altered represen-

tation compared to larger patient groups. Moreover, the graphs' extension and larger flexion angles portions are based on only part of the data set.

6.2. Intercondylar axes

The intercondylar axes were plotted for certain flexion angles to combine the translations and rotations into one figure. An larger increase in AP translation could be seen for the ACLD knees compared to the uninjured knees, which is interesting as the graphs did not show these differences as clearly. However, this may be related to the fact that the translation of a point on the ML axis of the femur is calculated here instead of that of the origin, which was done for the graphs.

An interesting, visible phenomenon is that the axis moves anteriorly during approximately the first 30° of flexion before it moves posteriorly again. This can be related to the a more prominent sliding movement of the femur at the beginning of the movement, which also results in the anterior movement of the intercondylar axes, which seems to be over a more extended portion of the flexion angle in ACLD patients (see tables in section 5.3). Following this, the rotational component becomes more prominent, which moves the axis posterior again. In addition, the axes are oriented more parallel in the ACLD knees due to the lack of restriction on internal/external rotation. Therefore, the medial pivot, where the lateral femoral condyle presents with a sliding movement toward the anterior side of the tibia plateau while the medial condyle simultaneously pivots, is less visible for the ACLD knees [78]. Here, the movement seems more consistent between the two sides due to the lack of resistance to rotations about the longitudinal axis.

These intercondylar axes are often used to approximate the finite helical axes of the joint [19]. This assumption would suffice for a circular object rolling over a surface, which is an appropriate assumption for the posterior part of the distal femur. More anteriorly, the shape of the distal femur can no longer be approximated as a circle, and the helical axis will start to differ from the intercondylar axes. Moreover, the location of the intercondylar axes is restricted to the ML axis of the femur, unlike the helical axes. For example, suppose a cylinder rolls over a flat surface. In that case, the finite helical axis will be at the point of contact between the two, while the 'intercondylar' axis will be through the centre of this cylinder. Therefore, the finite helical axis may be situated at another point in the femur than the intercondylar axis. This can also be seen in the study by Sheehan [81], where the finite helical axis is close to the articulation surface in flexion, which the intercondylar axis would not appropriately represent.

6.3. Centers of proximity

The plots of the centres of proximity onto the tibia showed a substantial variation among the patients. Because of this, a clear pattern in the differences between the ACLD and uninjured knees could not be established for this patient group. Interestingly, the patterns of the intercondylar axes and the plots of the centres of proximity onto the tibia differed substantially. This is because the intercondylar axes do not give insight into movements like slip and roll occurring at the surface of articulation, which the plots of the centres of proximity onto the tibia and femur do. Using these centers, the relative movements were determined, which was mostly slip or a combination of slip and roll throughout the flexion/extension movement. This may explain the differences between the two plots as the femur will, in this case, move substantially more anteriorly than the tibia does. These intercondylar axes do, therefore, not provide an adequate representation of the kinematics at the level of articulation even though they are a frequently used tool to visualize them [25, 37, 45, 51, 94].

Another explanation for the differences between the two plots may be due to the geometry of the distal femur as described by Asano et al. [7], who showed a substantial difference in the AP translation between the intercondylar axis and the contact point. Here, the differences are most prominent at extension and the lower flexion angles. As circles can approximate the posterior side of the femur, the locations of the intercondylar axis and the centre of proximity are better aligned here. However, the anterior side of the distal femur can no longer be approximated by this circle, hence the difference in location (see figure 6.1).

Overall an increased amount of slip can be seen for most ACLD knees, mostly on the lateral side. Increased slip will result in more shear forces exerted onto the tibial cartilage. This, in turn, will cause altered loadings of the cartilage and can cause an increase in cartilage degeneration which can lead to osteoarthritis [5]. Only a little difference can be seen for patient003 in the tables, which could mean that this patient is coping well with the injury and may not need surgery. Some values in the table can

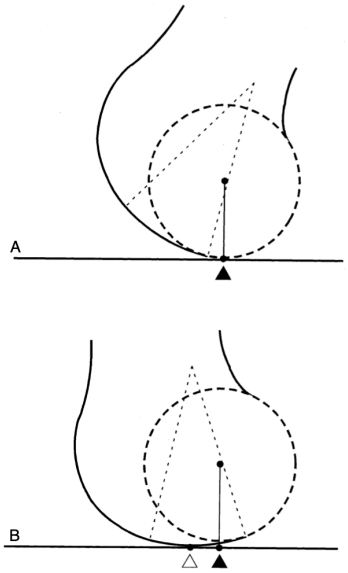

Figure 6.1: Relation of the intercondylar axis to the centre of proximity.
a. The centre of proximity is on the part of the distal femur that can be approximated by a circle. Hence, the centre of proximity is at the same location as the intercondylar axis when projected onto the tibia. b. The centre of proximity is not on the part of the distal femur that a circle can approximate. Therefore, the centre of proximity is located differently than the intercondylar axis [7].

be seen to be exceptionally high. An explanation for this is that the distance between two subsequent centres of proximity on the tibia is sometimes nearly identical, causing a division by a value close to 0 (see Appendix D) and, thereby, a high coefficient.

6.4. Clinical relevance

This thesis showed that some kinematic changes due to ACL injuries can be visualized using 4DCT and the graphs of the translations and rotations or the plots of the intercondylar axes. However, the differences are minor, and these figures do not accurately represent the kinematics at the articulation surface. The plots of the centres of proximity are better suited to evaluate the changes at this location, but a larger sample size is required to distinguish patterns between the ACLD and uninjured knees. Because of this, it may also be challenging to distinguish ACL deficiency for individual patients using these figures. 4DCT was chosen as it allows for easy implementation in the current care facilities, as the tools required are more commonly present than tools like motion capture labs. In addition, this technique allows the patient to move themselves, which is a more accurate representation of daily movement than other tests like the pivot shift. Moreover, the non-weight-bearing conditions increase usability as the setup is more accessible and less elaborate than weight-bearing alternatives and the kinematics can be evaluated based on the bone geometry directly. However, differences may be less evident than in weight-bearing conditions, and this technique subjects patients to radiation. Therefore, this technique may not be suited as a tool to evaluate knee injuries in all patients but only in patients that are expected to cope very well with the injury or where concomitant injury is expected, but future research should still evaluate the performance of the workflow for these situations.

6.5. Limitations

This thesis is subject to multiple assumptions and limitations. One of the assumptions is that all translations and rotations were calculated based on a fixed axis of rotation, namely, the ML axis of the femur ACS. However, knee flexion is a movement about a varying axis of rotation [43]. Even though this fixed axis is an assumption that is frequently used and is suitable for small movements, it is an approximation of reality, and minor deviations can cause errors in the calculated angles due to cross-talk [73, 3]. In addition, the graphs containing the translations and rotations provide a straightforward interpretation of the contributions of each DoF. Still, it isn't easy to understand the combined movements that oc-

cur. Moreover, potential errors in the calculated angles would influence all subsequent results as the calculated translations and rotations were used as input for all subsequent analyses.

For the definition of the ACSs, the mesh file of the static scan of the tibia still contained the fibula. Even though the ACS of the tibia is defined based on the tibial plateau only, the presence of the fibula may have altered the cut-off of the tibial plateau slightly. This is because this was done based on the cross-sectional area to which the fibula was added. Moreover, the separated tibial plateau may still have included part of the fibular head. This could have influenced the definition of the ACS, as the inertial axes are calculated based on the separated geometry and then directly used as the ACS. However, differences are assumed minor because of the difference in size of the tibia and fibula. In addition, the defined ACSs of the static scans were manually checked and showed no visible deviations.

For the centres of proximity, differences among patients may be explained by different bone geometries. For example, if the tibia or femur has a slight protrusion, this point will be closer to the other bone than the surrounding points causing the centre of proximity to stay in this position longer. Such a point is visible in the plot of the centres of proximity of the ACLD knee of patient 005 at the lateral side, where a protrusion can be seen extending from the medial-posterior side to a more anterior and lateral location. Here a cluster of centres of proximity over several flexion angles can be seen around that protrusion. Protrusions like this may also cause sudden jumps in the distances as the centre of proximity will remain at the protrusion over a few flexion angles and suddenly jump away from it.

A constant thickness was assumed for the cartilage to ease modelling as the contours of the cartilage could not be extracted from the 4DCT data, and determining a cartilage model of varying thickness based on the geometry would be outside the scope of this thesis. This assumption may have altered the results as proximities are calculated based on the overlap of the cartilage layers. This means that the overlap may have been more extensive when the cartilage was modelled thicker than it is and smaller for the regions where it should have been thinner. However, the cartilage is generally at its thickest at the regions of highest proximity, which is the thickness used here. Nonetheless, cartilage may be affected by the ACL injury, but as the extent of this was unknown for the patient group, this assumption was used throughout [18, 90]. In addition, as we only evaluated the centre of proximity, outliers or regions that were included due to the increased thickness at the peripheries should not affect results.

Only patients with unilateral complete ACL tears were evaluated within this thesis, and their contralateral knee was evaluated as a control. In addition, only a few patients were evaluated. Therefore, conclusions drawn may differ from this patient group when tested in a larger patient group. For extension and the larger flexion angles the number of evaluated subjects becomes even lower (only one to two) as not all patients reached the same range of angles. However, angles may be relevant to analyze as certain phenomenons, especially as the difference in AP translation is only visible in these ranges.

Lastly, automating the workflow allows for a less hands-on evaluation. The results of intermittent steps cannot be easily assessed, allowing for possible faulty results at these points. Even though each step was evaluated throughout the scripting process, an evaluation of the repeatability and accuracy of the process was not performed. This problem is expected to be most prominent in the segmentation and registration steps due to the movement artefacts in the scans. The process was optimized as much as possible with the current techniques and time frame available (see Appendix A). However, further development is desirable to overcome the movement artefacts in these steps fully.

6.6. Future research

Future research should focus on the further development of this workflow. The main difficulty in this process was the registration. This is a problem that could potentially be solved at multiple levels. A first solution would be to improve the images from the 4DCT scan by increasing the 'shutter speed' of the scanner, like in cameras that can visualize swift movements statically. Even though this would solve the problem at its core, developing such a system takes great effort and time and may not be feasible. Moreover, this adaptation was outside the scope of this thesis and would subject patients to more radiation. Another solution would be to adapt the settings of the scanner, such as using a high tube rotation speed and half reconstruction as proposed by Gondim Teixeira et al. [36], but this might reduce image quality [8]. Reducing the speed of the flexion/extension movement might also be an option to reduce the artefacts [36]. However, patients should be able to do so as it requires them to hold the position longer, which might not be possible due to injury. Moreover, patients will be exposed to radiation longer. Furthermore, this adaptation may result in less functional results as it is less of a

representation of daily life, and by moving too slowly, the movement may even become quasi-static, which can alter results [92]. Lastly, the size of the dynamic images may be reduced, which is essentially the same as the selection of the area to segment, only it will also reduce the amount of radiation the patient is subjected to.

An option that is more within the scope of this thesis might be to improve the segmentation or registration. As the movement artefacts are included in the segmentation, a solution would be to remove them manually. However, this is a time-consuming task, that decreases usability. Pre-processing the images might be an option to reduce the movement artefacts in the images and, thereby, the effect on the segmentation. An option might be to use a deep learning network to reduce the artefacts in the images before segmentation, as was done for fetal CT images by Lim et al.[56]. Improving the segmentation is expected to positively affect the registration as the distal part of the shaft would no longer have to be removed, and the geometries of the static and dynamic scans will be more similar.

Furthermore, more testing should be performed using this workflow to assess its quality and functions fully. These tests should include control subjects and subjects with other types of injuries or different concomitant injuries to ACL injury. Evaluating these patients allows for assessing the workflow's performance in evaluating the kinematics in other injuries or whether differences due to concomitant injuries can be distinguished, as this is still unknown. Moreover, as the differences found here were only minor, evaluating the technique in weight-bearing conditions may also be interesting as this is expected to enlarge the differences.

Another suggestion for future work is to improve the current OpenSim model, as the program allows for more elaborate applications than currently done, such as evaluating the effect of different ligament attachment sites or stiffnesses on the knee kinematics and evaluating pressures [33]. In doing so, the future user should consider further improvements. One example is that the current model, Lenhart2015, does not include a meniscus. Depending on the application, adding a meniscus may give more accurate results, like evaluating pressures exerted onto the cartilage or if the meniscus needs to be evaluated. In those cases, further work should look into the inclusion of this structure by using the Smith2019 model, for example, as this model is a further improvement of the Lenhart2015 model that does include the meniscus [85]. Inherent to this adaptation is the further refinement of the cartilage models. The best would be to obtain these based on a patient-specific MRI. However, this would subject the patient to additional scanning and, thereby, costs, which may be unnecessary. A technique developed for the hip joint may be interesting to adapt for the knee as it would not require additional scans. It defines the shape and thickness based on the bone geometry from the already acquired CT scans and population-averaged cartilage thickness maps or geometric constraints [64]. A method based on statistical shape modelling also exists for this application which may be interesting [89]. However, this method was inaccessible at the time of this project.

Our simulation did not include the attachment sites and properties of muscles, ligaments, and tendons, as kinematics were obtained directly from the 4DCT scans. Therefore, the influence of these structures was already included in the definition of the movement. However, further work should pay attention to these as they may be necessary for other work, like when the user is interested in analyzing the ligament stiffnesses.

Furthermore, this type of research may, in the future, aid surgeons in assessing patients' surgical needs better than the current techniques, as active kinematics can be assessed, thereby also evaluating the potential coping mechanisms of some patients, which can prevent unnecessary surgery. In addition, it may also be a technique that can evaluate the effects of concomitant injuries, which may also require surgical intervention. However, more research is needed on these effects. Moreover, it also allows for the better evaluation of kinematics post-surgery, which can help to improve surgical techniques further.

7

Conclusion

This thesis showed that some kinematic changes due to ACL injuries can be visualized using 4DCT and the graphs of the translations and rotations or the plots of the intercondylar axes. However, the differences found are only minor and these graphs and plots do not adequately represent the kinematics at the articulation surface. The plots of the centres of proximity are better suited to evaluate the changes at this location, but clear patterns between the ACLD and uninjured knees could not be distinguished. A larger sample size may give more insight into the pattern, but it may remain difficult to determine ACL deficiency for individual patients using these visualizations. Because of this, it may be beneficial to evaluate this technique in weight-bearing conditions as this is expected to enlarge the differences between ACLD and uninjured knees. Altogether, this technique may not be suited as a tool to evaluate knee injuries in all patients However, it shows potential to evaluate patients that are expected to cope very well or where a concomitant injury is expected, but future research should still evaluate the performance of the workflow for these situations. Moreover, the OpenSim model could be further developed to evaluate the effects of ligament stiffnesses and attachment locations which can also aid in the making of surgical decisions.

Bibliography

[1] *3D Slicer*. URL: https://www.slicer.org/ (visited on 04/10/2023).

[2] Fedorov A. et al. “3D Slicer as an Image Computing Platform for the Quantitative Imaging Network”. In: *Magnetic Resonance Imaging* 30.9 (2012), pp. 1323–41.

[3] Andrea Ancillao et al. “A Novel Procedure for Knee Flexion Angle Estimation Based on Functionally Defined Coordinate Systems and Independent of the Marker Landmarks”. In: *International Journal of Environmental Research and Public Health* 20.1 (2022), p. 500.

[4] Sebastian Andreß et al. “A method for finding high accuracy surface zones on 3D printed bone models”. In: *Computers in Biology and Medicine* 135 (2021), p. 104590.

[5] Thomas P Andriacchi et al. “Rotational changes at the knee after ACL injury cause cartilage thinning”. In: *Clinical Orthopaedics and Related Research®* 442 (2006), pp. 39–44.

[6] Edith M Arnold et al. “A model of the lower limb for analysis of human movement”. In: *Annals of biomedical engineering* 38 (2010), pp. 269–279.

[7] Taiyo Asano et al. “In vivo three-dimensional knee kinematics using a biplanar image-matching technique.” In: *Clinical Orthopaedics and Related Research (1976-2007)* 388 (2001), pp. 157–166.

[8] Mathias Prokop Ashley S. Shaw. *Computed Tomography*. URL: https://radiologykey.com/computed-tomography-5/#:~:text=CT%5C%20data%5C%20acquisitions%5C%20that%5C%20involve,%5C%27full%5C%2Dscan%5C%27%5C%20reconstructions.. (accessed: 04.05.2023).

[9] GA Ateshian, LJ Soslowsky, and Van C Mow. “Quantitation of articular surface topography and cartilage thickness in knee joints using stereophotogrammetry”. In: *Journal of biomechanics* 24.8 (1991), pp. 761–776.

[10] V Baltzopoulos. “A videofluoroscopy method for optical distortion correction and measurement of knee-joint kinematics”. In: *Clinical Biomechanics* 10.2 (1995), pp. 85–92.

[11] Anne Benjaminse, Alli Gokeler, and Cees P van der Schans. “Clinical diagnosis of an anterior cruciate ligament rupture: a meta-analysis”. In: *Journal of orthopaedic & sports physical therapy* 36.5 (2006), pp. 267–288.

[12] Paul J Besl and Neil D McKay. “Method for registration of 3-D shapes”. In: *Sensor fusion IV: control paradigms and data structures*. Vol. 1611. Spie. 1992, pp. 586–606.

[13] Bruce D Beynnon et al. “Chronic anterior cruciate ligament deficiency is associated with increased anterior translation of the tibia during the transition from non-weightbearing to weightbearing”. In: *Journal of orthopaedic research* 20.2 (2002), pp. 332–337.

[14] Barry P Boden et al. *Mechanisms of anterior cruciate ligament injury*. 2000.

[15] Sveinbjörn Brandsson et al. “Kinematics after tear in the anterior cruciate ligament: dynamic bilateral radiostereometric studies in 11 patients”. In: *Acta Orthopaedica Scandinavica* 72.4 (2001), pp. 372–378.

[16] Jeffrey R Brown and Thomas H Trojian. “Anterior and posterior cruciate ligament injuries”. In: *Primary Care: Clinics in Office Practice* 31.4 (2004), pp. 925–956.

[17] Canon Medical Systems. *Computed Tomography*. URL: https://nl.medical.canon/product-solutions/computed-tomography/aquilion-one. (accessed: 26.05.2023).

[18] AM Chaudhari et al. “Knee kinematics, cartilage morphology, and osteoarthritis after ACL injury.” In: *Medicine and science in sports and exercise* 40.2 (2008), pp. 215–222.

[19] Hao Chen et al. “A robust and semi-automatic quantitative measurement of patellofemoral instability based on four dimensional computed tomography”. In: *Medical engineering & physics* 78 (2020), pp. 29–38.

[20] Paolo Cignoni et al. “Meshlab: an open-source mesh processing tool.” In: *Eurographics Italian chapter conference*. Vol. 2008. Salerno, Italy. 2008, pp. 129–136.

[21] Zohara A Cohen et al. “Knee cartilage topography, thickness, and contact areas from MRI: in-vitro calibration and in-vivo measurements”. In: *Osteoarthritis and cartilage* 7.1 (1999), pp. 95–109.

[22] Louis E DeFrate et al. “The 6 degrees of freedom kinematics of the knee after anterior cruciate ligament deficiency: an in vivo imaging analysis”. In: *The American journal of sports medicine* 34.8 (2006), pp. 1240–1246.

[23] Scott L Delp et al. “OpenSim: open-source software to create and analyze dynamic simulations of movement”. In: *IEEE transactions on biomedical engineering* 54.11 (2007), pp. 1940–1950.

[24] Douglas A Dennis et al. “In vivo determination of normal and anterior cruciate ligament-deficient knee kinematics”. In: *Journal of biomechanics* 38.2 (2005), pp. 241–253.

[25] Ruediger von Eisenhart-Rothe et al. “Tibiofemoral and patellofemoral joint 3D-kinematics in patients with posterior cruciate ligament deficiency compared to healthy volunteers”. In: *BMC musculoskeletal disorders* 13.1 (2012), pp. 1–8.

[26] Nalan Ektas et al. “Recovery of knee extension and incidence of extension deficits following anterior cruciate ligament injury and treatment: a systematic review protocol”. In: *Journal of Orthopaedic Surgery and Research* 14.1 (2019), pp. 1–7.

[27] Fateme Esfandiarpour et al. “Comparison of kinematics of ACL-deficient and healthy knees during passive flexion and isometric leg press”. In: *The Knee* 20.6 (2013), pp. 505–510.

[28] Jennifer Evans et al. “Anterior cruciate ligament knee injuries”. In: *StatPearls [Internet]*. StatPearls Publishing, 2022.

[29] Peter D Fabricant et al. “Reconstruction of the anterior cruciate ligament in the skeletally immature athlete: a review of current concepts: AAOS exhibit selection”. In: *JBJS* 95.5 (2013), e28.

[30] Gregory C Fanelli, Daniel R Orcutt, and Craig J Edson. “The multiple-ligament injured knee: evaluation, treatment, and results”. In: *Arthroscopy: The Journal of Arthroscopic & Related Surgery* 21.4 (2005), pp. 471–486.

[31] *Figure of the anatomical planes*. URL: `https://opening.download/spring-2021.html`. (accessed: 18.04.2023).

[32] Jeremy S Frank and Peter L Gambacorta. “Anterior cruciate ligament injuries in the skeletally immature athlete: diagnosis and management”. In: *JAAOS-Journal of the American Academy of Orthopaedic Surgeons* 21.2 (2013), pp. 78–87.

[33] Toru Fukubayashi and Hlsashi Kurosawa. “The contact area and pressure distribution pattern of the knee: a study of normal and osteoarthrotic knee joints”. In: *Acta Orthopaedica Scandinavica* 51.1-6 (1980), pp. 871–879.

[34] Elizabeth B Gausden et al. “Surgical options for anterior cruciate ligament reconstruction in the young child”. In: *Current opinion in pediatrics* 27.1 (2015), pp. 82–91.

[35] Anastasios D Georgoulis et al. “Three-dimensional tibiofemoral kinematics of the anterior cruciate ligament-deficient and reconstructed knee during walking”. In: *The American journal of sports medicine* 31.1 (2003), pp. 75–79.

[36] Pedro Augusto Gondim Teixeira et al. “Evidence-based recommendations for musculoskeletal kinematic 4D-CT studies using wide area-detector scanners: a phantom study with cadaveric correlation”. In: *European radiology* 27 (2017), pp. 437–446.

[37] Alberto Grassi et al. “No differences in knee kinematics between active and passive flexion-extension movement: an intra-operative kinematic analysis performed during total knee arthroplasty”. In: *Journal of Experimental Orthopaedics* 7.1 (2020), pp. 1–8.

[38] Letha Y Griffin et al. “Noncontact anterior cruciate ligament injuries: risk factors and prevention strategies”. In: *JAAOS-Journal of the American Academy of Orthopaedic Surgeons* 8.3 (2000), pp. 141–150.

[39] Edward S Grood and Wilfredo J Suntay. “A joint coordinate system for the clinical description of three-dimensional motions: application to the knee”. In: (1983).

[40] Ayman Habib. *Force reporter tool OpenSim*. URL: https://opensim-org.github.io/opensim-moco-site/docs/1.1.0/html_user/classOpenSim_1_1ForceReporter.html. (accessed: 26.04.2023).

[41] Chen Hao. *Code Chen et al.* URL: https://github.com/BioMechTools/QDKCT. (accessed: 22.04.2023).

[42] KCT Ho et al. “Computed tomography analysis of knee pose and geometry before and after total knee arthroplasty”. In: *Journal of biomechanics* 45.13 (2012), pp. 2215–2221.

[43] A.M. Hollister et al. “The axes of rotation of the knee”. In: *Clin Orthop Relat Res* 290 (1993), pp. 259–268.

[44] Berthold KP Horn. “Closed-form solution of absolute orientation using unit quaternions”. In: *Josa a* 4.4 (1987), pp. 629–642.

[45] Futoshi Ikuta et al. “Knee kinematics of severe medial knee osteoarthritis showed tibial posterior translation and external rotation: a cross-sectional study”. In: *Aging Clinical and Experimental Research* 32 (2020), pp. 1767–1775.

[46] The MathWorks Inc. *MATLAB version: 9.13.0 (R2022b)*. Natick, Massachusetts, United States, 2022. URL: https://www.mathworks.com.

[47] Wan Noorshahida Mohd Isa. “Analysis on spatial and temporal features of gait kinematics”. In: *Fourth IEEE Workshop on Automatic Identification Advanced Technologies (AutoID’05)*. IEEE. 2005, pp. 130–133.

[48] Sarah M Jenkins et al. “Rehabilitation after anterior cruciate ligament injury: Review of current literature and recommendations”. In: *Current Reviews in Musculoskeletal Medicine* 15.3 (2022), pp. 170–179.

[49] Christopher C Kaeding, Benjamin Léger-St-Jean, and Robert A Magnussen. “Epidemiology and diagnosis of anterior cruciate ligament injuries”. In: *Clinics in sports medicine* 36.1 (2017), pp. 1–8.

[50] Stefan Klein et al. “Elastix: a toolbox for intensity-based medical image registration”. In: *IEEE transactions on medical imaging* 29.1 (2009), pp. 196–205.

[51] Michal Kozanek et al. “Tibiofemoral kinematics and condylar motion during the stance phase of gait”. In: *Journal of biomechanics* 42.12 (2009), pp. 1877–1884.

[52] Yune Kwong et al. “F our-dimensional computed tomography (4DCT): A review of the current status and applications”. In: *Journal of medical imaging and radiation oncology* 59.5 (2015), pp. 545–554.

[53] C.G. Lane, R. Warren, and A.D. Pearle. “The pivot shift”. In: *J Am Acad Orthop Surg* 16.12 (2008), pp. 679–688.

[54] Rachel L Lenhart et al. “Prediction and validation of load-dependent behavior of the tibiofemoral and patellofemoral joints during movement”. In: *Annals of biomedical engineering* 43 (2015), pp. 2675–2685.

[55] Guoan Li et al. “The cartilage thickness distribution in the tibiofemoral joint and its correlation with cartilage-to-cartilage contact”. In: *Clinical biomechanics* 20.7 (2005), pp. 736–744.

[56] Adam Lim et al. “Motion artifact correction in fetal MRI based on a Generative Adversarial network method”. In: *Biomedical Signal Processing and Control* 81 (2023), p. 104484.

[57] Kenneth M Lin, Evan W James, and Robert G Marx. “Who Needs ACL Surgery?” In: *Advances in Knee Ligament and Knee Preservation Surgery* (2022), pp. 1–9.

[58] Robert A Magnussen, James L Carey, and Kurt P Spindler. “Does autograft choice determine intermediate-term outcome of ACL reconstruction?” In: *Knee Surgery, Sports Traumatology, Arthroscopy* 19 (2011), pp. 462–472.

[59] K Markatos et al. “The anatomy of the ACL and its importance in ACL reconstruction”. In: *Eur J Orthop Surg Traumatol* 23.7 (2013), pp. 747–752.

[60] William Micheo, Liza Hernández, and Carlos Seda. “Evaluation, management, rehabilitation, and prevention of anterior cruciate ligament injury: current concepts”. In: *PM&R* 2.10 (2010), pp. 935–944.

[61] Daniel L Miranda et al. “Automatic determination of anatomical coordinate systems for three-dimensional bone models of the isolated human knee”. In: *Journal of biomechanics* 43.8 (2010), pp. 1623–1626.

[62] Johnny UV Monu and Thomas L Pope Jr. “MAGNETIC RESONANCE IMAGING OF THE KNEE”. In: *Orthopedics* 17.11 (1994), p. 1067.

[63] Yutaro Morishige et al. “Four-dimensional computed tomographic analysis of screw home movement in patients with anterior cruciate ligament deficient knee—a 3D-3D registration technique”. In: *Skeletal Radiology* 51.8 (2022), pp. 1679–1685.

[64] Faezeh Moshfeghifar et al. “A direct geometry processing cartilage generation method using segmented bone models from datasets with poor cartilage visibility”. In: *Computational Biomechanics for Medicine: Towards Translation and Better Patient Outcomes*. Springer, 2022, pp. 155–169.

[65] M K Mulcahey. *Knee anatomy*. URL: `https://orthoinfo.aaos.org/en/diseases--conditions/common-knee-injuries/`. (accessed: 22.05.2023).

[66] M.M Murray, P. Vavken, and B.C. Fleming. “The ACL handbook”. In: *NY: Springer* (2013).

[67] Volker Musahl and Jon Karlsson. “Anterior cruciate ligament tear”. In: *New England Journal of Medicine* 380.24 (2019), pp. 2341–2348.

[68] Volker Musahl et al. *ACL surgery: when to do it?* 2020.

[69] Christopher V Nagelli and Timothy E Hewett. “Should return to sport be delayed until 2 years after anterior cruciate ligament reconstruction? Biological and functional considerations”. In: *Sports Medicine* 47.2 (2017), pp. 221–232.

[70] F.R. Noyes. “The function of the human anterior cruciate ligament and analysis of single-and double-bundle graft reconstructions”. In: *Sports Health* 1.1 (2009), pp. 66–75.

[71] Todd Pataky. *SPM1d*. URL: `https://spm1d.org`. (accessed: 29.05.2023).

[72] *Python*. URL: `https://www.python.org/` (visited on 04/10/2023).

[73] HK Ramakrishnan and MP Kadaba. “On the estimation of joint kinematics during gait”. In: *Journal of biomechanics* 24.10 (1991), pp. 969–977.

[74] Jean-Baptiste Renault. *Code Renault et al.* URL: `https://github.com/renaultJB/GIBOC-Knee-Coordinate-System`. (accessed: 22.04.2023).

[75] Jean-Baptiste Renault et al. “Articular-surface-based automatic anatomical coordinate systems for the knee bones”. In: *Journal of Biomechanics* 80 (2018), pp. 171–178.

[76] Per A Renström. “Eight clinical conundrums relating to anterior cruciate ligament (ACL) injury in sport: recent evidence and a personal reflection”. In: *British journal of sports medicine* 47.6 (2013), pp. 367–372.

[77] SI Ringleb et al. “The effect of ankle ligament damage and surgical reconstructions on the mechanics of the ankle and subtalar joints revealed by three-dimensional stress MRI”. In: *Journal of orthopaedic research* 23.4 (2005), pp. 743–749.

[78] Luigi Sabatini et al. “Medial pivot in total knee arthroplasty: literature review and our first experience”. In: *Clinical Medicine Insights: Arthritis and Musculoskeletal Disorders* 11 (2018), p. 1179544117751431.

[79] Pierce E Scranton Jr et al. “A review of selected noncontact anterior cruciate ligament injuries in the National Football League”. In: *Foot & ankle international* 18.12 (1997), pp. 772–776.

[80] Ajay Seth et al. “OpenSim: Simulating musculoskeletal dynamics and neuromuscular control to study human and animal movement”. In: *PLoS computational biology* 14.7 (2018), e1006223.

[81] Frances T Sheehan. “The finite helical axis of the knee joint (a non-invasive in vivo study using fast-PC MRI)”. In: *Journal of biomechanics* 40.5 (2007), pp. 1038–1047.

[82] James R Slauterbeck et al. “The menstrual cycle, sex hormones, and anterior cruciate ligament injury”. In: *Journal of athletic training* 37.3 (2002), p. 275.

[83] Colin Smith. *Forsim Tool*. URL: https://github.com/clnsmith/opensim-jam/blob/master/src/ForsimTool.h. (accessed: 22.04.2023).

[84] Colin Smith. *Joint Mechanics tool*. URL: https://github.com/clnsmith/opensim-jam/blob/master/src/JointMechanicsTool.h. (accessed: 22.04.2023).

[85] Colin R Smith, Scott CE Brandon, and Darryl G Thelen. “Can altered neuromuscular coordination restore soft tissue loading patterns in anterior cruciate ligament and menisci deficient knees during walking?” In: *Journal of Biomechanics* 82 (2019), pp. 124–133.

[86] K Sri-Ram et al. “The incidence of secondary pathology after anterior cruciate ligament rupture in 5086 patients requiring ligament reconstruction”. In: *The bone & joint journal* 95.1 (2013), pp. 59–64.

[87] Nicholas Stergiou et al. “Tibial rotation in anterior cruciate ligament (ACL)-deficient and ACL-reconstructed knees: a theoretical proposition for the development of osteoarthritis”. In: *Sports medicine* 37 (2007), pp. 601–613.

[88] Scott Tashman et al. “Dynamic function of the ACL-reconstructed knee during running”. In: *Clinical Orthopaedics and Related Research®* 454 (2007), pp. 66–73.

[89] Christophe Van Dijck et al. “Statistical shape model-based prediction of tibiofemoral cartilage”. In: *Computer methods in biomechanics and biomedical engineering* 21.9 (2018), pp. 568–578.

[90] Kelly J Vazquez, Jacob T Andreae, and Corinne R Henak. “Cartilage-on-cartilage cyclic loading induces mechanical and structural damage”. In: *Journal of the mechanical behavior of biomedical materials* 98 (2019), pp. 262–267.

[91] Jian-ping Wang et al. “A data process of human knee joint kinematics obtained by motion-capture measurement”. In: *BMC medical informatics and decision making* 21.1 (2021), pp. 1–18.

[92] G Wu and Z Ladin. “Limitations of quasi-static estimation of human joint loading during locomotion”. In: *Medical and Biological Engineering and Computing* 34 (1996), pp. 472–476.

[93] Ji Hyeon Yim et al. “Anterior translation and rotational stability of anterior cruciate ligament-deficient knees during walking: speed and turning direction”. In: *Journal of Orthopaedic Science* 20 (2015), pp. 155–162.

[94] Stefano Zaffagnini et al. “Comparison of stability and kinematics of the natural knee versus a PS TKA with a ‘third condyle’”. In: *Knee Surgery, Sports Traumatology, Arthroscopy* 22 (2014), pp. 1778–1785.

A

Registration

Multiple difficulties arose during the registration of the tibia. The first section of this chapter describes why this registration is more complex than that of the femur and patella. The second section describes the process of deciding on a workflow for the registration of the tibia.

A.1. Difficulties

Compared to the femur and patella, the movement of the tibia is more extensive. Therefore, the tibia's dynamic scans contain more movement artefacts, making the processing of these images more complex than those of the femur and patella and the static images. The most visible artefacts are the hazes and double images along the shaft (see figure 4.3 in chapter 4). These artefacts became worse when moving more distally as the movement of the bone becomes faster when moving further from the centre of rotation. As an automatic segmentation that would exclude these artefacts was too elaborate for the duration of this thesis, and including these artefacts would interfere with the registrations, we decided to cut off (part of) the tibial shaft before registration. A downside is that we only had the tibial head to perform a registration with. In addition to these artefacts, the dynamic scans seem more sizable than the static scans (see figure A.1).

A.2. Workflow definition

Initially, we tried using the ICP algorithm from the Trimesh package in Python directly, as this was the workflow used for the femur and patella, and another member of the research group had also used this for the tibial registration of segmented 4DCT images. However, this did not work. A possible explanation is that, in contrast to the other researcher, we segmented the data automatically, which may be less accurate than the manual segmentation. Moreover, we decided to cut off (part of) the tibial shaft, thereby reducing the surface that could be used for the registration.

The ICP algorithm mentioned before, requires a relatively close initial position to prevent it from finding a local minimum instead of the global one (see section 4.4 in chapter 4). As this is a common problem with the ICP algorithm, the Trimesh package also offers registration technique that includes a pre-registration step. This technique starts by defining the inertial axis of the two meshes and aligns these as an initial registration which is then refined by applying the ICP algorithm. However, the orientation of the inertial axis defined for the two meshes differed, causing the ICP algorithm to find a local minimum again (see figure A.2). Other registration techniques offered in the Trimesh package were unsuitable as all were non-rigid, which was undesirable as the geometry should not be changed because it was patient-specific.

As the Trimesh package did not offer a technique suitable for our application, we started looking into the techniques offered in the 3D Slicer software, which was already used for the segmentations. Limited options were available for the registration of meshes in 3D Slicer, and most apply the ICP algorithm directly, resulting in erroneous results. An option was to manually transform the mesh in 3D Slicer and extract the transformation matrix to apply that as an initial guess in the Trimesh ICP registration. Subsequently, the resulting transformation matrix could be used as an initial guess for the

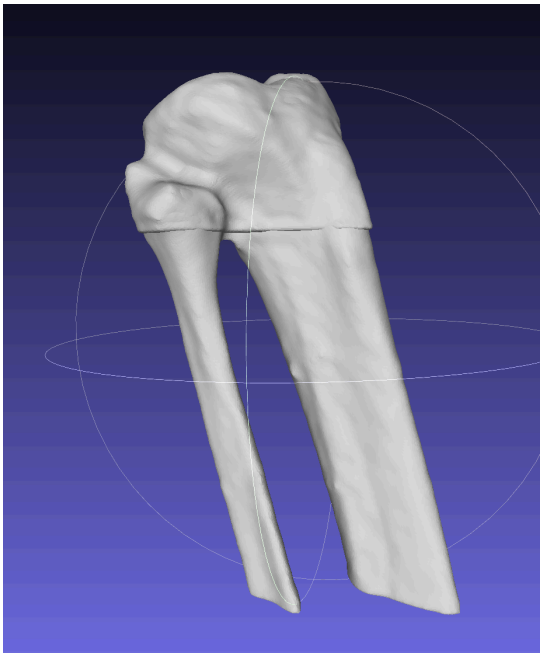

Figure A.1: Final registration of the static mesh onto the dynamic mesh of the tibia where the size difference between the two meshes can be seen.

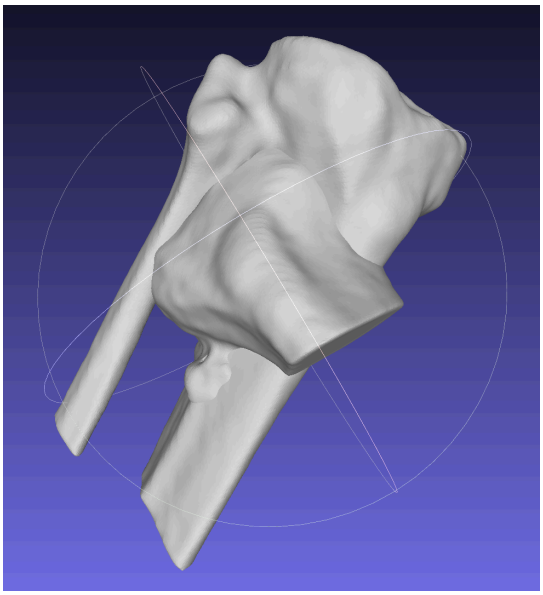

Figure A.2: Result from the Trimesh technique using the alignment of the inertial axes and the ICP algorithm.

mesh in the following image. Unfortunately, this resulted in long computational times or faulty results. We later discovered that this was due to the different definitions of the transformation matrices between the programs, but the registration was already performed at that point. In addition, the manual work required for this option was undesired as we aimed to automate the process as much as possible.

3D Slicer also offers other registration options, such as a registration based on images in the Elastix toolbox [50]. However, this tool does not allow for the registration of several segments in one image. Moreover, the images, like the segmented mesh files, also contain movement artefacts, potentially even more than the mesh files. Therefore, this technique may also result in problems. Nonetheless, we tried to contact the developers of this tool to discuss any possibilities of using this tool or if they had other suggestions but did not get a response.

We also contacted the research group of Prof. Verdonschot at Radboud University to discuss the possibilities. Through this group, we spoke with Ms Boot, who is currently doing a PhD, which focuses on evaluating surgical techniques for the knee using 4DCT. While planning a meeting with her, we continued exploring the registration options. We found the Surface Fragments Registration technique in 3D Slicer, which includes a pre-registration [44] and a non-rigid ICP algorithm and gave a good result [4]. This pre-registration technique allowed for a better initial fit than the pre-registration using the inertial axes in Trimesh did. Because of this, the ICP could find the global minimum, resulting in an adequate registration. However, it used a non-rigid ICP, which was undesire. Therefore, a rigid ICP was subsequently applied between the original and transformed static scan to eliminate the changes in geometry, which was possible because the geometries were now the same, except for some minor changes. In the meeting with Ms Boot, she said that she did recognize the problems and that the automated registration is complex due to the artefacts. Finally, we concluded that this was the best approach, with the current possibilities.

B

Hausdorff distances

The Hausdorff distances between the segmented dynamic mesh and the registered static scan were determined for each orientation to gain insight into the quality of the registration. Figure B.2 shows the heat maps of the Hausdorff distances for the left knee of patient001 to gain insight into the locations that differ most. Tables B.1 to B.6 show the mean Hausdorff distances and root mean square (RMS) errors calculated for each bone separately.

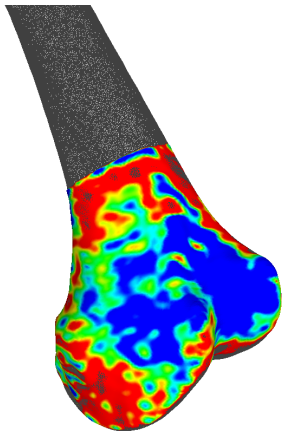

(a) Femur, anterior side.

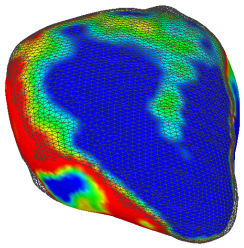

(b) Patella, anterior side.

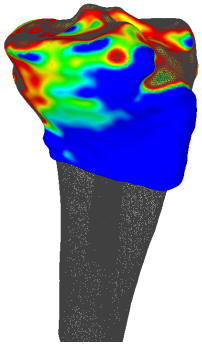

(c) Tibia, anterior side.

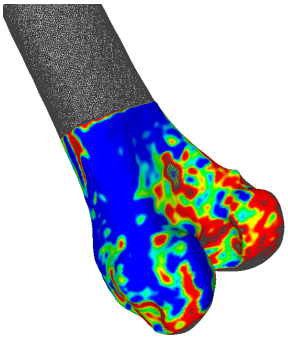

(a) Femur, posterior side.

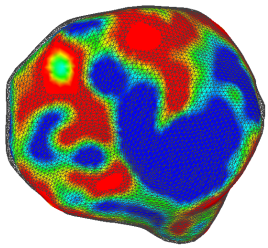

(b) Patella, posterior side.

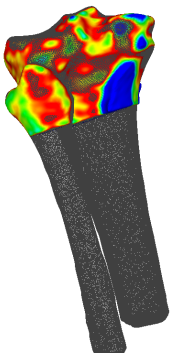

(c) Tibia, posterior side.

Figure B.2: Heat map of the Hausdorff distances for the left knee of patient 001.
The coloured mesh is the original segmentation, and the wireframe is the registered static scan. Blue represents the locations with the smallest Hausdorff distance, and red is the largest.

B.1. Left femur

Table B.1: Mean Hausdorff distances and RMS error for the left femur [mm].

	Patient001		Patient002		Patient003		Patient004		Patient005		Patient006		Patient008		Patient009	
Image (#)	**Mean**	**RMS**	**Mean**	**RMS**	**Mean**	**RMS**	**Mean**	**RMS**	**Mean**	**RMS**	**Mean**	**RMS**	**Mean**	**RMS**	**Mean**	**RMS**
0	0.46	1.23	0.45	1.22	0.29	1.21	0.30	1.22	0.48	1.92	0.43	1.50	0.43	1.65	0.33	1.28
1	0.43	1.26	0.39	1.24	0.40	1.24	0.32	1.25	0.59	2.13	0.45	1.54	0.44	1.67	0.38	1.30
2	0.44	1.27	0.39	1.24	0.35	1.23	0.33	1.25	0.61	2.16	0.46	1.55	0.47	1.68	0.38	1.30
3	0.46	1.28	0.38	1.24	0.33	1.22	0.33	1.25	0.62	2.17	0.48	1.56	0.46	1.69	0.40	1.31
4	0.45	1.28	0.41	1.25	0.31	1.21	0.32	1.25	0.61	2.17	0.49	1.57	0.46	1.70	0.41	1.32
5	0.47	1.28	0.42	1.26	0.33	1.22	0.33	1.26	0.62	2.19	0.46	1.58	0.47	1.71	0.39	1.32
6	0.48	1.29	0.43	1.27	0.36	1.23	0.33	1.27	0.67	2.26	0.47	1.58	0.47	1.71	0.40	1.31
7	0.51	1.31	0.42	1.27	0.34	1.23	0.34	1.27	0.70	2.29	0.47	1.58	0.51	1.72	0.39	1.32
8	0.51	1.31	0.42	1.27	0.36	1.24	0.33	1.27	0.73	2.34	0.48	1.58	0.48	1.74	0.41	1.34
9	0.52	1.32	0.44	1.28	0.36	1.23	0.34	1.28	0.74	2.36	0.48	1.59	0.48	1.74	0.39	1.34
10	0.51	1.31	0.43	1.28	0.34	1.23	0.33	1.28	0.74	2.36	0.48	1.59	0.49	1.74	0.41	1.34
11	0.43	1.22	0.42	1.21	0.30	1.21	0.31	1.22	0.48	1.94	0.46	1.52	0.44	1.65	0.35	1.28
12	0.51	1.31	0.44	1.28	0.36	1.24	0.34	1.29	0.75	2.37	0.48	1.58	0.50	1.75	0.41	1.35
13	0.51	1.31	0.43	1.28	0.36	1.25	0.34	1.29	0.74	2.36	0.48	1.58	0.51	1.78	0.40	1.35
14	0.44	1.23	0.42	1.23	0.29	1.20	0.29	1.22	0.50	1.95	0.44	1.52	0.44	1.65	0.34	1.28
15	0.39	1.23	0.39	1.21	0.31	1.20	0.34	1.23	0.51	1.97	0.44	1.53	0.44	1.65	0.35	1.28
16	0.39	1.24	0.46	1.24	0.32	1.22	0.30	1.23	0.51	1.99	0.44	1.53	0.44	1.65	0.38	1.29
17	0.41	1.26	0.52	1.31	0.32	1.21	0.31	1.23	0.53	2.01	0.44	1.52	0.46	1.66	0.38	1.28
18	0.43	1.26	0.36	1.22	0.30	1.22	0.31	1.23	0.53	2.03	0.43	1.53	0.44	1.67	0.37	1.28
19	0.42	1.26	0.41	1.24	0.31	1.21	0.32	1.23	0.57	2.06	0.45	1.54	0.45	1.67	0.47	1.31
20	0.42	1.26	0.41	1.24	0.31	1.21	0.35	1.24	0.58	2.09	0.46	1.55	0.46	1.67	0.42	1.30

B.2. Right femur

Table B.2: Mean Hausdorff distances and RMS error for the right femur [mm].

	Patient001		Patient002		Patient003		Patient004		Patient005		Patient006		Patient008		Patient009	
Image (#)	**Mean**	**RMS**	**Mean**	**RMS**	**Mean**	**RMS**	**Mean**	**RMS**	**Mean**	**RMS**	**Mean**	**RMS**	**Mean**	**RMS**	**Mean**	**RMS**
0	0.39	1.17	0.48	1.18	0.32	1.26	0.29	1.23	0.52	1.99	0.49	1.78	0.30	1.29	0.30	1.18
1	0.43	1.24	0.37	1.20	0.38	1.28	0.31	1.27	0.64	2.19	0.52	1.85	0.31	1.30	0.33	1.19
2	0.44	1.25	0.37	1.20	0.34	1.27	0.33	1.27	0.66	2.23	0.53	1.84	0.33	1.30	0.32	1.19
3	0.46	1.26	0.42	1.22	0.40	1.30	0.31	1.27	0.66	2.24	0.54	1.86	0.31	1.31	0.35	1.20
4	0.47	1.27	0.40	1.21	0.39	1.29	0.32	1.28	0.65	2.24	0.55	1.88	0.32	1.31	0.34	1.20
5	0.47	1.26	0.45	1.24	0.36	1.28	0.32	1.28	0.66	2.25	0.55	1.90	0.33	1.31	0.33	1.20
6	0.47	1.26	0.48	1.24	0.36	1.29	0.32	1.29	0.70	2.32	0.55	1.89	0.33	1.31	0.33	1.20
7	0.48	1.27	0.41	1.23	0.35	1.29	0.32	1.29	0.73	2.36	0.56	1.89	0.34	1.32	0.33	1.21
8	0.48	1.27	0.40	1.23	0.37	1.30	0.32	1.29	0.76	2.42	0.56	1.89	0.33	1.32	0.36	1.22
9	0.48	1.27	0.41	1.23	0.36	1.29	0.32	1.29	0.78	2.44	0.57	1.91	0.33	1.32	0.34	1.22
10	0.49	1.28	0.41	1.24	0.37	1.30	0.33	1.30	0.78	2.45	0.57	1.91	0.34	1.33	0.35	1.22
11	0.43	1.22	0.42	1.16	0.33	1.26	0.30	1.23	0.53	2.01	0.53	1.80	0.31	1.29	0.31	1.18
12	0.49	1.28	0.41	1.24	0.38	1.31	0.33	1.31	0.79	2.46	0.56	1.89	0.34	1.33	0.36	1.22
13	0.48	1.27	0.41	1.24	0.39	1.32	0.34	1.31	0.79	2.46	0.55	1.88	0.35	1.33	0.35	1.22
14	0.49	1.22	0.44	1.18	0.34	1.26	0.31	1.24	0.56	2.04	0.52	1.82	0.31	1.30	0.31	1.18
15	0.39	1.20	0.38	1.18	0.33	1.26	0.33	1.25	0.56	2.06	0.52	1.83	0.31	1.29	0.31	1.18
16	0.40	1.22	0.35	1.16	0.37	1.27	0.30	1.26	0.59	2.09	0.52	1.83	0.31	1.29	0.34	1.19
17	0.43	1.23	0.36	1.17	0.36	1.27	0.30	1.26	0.59	2.10	0.51	1.83	0.31	1.29	0.31	1.18
18	0.45	1.24	0.36	1.19	0.34	1.27	0.30	1.26	0.71	2.13	0.53	1.84	0.31	1.29	0.31	1.18
19	0.43	1.24	0.38	1.19	0.36	1.27	0.32	1.26	0.61	2.12	0.52	1.84	0.33	1.30	0.48	1.22
20	0.42	1.24	0.39	1.20	0.33	1.27	0.32	1.27	0.61	2.15	0.53	1.86	0.32	1.30	0.34	1.19

B.3. Left patella

Table B.3: Mean Hausdorff distances and RMS error for the left patella [mm].

	Patient001		Patient002		Patient003		Patient004		Patient005		Patient006		Patient008		Patient009	
Image (#)	**Mean**	**RMS**	**Mean**	**RMS**	**Mean**	**RMS**	**Mean**	**RMS**	**Mean**	**RMS**	**Mean**	**RMS**	**Mean**	**RMS**	**Mean**	**RMS**
0	0.42	0.52	0.30	0.33	0.15	0.19	0.14	0.19	0.13	0.16	0.16	0.18	0.24	0.38	0.14	0.17
1	0.24	0.31	0.22	0.26	0.24	0.30	0.13	0.17	0.19	0.23	0.25	0.32	0.21	0.31	0.21	0.29
2	0.18	0.22	0.21	0.26	0.22	0.29	0.15	0.21	0.21	0.26	0.25	0.33	0.23	0.32	0.22	0.28
3	0.20	0.26	0.23	0.28	0.18	0.21	0.17	0.21	0.25	0.31	0.27	0.36	0.22	0.33	0.21	0.28
4	0.20	0.25	0.23	0.28	0.16	0.19	0.16	0.20	0.27	0.35	0.28	0.37	0.24	0.33	0.28	0.35
5	0.21	0.26	0.24	0.30	0.19	0.24	0.17	0.21	0.29	0.37	0.28	0.37	0.26	0.35	0.19	0.24
6	0.21	0.25	0.22	0.28	0.20	0.26	0.16	0.20	0.32	0.40	0.31	0.44	0.23	0.31	0.19	0.26
7	0.23	0.27	0.26	0.33	0.17	0.22	0.18	0.22	0.29	0.38	0.35	0.47	0.35	0.46	0.19	0.25
8	0.22	0.27	0.21	0.26	0.28	0.41	0.17	0.22	0.32	0.42	0.36	0.48	0.25	0.35	0.23	0.31
9	0.22	0.27	0.23	0.30	0.34	0.49	0.18	0.22	0.37	0.48	0.37	0.48	0.24	0.33	0.26	0.35
10	0.22	0.27	0.22	0.31	0.18	0.24	0.18	0.22	0.38	0.50	0.36	0.47	0.25	0.34	0.28	0.36
11	0.38	0.46	0.26	0.29	0.16	0.20	0.16	0.23	0.13	0.16	0.19	0.23	0.24	0.38	0.15	0.18
12	0.22	0.27	0.21	0.27	0.28	0.37	0.19	0.25	0.41	0.53	0.37	0.48	0.31	0.42	0.26	0.34
13	0.21	0.26	0.19	0.25	0.23	0.30	0.20	0.26	0.41	0.53	0.37	0.49	0.32	0.43	0.26	0.34
14	0.35	0.43	0.30	0.33	0.15	0.19	0.13	0.18	0.14	0.18	0.16	0.19	0.25	0.40	0.15	0.18
15	0.36	0.53	0.20	0.24	0.16	0.22	0.17	0.21	0.14	0.19	0.16	0.19	0.25	0.41	0.13	0.17
16	0.24	0.33	0.30	0.37	0.15	0.19	0.12	0.16	0.13	0.17	0.17	0.19	0.25	0.40	0.35	0.47
17	0.26	0.40	0.31	0.37	0.16	0.20	0.13	0.17	0.15	0.20	0.18	0.21	0.27	0.41	0.28	0.35
18	0.21	0.33	0.21	0.25	0.15	0.18	0.13	0.17	0.15	0.21	0.16	0.20	0.24	0.38	0.18	0.22
19	0.25	0.36	0.29	0.33	0.14	0.18	0.13	0.18	0.20	0.26	0.18	0.22	0.25	0.37	0.21	0.25
20	0.17	0.22	0.22	0.26	0.15	0.18	0.19	0.26	0.17	0.23	0.20	0.25	0.28	0.40	0.28	0.38

B.4. Right patella

Table B.4: Mean Hausdorff distances and RMS error for the right patella [mm].

	Patient001		Patient002		Patient003		Patient004		Patient005		Patient006		Patient008		Patient009	
Image (#)	**Mean**	**RMS**	**Mean**	**RMS**	**Mean**	**RMS**	**Mean**	**RMS**	**Mean**	**RMS**	**Mean**	**RMS**	**Mean**	**RMS**	**Mean**	**RMS**
0	0.29	0.34	0.32	0.36	0.14	0.17	0.13	0.16	0.20	0.31	0.26	0.38	0.13	0.18	0.11	0.14
1	0.16	0.22	0.29	0.34	0.20	0.25	0.13	0.17	0.26	0.34	0.22	0.30	0.17	0.23	0.34	0.45
2	0.17	0.23	0.27	0.33	0.15	0.19	0.16	0.20	0.28	0.36	0.20	0.25	0.19	0.26	0.24	0.31
3	0.30	0.41	0.27	0.32	0.16	0.20	0.16	0.19	0.27	0.32	0.23	0.30	0.18	0.25	0.21	0.26
4	0.21	0.27	0.31	0.39	0.21	0.27	0.18	0.22	0.30	0.37	0.21	0.27	0.22	0.30	0.20	0.25
5	0.22	0.29	0.30	0.39	0.20	0.25	0.17	0.21	0.31	0.39	0.20	0.26	0.22	0.31	0.21	0.25
6	0.23	0.29	0.34	0.46	0.20	0.25	0.19	0.26	0.34	0.43	0.28	0.38	0.21	0.28	0.18	0.23
7	0.22	0.29	0.25	0.33	0.16	0.20	0.18	0.23	0.33	0.43	0.35	0.48	0.25	0.35	0.18	0.23
8	0.22	0.29	0.23	0.31	0.26	0.36	0.18	0.22	0.38	0.48	0.29	0.39	0.21	0.28	0.27	0.34
9	0.22	0.29	0.24	0.33	0.30	0.41	0.18	0.23	0.42	0.54	0.29	0.38	0.21	0.29	0.32	0.44
10	0.23	0.29	0.26	0.35	0.25	0.35	0.18	0.23	0.44	0.55	0.29	0.38	0.26	0.38	0.22	0.28
11	0.39	0.47	0.32	0.37	0.15	0.18	0.16	0.19	0.20	0.31	0.28	0.40	0.14	0.18	0.14	0.16
12	0.23	0.29	0.24	0.32	0.26	0.34	0.19	0.26	0.46	0.58	0.30	0.39	0.28	0.37	0.27	0.34
13	0.23	0.31	0.21	0.27	0.29	0.38	0.26	0.37	0.46	0.58	0.29	0.39	0.32	0.43	0.25	0.33
14	0.34	0.39	0.33	0.40	0.17	0.21	0.13	0.16	0.31	0.44	0.23	0.33	0.13	0.17	0.13	0.16
15	0.36	0.50	0.27	0.32	0.20	0.26	0.18	0.22	0.29	0.43	0.22	0.31	0.14	0.18	0.14	0.18
16	0.36	0.49	0.24	0.29	0.16	0.19	0.13	0.17	0.26	0.39	0.21	0.30	0.14	0.17	0.16	0.19
17	0.39	0.53	0.27	0.31	0.20	0.23	0.14	0.18	0.23	0.37	0.21	0.30	0.14	0.18	0.17	0.20
18	0.35	0.48	0.24	0.29	0.15	0.17	0.13	0.16	0.29	0.41	0.21	0.30	0.13	0.17	0.20	0.23
19	0.24	0.30	0.28	0.33	0.18	0.22	0.16	0.20	0.27	0.35	0.21	0.31	0.14	0.19	0.35	0.43
20	0.19	0.25	0.24	0.29	0.15	0.18	0.17	0.21	0.23	0.32	0.27	0.39	0.16	0.21	0.22	0.28

B.5. Left tibia

Table B.5: Mean Hausdorff distances and RMS error for the left tibia [mm].

	Patient001		Patient002		Patient003		Patient004		Patient005		Patient006		Patient008		Patient009	
Image (#)	**Mean**	**RMS**	**Mean**	**RMS**	**Mean**	**RMS**	**Mean**	**RMS**	**Mean**	**RMS**	**Mean**	**RMS**	**Mean**	**RMS**	**Mean**	**RMS**
0	0.99	1.83	0.85	2.21	3.45	5.77	2.42	4.29	0.79	2.16	0.49	1.82	0.37	1.29	0.34	1.31
1	0.88	1.60	0.95	2.38	3.72	5.92	2.41	4.38	3.25	5.24	0.59	1.72	0.46	1.37	3.01	5.20
2	0.97	1.78	1.03	2.42	3.58	5.85	2.96	4.54	1.03	2.19	1.13	2.64	0.57	1.40	1.01	2.09
3	1.11	2.02	1.01	2.41	1.00	2.79	2.46	4.38	1.18	2.37	0.75	1.73	0.69	1.57	0.73	1.64
4	0.47	1.04	1.08	2.45	1.21	2.82	2.47	4.35	0.82	2.07	0.65	1.66	0.65	1.41	1.17	2.41
5	0.47	1.05	1.05	2.40	3.57	5.90	2.74	4.42	0.79	2.03	0.50	1.55	0.81	1.77	0.39	1.27
6	0.60	1.37	1.00	2.34	3.46	5.76	2.53	4.33	0.93	2.05	1.02	2.19	0.52	1.34	0.57	1.38
7	0.62	1.56	1.07	2.36	3.58	5.81	2.48	4.34	1.01	2.05	1.15	2.31	1.46	2.69	0.82	1.59
8	0.61	1.79	1.00	2.31	3.54	5.64	2.61	4.36	1.17	2.19	0.67	1.59	0.45	1.26	1.31	2.32
9	1.20	2.21	1.07	2.25	3.50	5.58	2.54	4.32	1.14	2.28	0.55	1.55	0.47	1.27	1.32	2.70
10	0.65	1.95	1.00	2.19	1.50	2.83	2.44	4.23	1.33	2.31	0.58	1.62	0.55	1.33	0.83	2.10
11	1.16	1.98	0.77	2.12	3.48	5.82	2.55	4.38	0.85	2.20	0.78	1.99	0.37	1.29	0.36	1.32
12	0.68	1.98	0.90	2.05	3.60	5.48	2.85	4.32	0.92	1.89	1.54	2.32	0.72	1.42	0.61	1.72
13	0.63	1.86	0.86	2.04	3.26	5.22	2.73	4.18	1.52	2.22	0.58	1.60	1.22	2.28	0.62	1.76
14	1.28	2.15	0.79	2.13	3.49	5.84	2.46	4.35	0.90	2.19	0.65	1.83	0.37	1.28	0.35	1.31
15	2.91	4.41	0.80	2.18	3.56	5.87	3.02	4.55	0.88	2.18	1.02	2.29	0.37	1.29	0.38	1.32
16	0.85	1.58	0.94	2.24	3.46	5.83	2.45	4.35	0.89	2.20	0.64	1.83	0.44	1.33	0.85	1.79
17	1.63	2.57	1.00	2.24	3.49	5.86	2.42	4.35	0.84	2.17	0.56	1.79	0.78	1.52	0.83	1.85
18	0.87	1.66	0.81	2.23	3.55	5.93	2.57	4.38	0.95	2.20	0.54	1.77	0.75	1.73	0.63	1.54
19	1.10	2.30	1.21	2.36	3.56	5.94	2.44	4.36	0.95	2.20	0.57	1.75	0.63	1.47	0.89	1.71
20	0.50	1.26	1.04	2.32	3.59	5.98	2.82	4.55	1.01	2.22	0.75	1.92	0.90	1.87	3.23	5.15

B.6. Right tibia

Table B.6: Mean Hausdorff distances and RMS error for the right tibia [mm].

	Patient001		Patient002		Patient003		Patient004		Patient005		Patient006		Patient008		Patient009	
Image (#)	**Mean**	**RMS**	**Mean**	**RMS**	**Mean**	**RMS**	**Mean**	**RMS**	**Mean**	**RMS**	**Mean**	**RMS**	**Mean**	**RMS**	**Mean**	**RMS**
0	0.85	1.74	1.01	2.57	0.79	2.54	0.53	1.55	0.52	1.68	0.41	1.47	0.43	1.58	0.38	1.48
1	0.73	1.47	1.56	2.81	0.97	2.64	0.34	1.23	3.59	5.76	0.86	1.97	0.54	1.71	0.93	2.02
2	0.83	1.58	1.58	2.90	0.90	2.60	0.71	1.64	1.23	2.35	0.57	1.47	0.62	1.73	0.49	1.57
3	1.74	2.82	1.14	2.74	0.91	2.58	0.57	1.62	0.91	2.19	1.08	2.17	0.55	1.70	0.76	1.80
4	1.15	2.06	1.30	2.80	1.06	2.59	0.80	1.69	1.12	2.24	0.82	1.69	0.69	1.77	0.57	1.52
5	2.62	3.97	1.56	2.87	0.86	2.52	0.87	1.91	0.86	1.72	0.52	1.40	0.68	1.74	0.45	1.47
6	0.74	1.41	1.39	2.82	0.96	2.50	0.86	1.77	1.12	2.25	1.62	3.29	0.68	1.79	0.53	1.47
7	0.77	1.46	1.21	2.72	0.85	2.45	0.66	1.62	1.42	2.42	1.57	2.72	0.71	1.69	0.52	1.43
8	0.75	1.44	1.39	2.70	1.61	2.91	0.65	1.60	1.25	2.44	1.30	2.68	0.51	1.60	1.73	3.04
9	0.81	1.54	0.89	2.49	1.04	2.29	0.60	1.58	1.11	2.17	0.53	1.41	0.52	1.60	1.19	2.12
10	0.77	1.48	0.96	2.49	1.44	2.75	1.09	1.80	1.49	2.43	0.54	1.38	0.71	1.64	1.39	2.41
11	0.93	1.83	0.99	2.56	0.79	2.54	0.35	1.19	0.53	1.67	0.47	1.49	0.44	1.58	0.41	1.48
12	0.79	1.51	0.98	2.50	1.46	2.38	0.86	1.70	0.47	1.27	0.53	1.43	0.84	1.89	1.18	2.19
13	2.01	2.89	1.14	2.54	0.90	2.05	3.09	4.82	0.45	1.25	0.54	1.45	0.63	1.57	0.74	1.57
14	0.98	1.80	0.98	2.54	0.82	2.56	0.37	1.18	0.65	1.74	0.49	1.51	0.43	1.57	0.40	1.48
15	1.04	1.88	1.05	2.60	0.88	2.58	0.66	1.58	1.09	2.33	0.47	1.46	0.44	1.58	0.40	1.48
16	1.15	2.00	0.98	2.60	0.84	2.58	0.40	1.19	1.13	2.38	0.90	1.88	0.50	1.61	0.84	2.04
17	1.20	2.01	0.98	2.60	0.87	2.59	0.60	1.58	0.99	2.31	0.91	1.81	0.68	1.76	0.56	1.58
18	1.39	2.22	0.92	2.60	0.80	2.56	0.55	1.57	1.48	2.58	0.40	1.46	0.52	1.66	0.59	1.61
19	1.10	1.99	0.94	2.59	0.87	2.61	0.50	1.29	1.25	2.44	0.73	1.97	0.88	2.12	1.27	2.19
20	1.13	2.13	0.94	2.60	0.85	2.64	0.74	1.69	0.95	2.29	0.60	1.54	0.66	1.73	0.63	1.61

C

Patient-specific translations and rotations

Figure C.1 below shows the translations and rotations calculated for each patient plotted against the flexion angle. Figure C.2 shows the differences between the ACLD and uninjured knees for all patients. Patient 002 was excluded due to substantial outliers, which can be seen in figure C.3. Finally, C.4 shows the rotations against the image numbers from which the outliers have been defined for each patient individually.

C.1. Patient-specific translations and rotations

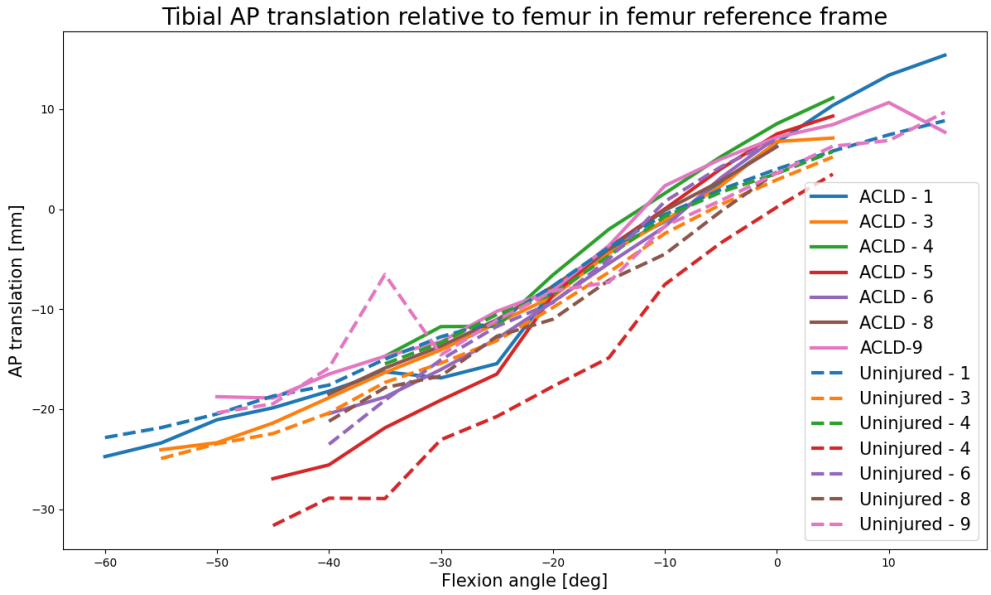

(a) Patient-specific AP translations, anterior positive.

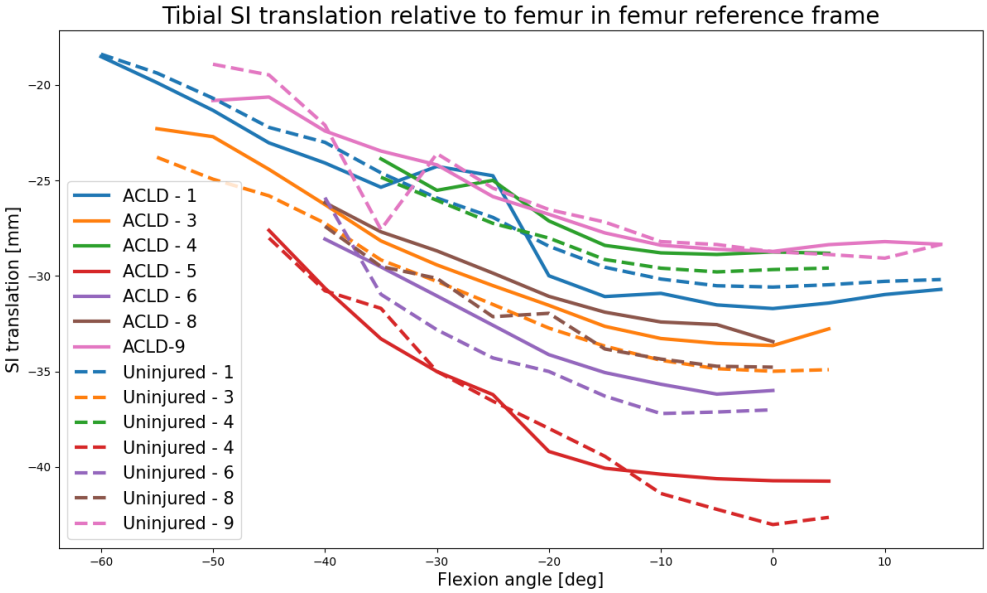

(b) Patient-specific SI translations, superior positive.

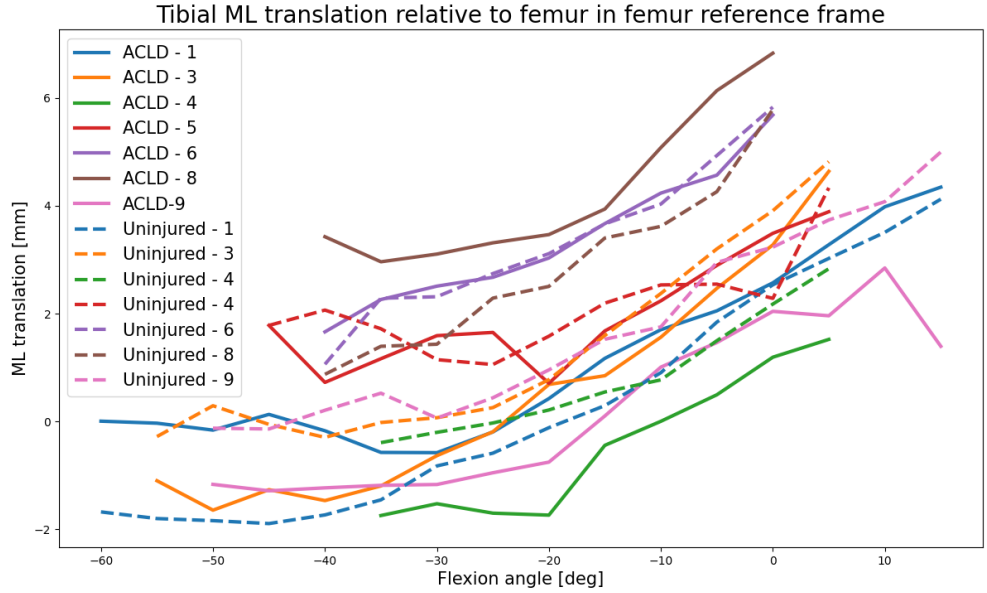

(c) Patient-specific ML translations, medial positive.

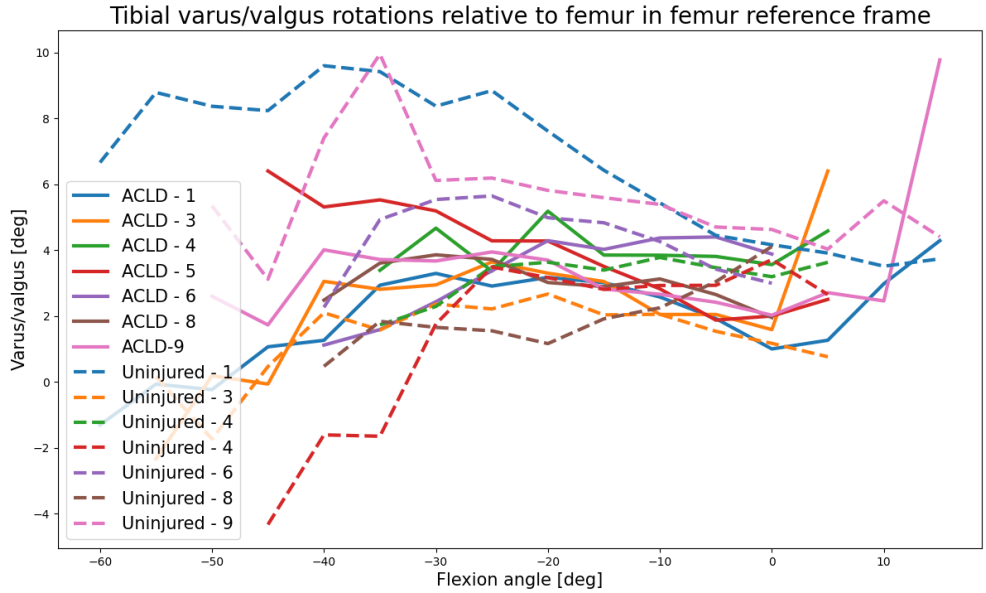

(d) Patient-specific varus/valgus rotations, varus positive.

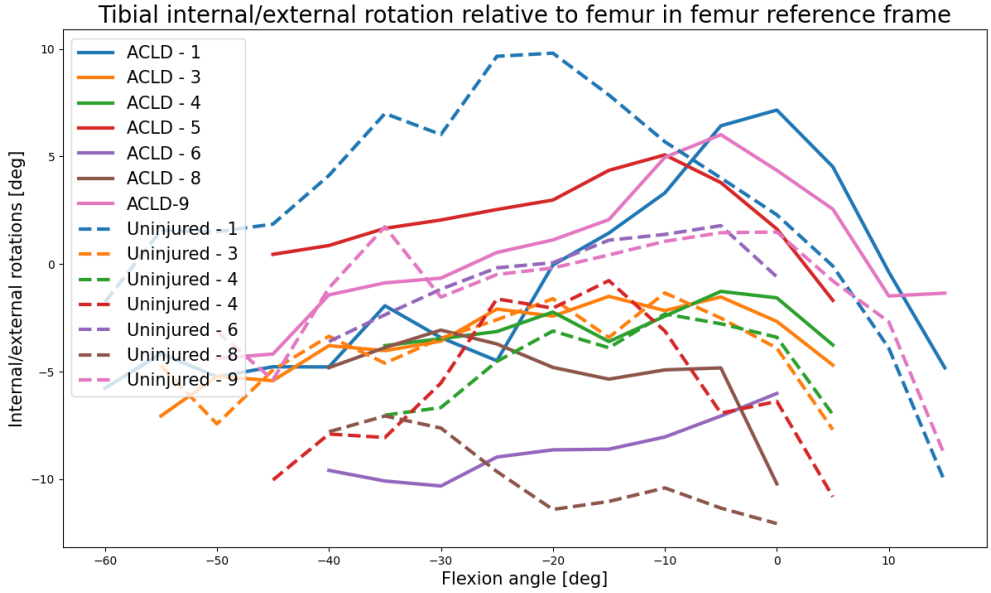

(e) Patient-specific internal/external rotations, internal positive.

Figure C.1: Plots of tibiofemoral translations and rotations for each patient specifically.

C.2. Patient-specific differences in translations and rotations between ACLD and uninjured knees

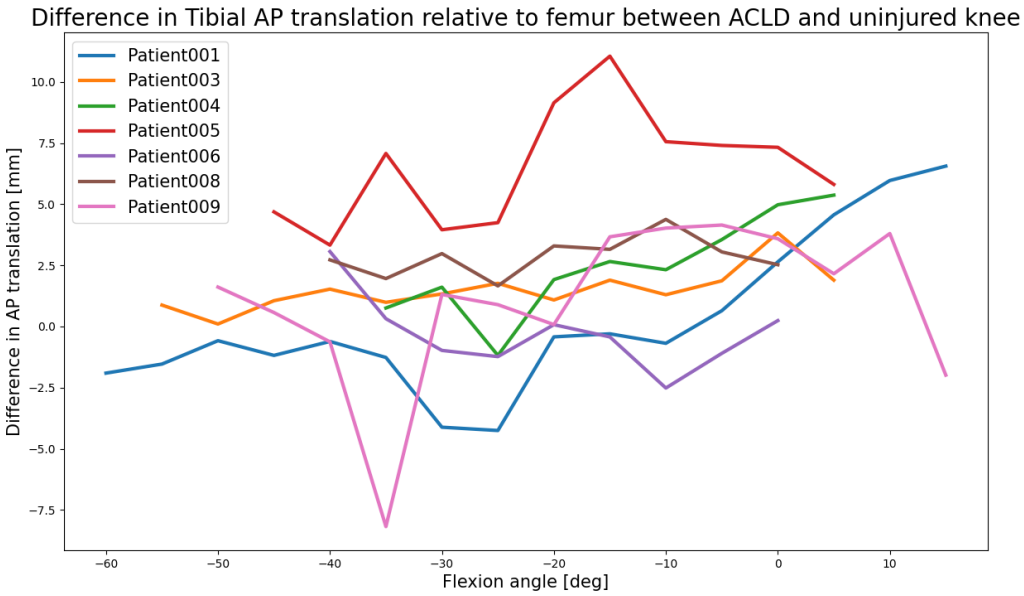

(a) Difference in AP translation between ACLD and uninjured knee, anterior positive.

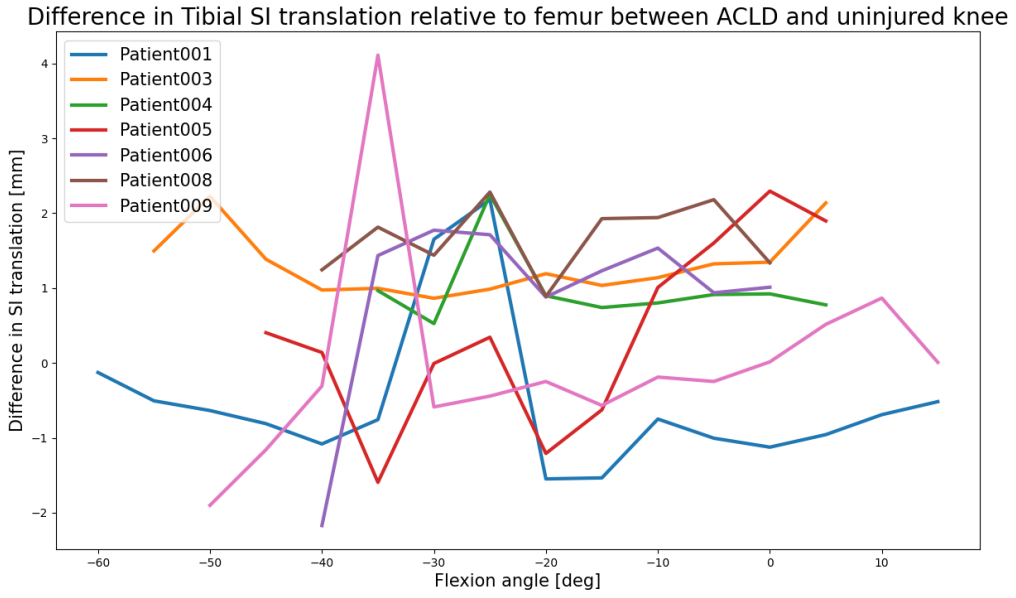

(b) Difference in SI translation between ACLD and uninjured knee, superior positive.

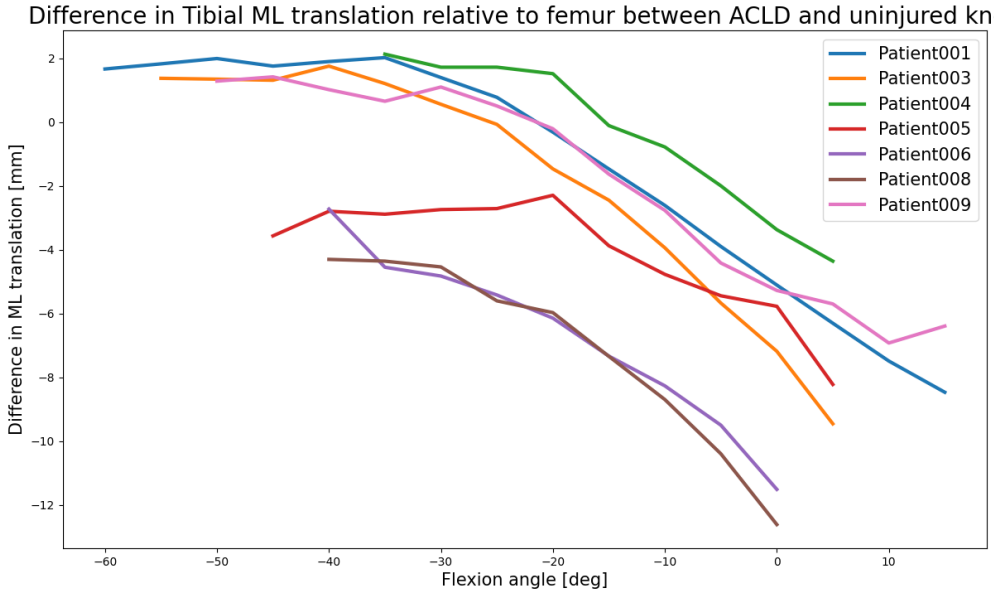

(c) Difference in ML translation between ACLD and uninjured knee, medial positive.

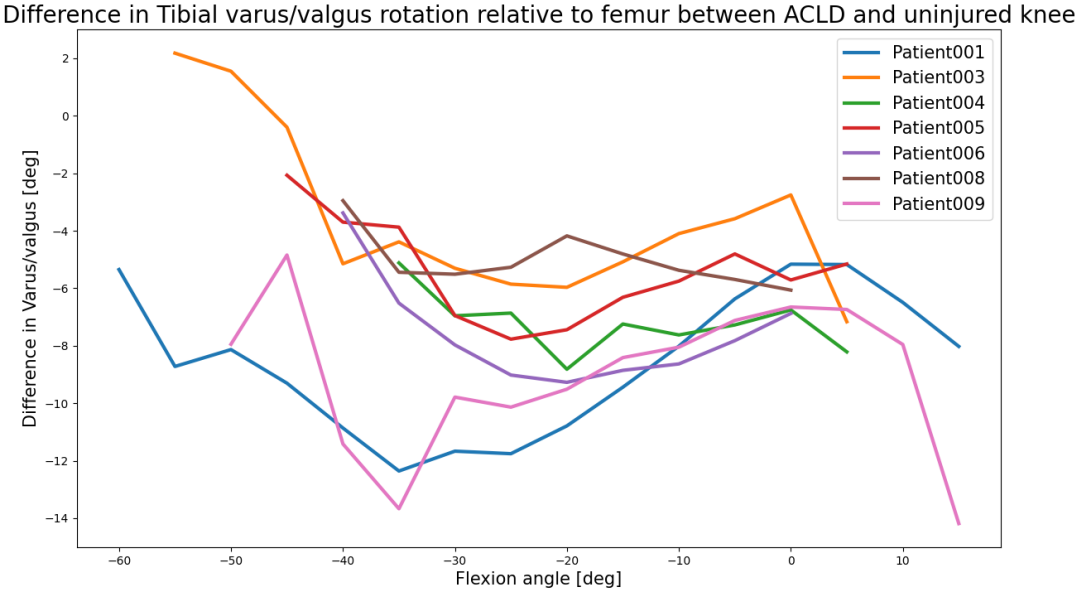

(d) Difference in varus/valgus rotation between ACLD and uninjured knee, varus positive.

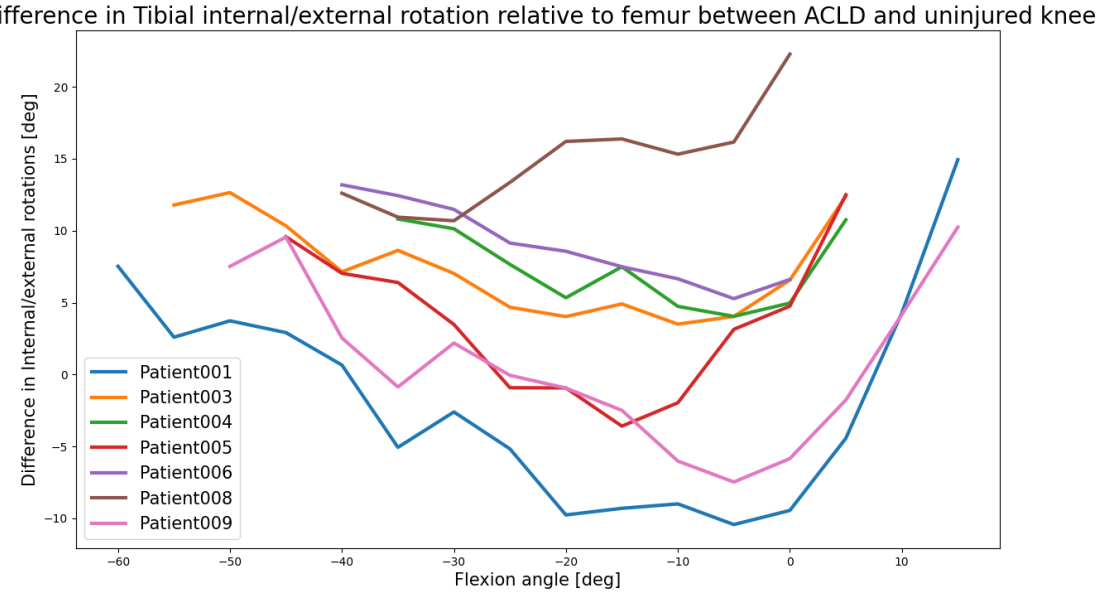

(e) Difference in internal/external rotation between ACLD and uninjured knee, internal positive.

Figure C.2: Plots of the differences in translations and rotations between ACLD and uninjured knee for each patient specifically.

C.3. Translations and rotations for Patient002

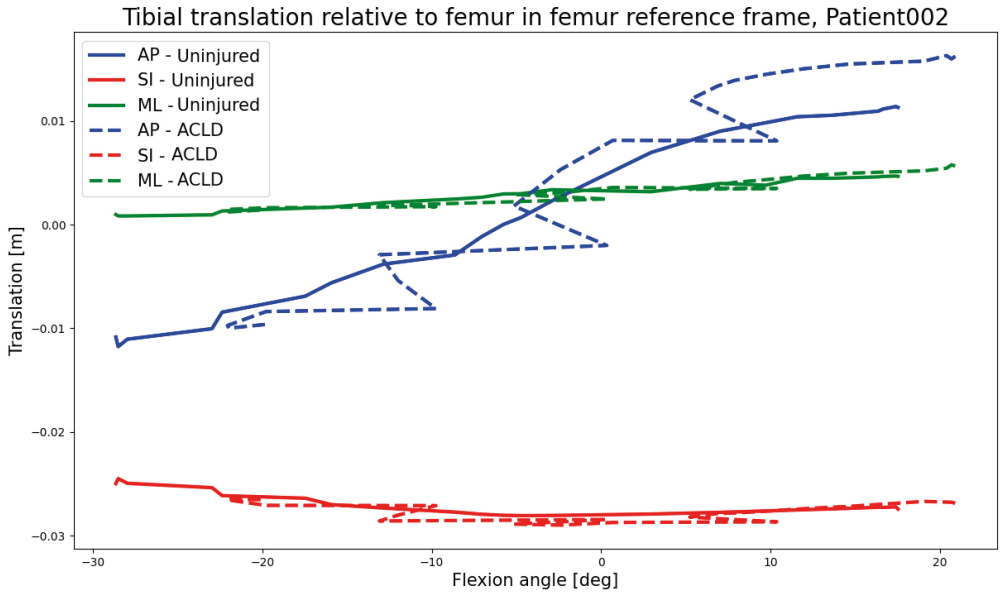

(a) Translations patient002.

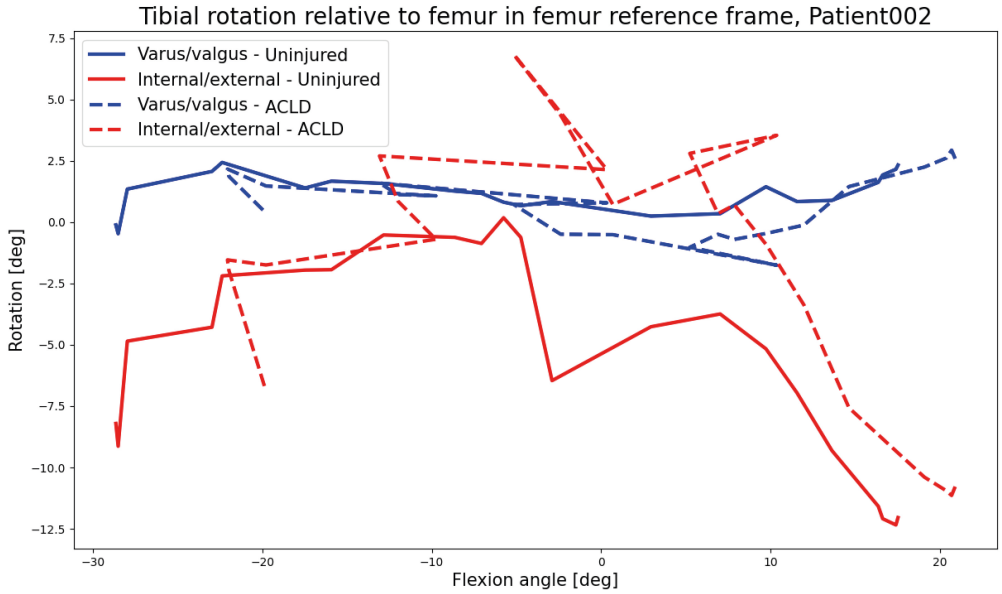

(b) Rotations patient 002.

Figure C.3: Translations and rotations for patient002.

C.4. Patient-specific rotations against image number

Initially, the rotations and translations were plotted against the image number instead of the flexion angles. These plots were used to define the images containing outliers which were excluded from subsequent analysis. The (dotted) lines in the figures represent the data used for analysis, and the dots and stars represent the calculated translations and rotations. Those that differed from the lines were excluded.

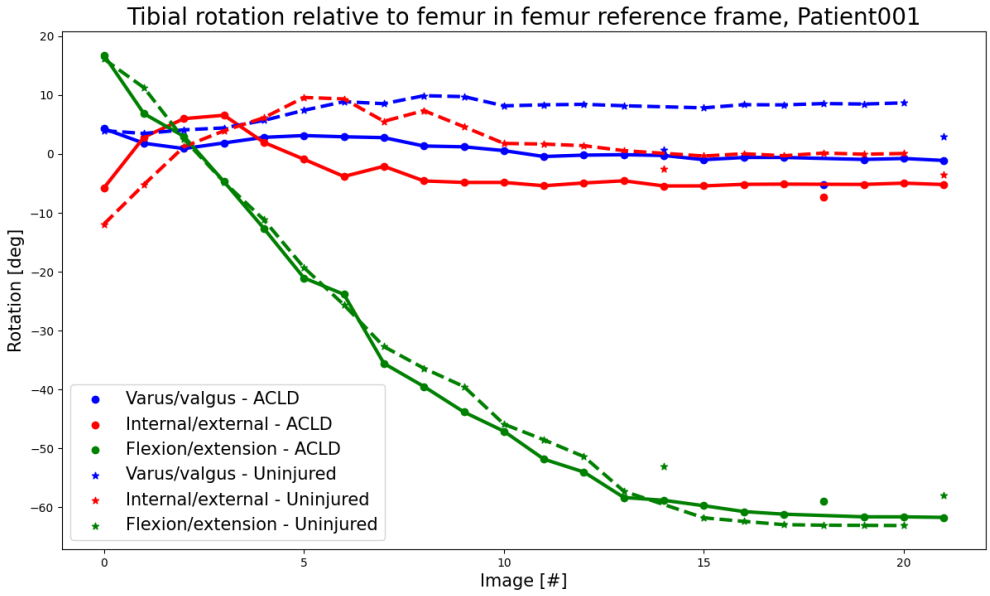

(a) Rotations against image number, patient001.

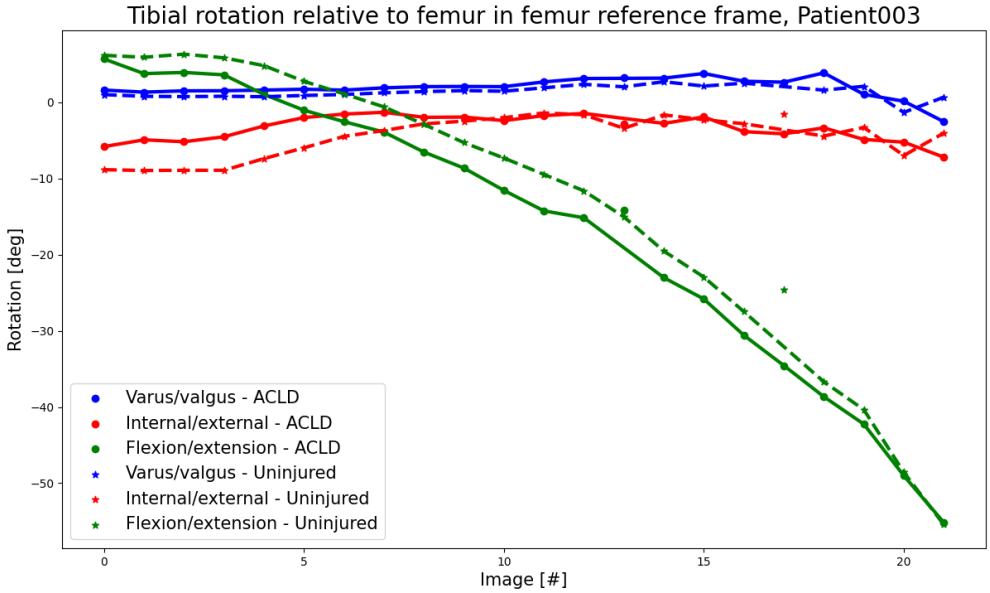

(b) Rotations against image number, patient003.

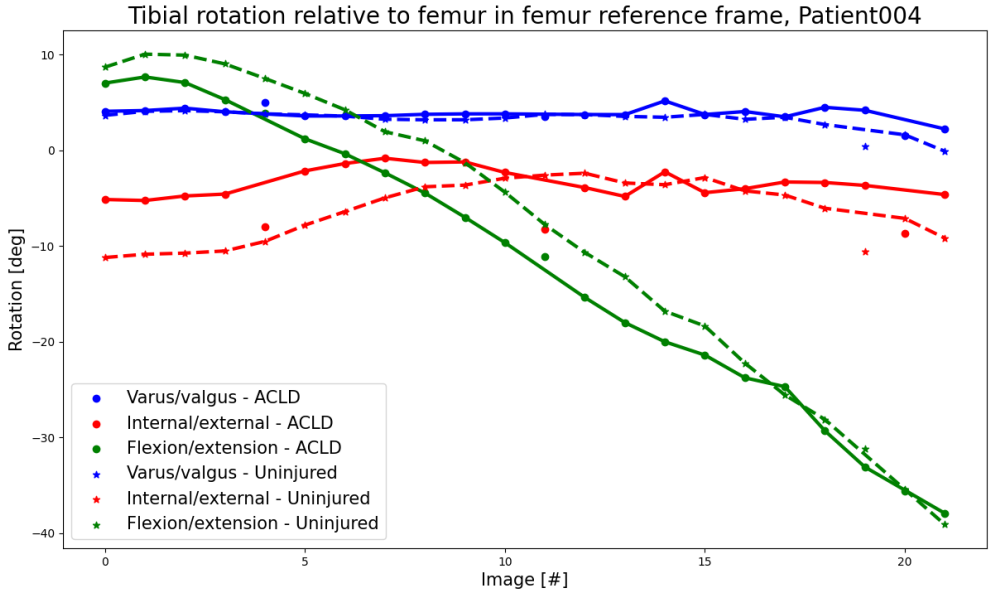

(c) Rotations against image number, patient004.

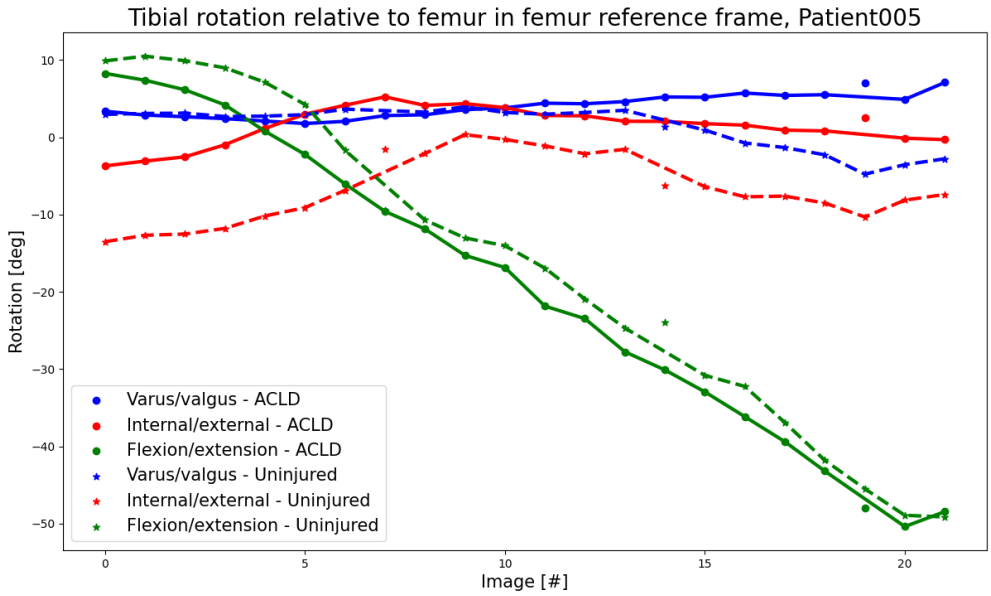

(d) Rotations against image number, patient005.

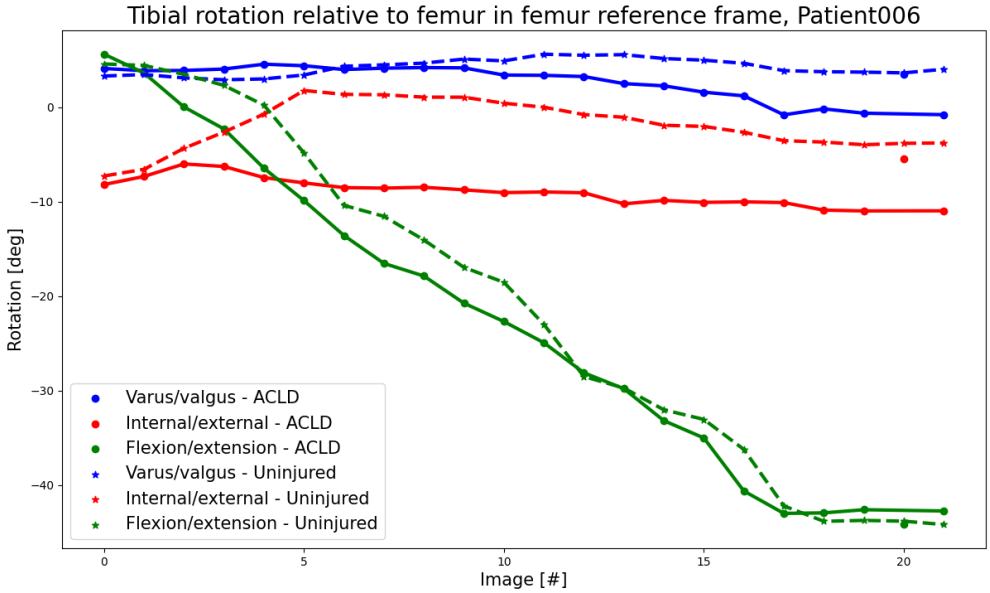

(e) Rotations against image number, patient006.

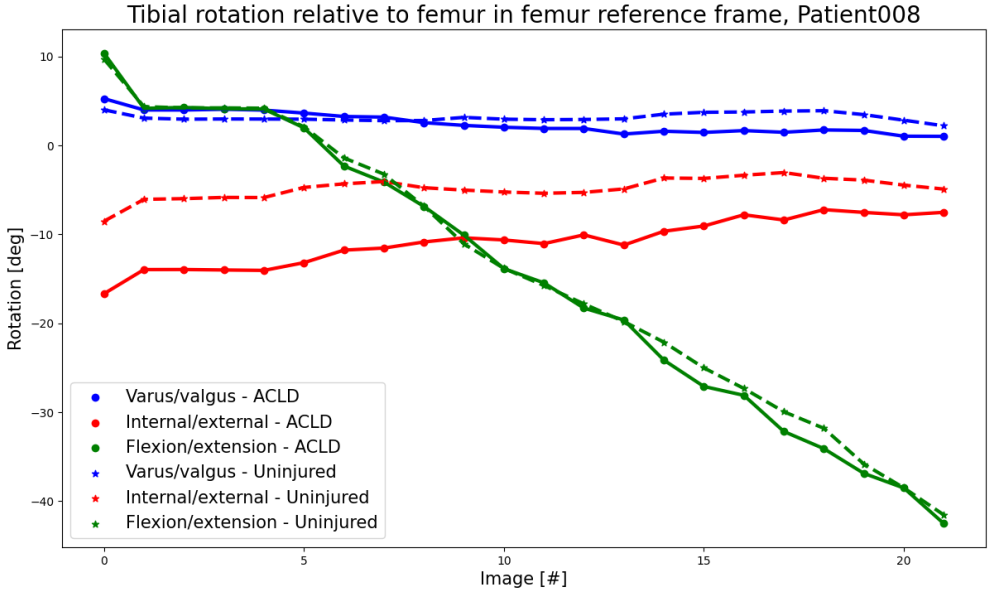

(f) Rotations against image number, patient008.

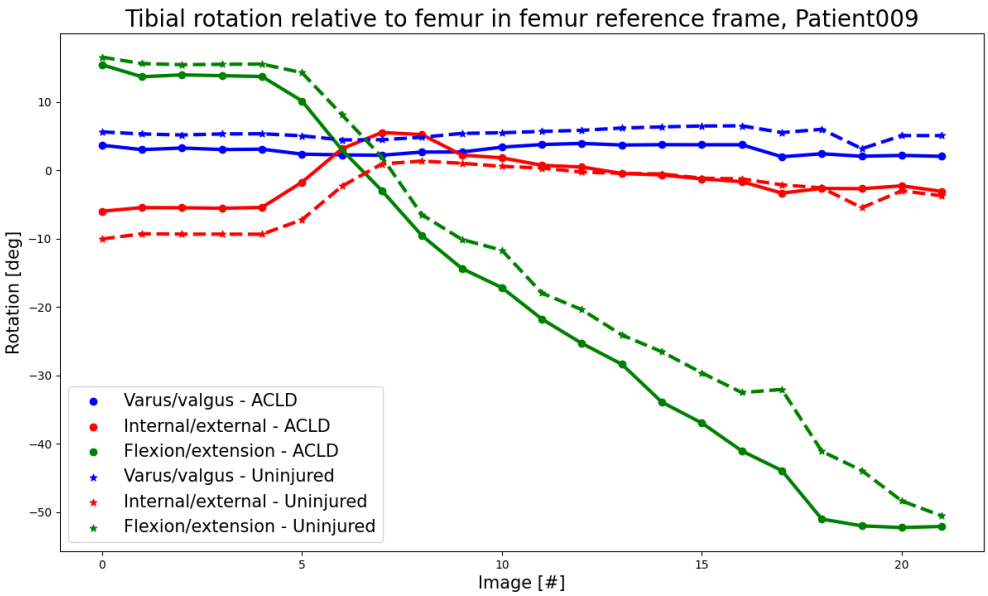

(g) Rotations against image number, patient009.

Figure C.4: Plots of the rotations against the image numbers where the lines represent the data used for the simulations and the dots the data values obtained from the 4DCT.

D

Distances between subsequent centers of proximity

To define whether roll or slip was occurring the distances between subsequent centers of proximity were calculated. These values can be found in tables D.1 to D.14.

Table D.1: Distances between subsequent centres of proximity, ACLD knee patient001.

Flexion angle	Distance femur (L)	Distance tibia (L)	Femur/ tibia (L)	Distance femur (M)	Distance tibia (M)	Femur/ tibia (M)
-10	3.52	4.27	0.82	5.51	1.35	4.08
-5	3.10	0.84	3.69	3.77	0.14	26.92
0	2.97	0.29	10.14	3.02	0.52	5.82
5	3.78	0.31	12.37	2.94	1.22	2.40
10	2.37	0.20	11.88	1.92	0.78	2.46
15	3.37	0.53	6.40	3.27	0.56	5.82
20	6.83	1.34	5.08	5.76	0.30	19.52
25	0.33	0.67	0.49	1.47	0.89	1.65
30	0.30	0.42	0.71	0.87	0.66	1.32
35	2.32	0.04	63.07	2.45	1.75	1.41
40	1.48	0.27	5.48	2.37	1.27	1.87
45	1.68	0.18	9.50	1.64	0.47	3.47

Table D.2: Distances between subsequent centres of proximity, uninjured knee patient001.

Flexion angle	Distance femur (L)	Distance tibia (L)	Femur/ tibia (L)	Distance femur (M)	Distance tibia (M)	Femur/ tibia (M)
-10	0.89	1.10	0.81	2.30	0.03	68.99
-5	1.33	1.09	1.23	2.52	0.33	7.70
0	2.04	1.34	1.52	2.85	0.78	3.66
5	2.71	1.43	1.89	3.25	0.85	3.80
10	2.74	0.84	3.26	3.46	0.03	117.37
15	2.76	0.25	11.02	3.39	0.55	6.19
20	2.63	0.65	4.07	3.06	0.09	32.82
25	1.88	1.06	1.77	1.92	1.31	1.46
30	2.16	0.42	5.21	2.58	0.70	3.69
35	2.36	1.04	2.26	2.32	0.64	3.62
40	1.44	0.32	4.57	1.64	1.56	1.05
45	1.89	0.09	21.38	2.21	0.68	3.25

Table D.3: Distances between subsequent centres of proximity, ACLD knee patient003.

Flexion angle	Distance femur (L)	Distance tibia (L)	Femur/ tibia (L)	Distance femur (M)	Distance tibia (M)	Femur/ tibia (M)
0	6.13	2.59	2.36	7.66	0.56	13.61
5	2.33	1.00	2.34	3.67	0.72	5.12
10	2.07	0.29	7.05	4.29	1.67	2.57
15	3.83	1.06	3.61	6.61	3.04	2.17
20	1.03	0.44	2.33	1.56	0.80	1.94
25	3.05	0.82	3.75	4.62	3.09	1.50
30	2.63	0.73	3.59	3.58	2.00	1.79
35	2.62	0.34	7.74	3.10	0.60	5.15
40	3.64	0.53	6.83	4.34	2.38	1.83
45	1.86	0.18	10.36	2.46	1.26	1.95

Table D.4: Distances between subsequent centres of proximity, uninjured knee patient003.

Flexion angle	Distance femur (L)	Distance tibia (L)	Femur/ tibia (L)	Distance femur (M)	Distance tibia (M)	Femur/ tibia (M)
0	2.17	1.67	1.29	3.31	1.07	3.10
5	2.70	1.42	1.90	3.85	1.08	3.57
10	3.14	1.03	3.05	4.27	2.04	2.09
15	2.46	0.93	2.64	3.98	0.54	7.40
20	2.81	0.44	6.38	4.75	2.46	1.93
25	2.41	0.30	8.02	4.16	2.95	1.41
30	2.44	0.43	5.71	3.62	2.81	1.29
35	2.33	0.59	3.95	2.65	0.76	3.50
40	3.23	0.88	3.67	5.05	4.92	1.03
45	1.68	0.40	4.18	3.11	3.11	1.00

Table D.5: Distances between subsequent centers of proximity, ACLD knee patient004.

Flexion angle	Distance femur (L)	Distance tibia (L)	Femur/ tibia (L)	Distance femur (M)	Distance tibia (M)	Femur/ tibia (M)
-5	0.98	0.29	3.37	1.80	0.20	8.96
0	2.15	0.54	3.99	3.48	0.90	3.87
5	2.89	0.70	4.15	3.65	0.80	4.57
10	3.02	0.77	3.91	3.86	0.97	3.96
15	2.99	0.80	3.76	3.98	0.70	5.67
20	4.28	0.73	5.89	3.38	0.93	3.65
25	0.74	0.69	1.06	1.95	1.92	1.02
30	2.74	0.14	19.61	2.97	0.67	4.44

Table D.6: Distances between subsequent centres of proximity, uninjured knee patient004.

Flexion angle	Distance femur (L)	Distance tibia (L)	Femur/ tibia (L)	Distance femur (M)	Distance tibia (M)	Femur/ tibia (M)
-5	2.25	1.86	1.21	3.24	0.35	9.15
0	2.23	1.18	1.88	2.39	0.54	4.39
5	1.93	1.24	1.56	3.19	1.39	2.30
10	2.75	0.81	3.42	2.70	0.19	13.93
15	3.51	0.36	9.80	3.85	0.32	12.17
20	2.26	0.21	10.60	2.78	1.28	2.17
25	3.11	0.55	5.66	3.16	1.27	2.49
30	2.23	0.37	6.10	3.00	1.67	1.79

Table D.7: Distances between subsequent centres of proximity, ACLD knee patient005.

Flexion angle	Distance femur (L)	Distance tibia (L)	Femur/ tibia (L)	Distance femur (M)	Distance tibia (M)	Femur/ tibia (M)
-5	12.49	13.67	0.91	1.97	0.86	2.30
0	3.59	2.47	1.45	3.78	0.08	46.45
5	2.24	0.28	8.11	3.80	0.46	8.23
10	1.46	2.23	0.66	3.76	1.08	3.48
15	0.51	4.36	0.12	4.73	0.94	5.00
20	3.25	3.82	0.85	6.03	0.29	21.06
25	1.92	1.33	1.45	3.31	1.40	2.37
30	2.20	0.62	3.55	3.56	1.35	2.65
35	3.27	0.64	5.09	2.84	0.37	7.73
40	4.60	2.23	2.06	5.31	3.49	1.52

Table D.8: Distances between subsequent centres of proximity, uninjured knee patient005.

Flexion angle	Distance femur (L)	Distance tibia (L)	Femur/ tibia (L)	Distance femur (M)	Distance tibia (M)	Femur/ tibia (M)
-5	10.34	8.50	1.22	14.03	2.83	4.96
0	8.49	6.09	1.39	10.10	1.19	8.47
5	8.12	5.77	1.41	9.33	1.06	8.77
10	5.15	1.64	3.14	6.12	1.94	3.16
15	3.70	1.00	3.70	2.54	1.08	2.35
20	3.69	1.95	1.90	3.82	1.20	3.20
25	3.58	1.68	2.13	4.38	4.25	1.03
30	4.87	1.55	3.13	1.69	1.72	0.98
35	0.66	0.48	1.38	0.72	0.73	0.98
40	5.34	0.39	13.77	0.07	0.07	0.98

Table D.9: Distances between subsequent centres of proximity, ACLD knee patient006.

Flexion angle	Distance femur (L)	Distance tibia (L)	Femur/ tibia (L)	Distance femur (M)	Distance tibia (M)	Femur/ tibia (M)
0	3.32	0.61	5.48	4.46	1.93	2.31
5	4.05	0.24	17.22	5.01	2.13	2.35
10	3.41	0.16	21.73	6.87	4.33	1.59
15	3.23	0.22	15.02	6.51	3.29	1.98
20	3.74	0.79	4.72	3.91	1.74	2.25
25	3.09	0.49	6.28	7.19	5.29	1.36
30	2.31	0.17	13.66	8.02	6.55	1.22

Table D.10: Distances between subsequent centres of proximity, uninjured knee patient006.

Flexion angle	Distance femur (L)	Distance tibia (L)	Femur/ tibia (L)	Distance femur (M)	Distance tibia (M)	Femur/ tibia (M)
0	1.53	2.02	0.76	2.98	0.60	4.99
5	2.70	1.22	2.21	3.31	1.42	2.34
10	4.07	1.46	2.80	5.61	1.11	5.07
15	4.29	0.34	12.77	6.72	3.25	2.07
20	0.71	0.33	2.16	1.43	1.00	1.42
25	5.80	1.77	3.27	7.87	4.79	1.64
30	0.22	0.11	1.97	0.24	0.22	1.10

Table D.11: Distances between subsequent centres of proximity, ACLD knee patient008.

Flexion angle	Distance femur (L)	Distance tibia (L)	Femur/ tibia (L)	Distance femur (M)	Distance tibia (M)	Femur/ tibia (M)
5	7.66	2.30	3.32	9.77	1.52	6.45
10	1.48	0.21	6.94	1.79	0.15	12.14
15	2.75	0.10	28.48	3.62	0.11	33.50
20	2.49	0.14	18.37	3.29	0.17	19.24
25	2.27	0.35	6.57	2.80	0.26	10.64
30	2.45	0.35	7.11	2.79	0.93	3.00
35	2.47	0.20	12.11	2.94	0.91	3.25

Table D.12: Distances between subsequent centres of proximity, uninjured knee patient008.

Flexion angle	Distance femur (L)	Distance tibia (L)	Femur/ tibia (L)	Distance femur (M)	Distance tibia (M)	Femur/ tibia (M)
5	3.11	0.34	9.09	3.44	0.99	3.48
10	2.31	0.18	12.67	2.33	0.02	134.28
15	3.45	0.26	13.32	3.50	0.31	11.25
20	0.91	0.52	1.76	1.92	0.21	9.32
25	3.18	0.69	4.60	4.00	0.60	6.72
30	1.23	0.55	2.25	2.42	0.78	3.09
35	3.22	0.09	37.82	4.00	1.18	3.37

Table D.13: Distances between subsequent centres of proximity, ACLD knee patient009.

Flexion angle	Distance femur (L)	Distance tibia (L)	Femur/ tibia (L)	Distance femur (M)	Distance tibia (M)	Femur/ tibia (M)
0	15.24	5.53	2.76	17.86	0.14	128.87
5	4.83	4.63	1.04	5.38	1.19	4.52
10	3.94	3.99	0.99	4.30	0.77	5.60
15	2.68	1.17	2.29	3.54	0.30	11.61
20	2.23	0.13	17.00	3.36	1.59	2.12
25	2.56	0.79	3.24	3.22	0.75	4.27
30	1.72	0.68	2.55	2.88	1.90	1.52
35	2.41	0.10	24.77	3.47	1.75	1.98
40	4.11	0.85	4.83	5.48	2.34	2.35

Table D.14: Distances between subsequent centres of proximity, uninjured knee patient009.

Flexion angle	Distance femur (L)	Distance tibia (L)	Femur/ tibia (L)	Distance femur (M)	Distance tibia (M)	Femur/ tibia (M)
0	0.10	0.02	5.27	0.15	0.05	2.98
5	1.44	0.37	3.88	1.88	0.36	5.27
10	3.47	0.98	3.53	4.01	0.15	26.67
15	1.58	0.26	5.97	2.52	1.50	1.67
20	2.21	0.30	7.49	3.11	0.78	4.00
25	2.22	0.13	17.32	2.91	1.16	2.50
30	2.01	1.62	1.24	0.56	2.31	0.24
35	1.94	0.63	3.08	3.63	2.36	1.54
40	3.06	0.19	15.91	3.83	3.36	1.14